THE REDUCED-ALPHA-WIDTH OF THE LOWEST 1^- STATE OF ^{16}O

Thesis by

Peggy L. Dyer

In Partial Fulfillment of the Requirements

For the Degree of

Doctor of Philosophy

California Institute of Technology
Pasadena, California

1973

(Submitted December 15, 1972)

ACKNOWLEDGMENTS

I am especially grateful to Professor C. A. Barnes, who provided guidance and encouragement throughout this work. It was a pleasure to work with him. Appreciation goes also to Professor W. A. Fowler, whose unfading interest in the $^{12}C(\alpha,\gamma)^{16}O$ reaction rate motivated us to attempt these formidable measurements.

The technique adopted for these measurements was explored first by Dr. Barnes with Drs. A. Adams, M. H. Shapiro, and E. G. Adelberger, and later, in more detail, by Drs. D. C. Weisser and J. F. Morgan. Dr. H. B. Mak designed the amplifiers which made possible the extraction of a time-reference pulse from the target. The chopping and bunching system on the 3 MV generator was constructed by Dr. M. R. Dwarakanath. Dr. Dwarakanath and Mr. J. G. Polchinski aided in setting up the experimental apparatus on the 3 MV generator and in taking data.

Dr. Eileen Hess of DHOM Products Ltd. carried out the conversion of amorphous carbon to methyl iodide required for target preparation.

Two methods of extrapolating the $^{12}C(\alpha,\gamma)^{16}O$ excitation function to low energies are described in this thesis. The 3-level R-matrix computer code was written by Drs. D. R. Thompson, D. C. Weisser and J. F. Morgan; the "hybrid" R-matrix-optical-model fit was developed by Mr. S. E. Koonin and Professor T. A. Tombrello.

A special thank-you goes to the following members of the Kellogg Radiation Laboratory staff: Vic Ehrgott, Barbara Zimmerman,

Laurie Graham, Don Kinley, Bud Warrick, George Fastle, Don Woshnak, Will Schick, and Don McGrath. I am also indebted to the many graduate students and research fellows who helped during the long data-accumulation periods.

I am grateful for financial assistance provided by a NASA Traineeship and by Graduate Research Assistantships from the California Institute of Technology. This research was supported in part by the National Science Foundation (GP-28027).

ABSTRACT

Cross sections for the reaction $^{12}C(\alpha,\gamma)^{16}O$ have been measured for a range of center-of-mass alpha particle energies extending from 1.72 MeV to 2.94 MeV. Two 8"×5" NaI(Tℓ) crystals were used to detect gamma rays; time-of-flight technique was employed to suppress cosmic ray background and background due to neutrons arising mainly from the $^{13}C(\alpha,n)^{16}O$ reaction. Angular distributions were measured at center-of-mass alpha energies of 2.18, 2.42, 2.56 and 2.83 MeV. Upper limits were placed on the amount of radiation cascading through the 6.92 or 7.12-MeV states in ^{16}O. By means of theoretical fits to the measured electric dipole component of the total cross section, in which interference between the 1^- states in ^{16}O at 7.12 MeV and at 9.60 MeV is taken into account, it is possible to extract the dimensionless, reduced-alpha-width of the 7.12-MeV state in ^{16}O. A three-level R-matrix parameterization of the data yields the width $\Theta^2_{\alpha,F} = 0.14\ ^{+0.10}_{-0.08}$. A "hybrid" R-matrix-optical-model parameterization yields $\Theta^2_{\alpha,F} = 0.11\ ^{+0.11}_{-0.07}$. This quantity is of crucial importance in determining the abundances of ^{12}C and ^{16}O at the end of helium burning in stars.

TABLE OF CONTENTS

LIST OF TABLES

LIST OF FIGURES

I. GENERAL INTRODUCTION

A. Astrophysical Implications

The $^{12}C(\alpha,\gamma)^{16}O$ reaction follows the $3\alpha \rightarrow {}^{12}C$ reaction in the chain of helium-burning reactions which can occur in the interior of a star which has exhausted the hydrogen fuel in its core. The ratio of the rates of the $^{12}C(\alpha,\gamma)^{16}O$ and the $3\alpha \rightarrow {}^{12}C$ reactions (at the relevant stellar temperatures) effectively determines the mass fractions of ^{12}C and ^{16}O at the end of helium burning in massive or intermediate-mass stars, since the succeeding reaction $^{16}O(\alpha,\gamma)^{20}Ne$ is very slow at helium-burning temperatures. Whereas the $3\alpha \rightarrow {}^{12}C$ rate is relatively well known at the present time (Barnes 1971), the $^{12}C(\alpha,\gamma)^{16}O$ rate was so highly uncertain prior to the present measurements, that the mass fraction of ^{12}C at the end of helium burning was left completely unresolved. It was thus difficult for astrophysicists to calculate relative abundances of ^{12}C and ^{16}O in the universe or to follow the evolution of a star past helium burning.

As an example of the importance of the $^{12}C(\alpha,\gamma)^{16}O$ reaction rate, we consider here helium burning in intermediate mass ($4 < M/M_{\odot} < 10$) and massive ($10 < M/M_{\odot} < 100$) stars.

Helium burning follows hydrogen burning. Following exhaustion of the hydrogen fuel by the conversion of hydrogen to helium, which takes place through the various chains of reactions characteristic of hydrogen burning, the central region of a star contracts and heats up. When this core becomes hot enough, helium burning begins and gravitational collapse is halted. At this point the central density is about

$10^4 g/cm^3$ and the central temperature is of the order of 10^8 ^oK. The reaction chain for nucleosynthesis of ^{12}C and ^{16}O in helium burning is primarily concerned with the following three reactions:

$$3\alpha \rightarrow {}^{12}C ,$$

$$^{12}C(\alpha,\gamma)^{16}O ,$$

$$^{16}O(\alpha,\gamma)^{20}Ne .$$

The relative rates of these three reactions at the appropriate effective interaction energies determine the abundances of elements left in the core at the end of helium burning. If the $^{12}C(\alpha,\gamma)^{16}O$ rate is slow compared with the $3\alpha \rightarrow {}^{12}C$ rate, then a large fraction of ^{12}C will remain at the end of helium burning; if $^{12}C(\alpha,\gamma)^{16}O$ is fast compared with $3\alpha \rightarrow {}^{12}C$, then the end-product of helium burning will be ^{16}O, since the $^{16}O(\alpha,\gamma)^{20}Ne$ reaction rate is very small. For intermediate $^{12}C(\alpha,\gamma)^{16}O$ rates there will be some mixture of ^{12}C and ^{16}O remaining.

The stellar reaction rate of the $^{12}C(\alpha,\gamma)^{16}O$ reaction is commonly parameterized in terms of a dimensionless, reduced-alpha-width of the state in ^{16}O at 7.12 MeV, a quantity denoted $\Theta^2_{\alpha,F}$*. The relation between the rate at astrophysically important energies, which are of the order of 300 keV c.m., and $\Theta^2_{\alpha,F}$ is given in Appendix A. The stellar reaction rate is directly proportional to the magnitude of $\Theta^2_{\alpha,F}$. The mass fraction of ^{12}C remaining at the end of helium burning, a quantity

---

*In this work the symbol Θ^2_α will refer to the 7.12-MeV state in ^{16}O unless otherwise noted. The subscript "F" refers specifically to the quantity Θ^2_α as defined by Fowler et al. (1967). See Appendix A.

denoted by X_C , may thus be expressed as a function of the mass of the star and of the quantity $\Theta^2_{\alpha,F}$. (See Section IV.A for a more quantitative discussion of the relation between X_C and $\Theta^2_{\alpha,F}$.)

A basic premise of current astrophysical theory is that most of the synthesis of elements heavier than helium has taken place in the interior of stars and that these elements have in some way been ejected into the interstellar medium (Fowler 1968). Recent calculations (Arnett 1972) suggest that massive stars ($10 < M/M_\odot < 100$) are the primary source of ^{12}C and ^{16}O . Once $\Theta^2_{\alpha,F}$ is known, it should be possible to calculate the relative abundances of ^{12}C and ^{16}O at the end of helium burning, and from current astrophysical theory, to predict the observed "cosmological" abundance ratio X_C/X_O . (X_O is the mass fraction of ^{16}O.) If the calculated and observed values do not agree, the astrophysical theory must be modified.

Such an astrophysical theory must treat the following topics (Arnett 1971): (1) galactic evolution theory, in order to interpret present abundances in terms of continuous nucleosynthesis beginning billions of years ago, (2) the mass distribution of stars formed from the interstellar medium, (3) the range of mass of stars contributing to nucleosynthesis of ^{12}C and ^{16}O, (4) the rates of nucleosynthesis during quiescent quasi-static helium burning in the core and in shells of the star, and during possible explosive stages, (5) the mechanisms for mass ejection, and (6) the fractions of mass ejected. None of these topics can presently be treated unambiguously. However, once the relevant nuclear reaction rates are determined empirically, severe constraints are placed on any viable astrophysical theory.

Much effort has been spent recently in an attempt to follow the evolution of a star after core helium burning is completed. Because the helium fuel has now been used up, the core will contract, converting gravitational energy to heat, until a temperature is reached which is high enough for further nuclear reactions to take place. What these reactions will be depends upon what nuclei are present. Whether these reactions will ignite quiescently or explosively depends on many factors, which include the amount and type of fuel available.

One possible path at this point, for stars in the intermediate mass range ($4 < M/M_\odot < 10$), is explosive ignition of either ^{12}C, by the $^{12}C+^{12}C$ reaction, or ^{16}O, by the $^{16}O+^{16}O$ reaction. The resulting detonation could end with a catastrophic mass loss, with or without a remnant. This stage of evolution has become of great interest in the last few years, especially because of the apparent concurrence of an analysis of pulsar observations made by Gunn and Ostriker (1970) and calculations of stellar models made by Paczyński (1970) and others.

Gunn and Ostriker statistically analyzed data on 40 observed pulsars, using a rotating, highly magnetized neutron star as their model for a pulsar. The derived information such as the birth rate of pulsars and their scale height from the galactic plane indicates that pulsars may be the remnants of Type II supernovae, and that all Population I stars in the mass range $2 < M/M_\odot < 10$ could be progenitors of pulsars.

On the other hand, evolutionary models of stars calculated by Paczyński show that stars in the mass range $4 < M/M_\odot < 10$ all develop a carbon-oxygen core of about 1.4 $M_\odot$ and converge onto a single

evolutionary track. After this, the core may become dynamically unstable and collapse, or may ignite carbon explosively, leading to the type of supernova explosion suggested by Arnett (1969).

At this stage, however, the unknown $^{12}C(\alpha,\gamma)^{16}O$ rate allows only speculation, for the further evolution of the star is critically dependent on the amount of ^{12}C remaining at the end of helium burning. If there is a large fraction of ^{12}C ($^{12}C(\alpha,\gamma)^{16}O$ rate low, small $\Theta^2_{\alpha,F}$), a carbon detonation could be initiated by the $^{12}C+^{12}C$ reaction, and the star could explode. Arnett (1969) and Wheeler et al. (1970) agree that if such a carbon detonation takes place, there would be no remnant, and thus no neutron star. On the other hand, if there is not enough ^{12}C to initiate a $^{12}C+^{12}C$ detonation ($^{12}C(\alpha,\gamma)^{16}O$ rate high, large $\Theta^2_{\alpha,F}$), the core will continue to contract until ^{16}O detonates; however, such an ^{16}O detonation would occur at higher densities than would obtain for a ^{12}C detonation. At these higher densities, electron capture processes are very rapid, and the core of the star would implode rather than explode. There would in this case be a remnant.

The $^{12}C(\alpha,\gamma)^{16}O$ reaction rate is thus a critical factor in predicting the relative abundances of ^{12}C and ^{16}O from astrophysical theory and in specifying the amount of ^{12}C left in the interior of an intermediate-mass star at the end of helium burning, a quantity which is of decisive importance in determining the further evolution of the star.

The discussion thus far has been primarily concerned with helium burning in the core of a star. An interesting phenomenon, which is perhaps related to helium burning in a shell outside the core, is

the abnormally high carbon content of the atmospheres of certain very luminous, highly-evolved stars, called carbon stars. Such carbon abundances are measured by observations of molecular bands of carbon-containing molecules such as CN. A carbon star is defined as a star in which the number ratio of carbon to oxygen in the atmosphere is greater than unity. When this is true, carbon molecules other than CO can form. In terms of the mass fractions, the criterion is that X_C be greater than 1.33 X_O. Since the measured abundances for the solar system give $X_C = 0.4\ X_O$ (Cameron 1968), it is thought that these stars were not formed as carbon stars, but that they have evolved to that stage.

Such high carbon abundances may reflect the abundance of carbon in a helium-burning shell inside the star. The temperature and density of a helium-burning shell are different from those of a helium-burning core (for a star of the same mass); the relative rate of the $^{12}C(\alpha,\gamma)^{16}O$ reaction may thus be smaller in the shell. The ratio of ^{12}C to ^{16}O at the end of helium burning in a shell will then be higher than that characterizing core helium burning (Paczyński 1971). At this stage of evolution, a star of a few solar masses is expected to have a carbon-oxygen core where helium burning has been completed, a helium-burning shell, an intershell zone of helium where hydrogen burning has been completed but helium burning has not yet begun, a hydrogen-burning shell, and an envelope made up mostly of hydrogen. If the carbon content of the envelope is to be described in terms of the carbon content of the helium-burning shell, there must be derived some mechanism for convective mixing between the two zones.

A star in the red giant stage has a deep convective envelope; however, this convective zone will never reach into the hydrogen-burning shell. Schwarzschild and Härm (1967) and Weigert (1966) have found that during helium shell flashes, "convective tongues" may extend from the helium-burning shell to the intershell zone. After several flashes, the convective tongue can penetrate the hydrogen-burning shell. The intershell zone and the hydrogen-burning shell then contain carbon and oxygen. It now remains to find a mechanism for convective mixing of the hydrogen-burning shell and the convective region of the envelope. Smith and Sackmann (1972) have done so by considering the protons brought down from the hydrogen-burning shell to the carbon-enriched intershell zone. The energy release from the $^{12}C(p,\gamma)^{13}N(e^+,\nu)^{13}C$ reaction raises the temperature gradient to the extent that another convective tongue reaches from the hydrogen-burning shell to the convective region of the envelope. In order to calculate the amount of atmospheric carbon enrichment, it is necessary to know the ratio of ^{12}C to ^{16}O produced by the helium-burning shell. Again, however, the unknown rate of the $^{12}C(\alpha,\gamma)^{16}O$ reaction limits one's ability to calculate the abundance ratio in the shell, and thus in the atmosphere. If the $^{12}C(\alpha,\gamma)^{16}O$ rate were very small, so that ^{12}C would be the main product in the helium-burning shell, one helium flash in a 1 $M_\odot$ star would be more than adequate to produce a carbon star. Since there are probably several such flashes in a 1 $M_\odot$ star, this theory predicts too much carbon enrichment if the $^{12}C(\alpha,\gamma)^{16}O$ rate is very small. In the case of a 5 $M_\odot$ star, it is more difficult to enrich the atmosphere with ^{12}C; the intershell mass is smaller, and the envelope is larger

and thus contains a greater quantity of oxygen before mixing. The theory will then predict too small an enrichment of ^{12}C if the $^{12}C(\alpha,\gamma)^{16}O$ rate is very large. There are, of course, many uncertainties in the astrophysical description of carbon stars. For example, the masses of observed carbon stars are, at best, very poorly known, and cannot be determined by simply observing the luminosities, since evolutionary tracks of stars of different masses tend to converge at this stage of evolution. A knowledge of the $^{12}C(\alpha,\gamma)^{16}O$ rate will, therefore, impose a serious constraint on any theory of carbon star formation.

B. Theoretical Description of the ^{16}O Nucleus

The dimensionless reduced-alpha-width θ_α^2 is expected to have a value between 0 and 1. Crudely speaking, it is a measure of the fraction of the time that the 7.12-MeV state of ^{16}O looks like a ^{12}C nucleus plus an alpha particle.

Because the ^{16}O nucleus is one of the alpha-particle series nuclei, it might be expected that an alpha-particle, or cluster model, would describe the states of the nucleus well. However, such simple models have not been able to describe quantitatively even the low-lying states in ^{16}O.

A model which has had more success is one developed by Brown and Green (1965, 1966). They account for the low-lying odd-parity states by mixing a deformed odd-parity state, formed by excitation of three nucleons out of a deformed core, with a spherical shell-model state corresponding to a 1 particle- 1 hole excitation. In this picture the

7.12-MeV state of ^{16}O is predominantly 1 particle - 1 hole, whereas the 9.60-MeV state is predominantly 3 particle - 3 hole. Low-lying even-parity states are expressed as mixtures of a spherical shell-model ground state with deformed states formed by mixing 2 particle - 2 hole and 4 particle - 4 hole excitations out of a deformed core. Although it has had only moderate success at predicting transition probabilities, this model does well in predicting the energies of levels in ^{16}O (with the proper choice of free parameters).

Stephenson (1966) has used such a model to calculate $\Theta_\alpha^2(7.12\text{-MeV}, ^{16}O)$. He finds this quantity to be 0.08 ± 0.04, with the major uncertainty attributed to neglect of coupling to higher-energy configurations.

C. Previous Attempts to Determine $\Theta_\alpha^2(7.12\text{-MeV}, ^{16}O)$

There have been many previous attempts to measure the alpha width of the 7.12-MeV state of ^{16}O; the results have varied widely.

Loebenstein et al. (1967) measured the angular distributions of deuterons from the reaction $^{6}Li(^{12}C,d)^{16}O$, hoping to measure Θ_α^2 by observing the transfer of an alpha particle from ^{6}Li into the 7.12-MeV state in ^{16}O. However, it was found that the reaction proceeded not only by this direct process, but also through formation of a compound nucleus. The compound nuclear contribution was estimated theoretically and found to be, for the energies studied, two-thirds or more of the total cross section for the reaction leading to the 7.12-MeV state. Their result, $0.06 \leq \Theta_\alpha^2 \leq 0.14$, does not include any uncertainty in the theoretical estimate of the compound nuclear contribution

to the cross section.

Pühlhofer et al. (1970) attempted a similar measurement. They measured triton angular distributions from the reaction $^{12}C(^{7}Li,t)^{16}O$. This reaction was expected by the authors to proceed more strongly by direct reaction than the $^{6}Li(^{12}C,d)^{16}O$ reaction studied by Loebenstein et al. The compound nuclear part of the cross section extracted for the case of the 7.12-MeV state was still high--about 50% of the total cross section. It was again necessary to subtract the compound contribution in order to find Θ_α^2. The result given is $\Theta_\alpha^2 = 0.025$, uncertain by a factor of 1.5 or 2, although this factor may well be much larger since the theoretical framework employed by Pühlhofer et al. could not be applied to the unbound states of ^{16}O for which Θ_α^2 is already known.

An attempt has been made to obtain Θ_α^2 by a multilevel R-matrix fit to the p-wave phase shifts for $^{12}C+\alpha$ elastic scattering (Clark 1969). However, the present data are not accurate enough at low energies to put useful limits on the value of Θ_α^2, as our own analysis shows clearly.

The alpha spectrum following the beta decay of ^{16}N to ^{16}O (Hättig 1969) has been fitted by Werntz (1971) and Barker (1971), in attempts to see interference between the tail of the 9.60-MeV state in ^{16}O and the tail of the 7.12-MeV state. Barker considered contributions of 6 levels (three 1^- and three 3^-) to the spectrum. He fitted the p-wave and f-wave $^{12}C+\alpha$ elastic scattering phase shifts, each with a 3-level R-matrix formula, in order to determine some of the parameters required for a description of the alpha spectrum. From a fit to the ^{16}N alpha spectrum, he determined that the interference in the ^{16}N case is destructive between levels and that Θ_α^2 is in the range 0.06

to 0.24. Werntz considered only three 1^- levels. Some of the parameters were constrained by the 1^- phase shifts of $^{12}C+\alpha$ elastic scattering and by known ft values for the beta decay. Two parameters, one of which is Θ_α^2, were varied to fit the alpha spectrum. The resulting range for Θ_α^2 is 0.013 to 0.105. Barnes and Fowler (1970) have also investigated the implications of the measured α-spectrum from ^{16}N beta decay. They found that the interference between the 7.12-MeV and 9.60-MeV levels is destructive in the ^{16}N case, and that $\Theta_\alpha^2(7.12)$ is not negligibly small. This result is confirmed by the more detailed analyses of Werntz and Barker.

The most direct way to obtain the astrophysical rate of the $^{12}C(\alpha,\gamma)^{16}O$ reaction, is to measure the cross section for that reaction to as low an alpha energy as possible. Early measurements of the $^{12}C(\alpha,\gamma)^{16}O$ cross section did not extend low enough in energy that a reliable estimate of the rate at a few hundred keV could be made. Larson and Spear (Larson 1964, Larson 1965) measured the gamma-ray yield with a NaI(Tℓ) detector, and found the cross section at $E_\alpha(c.m.) = 2.4$ MeV (at the peak of the resonance corresponding to the 9.60-MeV state in ^{16}O) to be about 36 nb. Adams et al. (1968) introduced the time-of-flight technique to suppress the background of neutrons from the $^{13}C(\alpha,n)^{16}O$ reaction; they found $\sigma \simeq 10$ nb at $E_\alpha(c.m.) = 2.0$ MeV. Ewen (1970) used an NE226 non-hydrogenous liquid scintillator to suppress neutron background; he obtained $\sigma = 120 \pm 80$ nb at $E_\alpha(c.m.) = 2.4$ MeV. Jaszczak et al. (1970, 1970a), by a method similar to the one described in this work, have measured the cross section down to a c.m. alpha energy of 1.4 MeV, but the statistical errors are so large

that the extrapolated cross section for astrophysically interesting energies is still highly uncertain (Weisser 1970). In addition, the energy dependence of the cross sections measured by Jaszczak et al. is not in agreement with the work reported in this thesis. Since an extrapolation to stellar energies is involved, any error in the energy dependence is greatly amplified in the extrapolation.

D. Scheme of the Present Experiment

Since the $^{12}C(\alpha,\gamma)^{16}O$ cross section at c.m. alpha energies near 300 keV is expected to be of the order of 10^{-8} nanobarns, it is not possible to measure the yield directly in the laboratory by any known method. The best that can be done is to measure the cross section over a wide range of energies which extends as low as possible, and to extrapolate to astrophysically important energies.

Figure 1 shows an energy level diagram of the ^{16}O nucleus (Ajzenberg-Selove 1971). The states which are of immediate interest in this work are the 7.12-MeV state and the 9.60-MeV state, both of which have 1^- spin and parity. At a c.m. alpha energy of 2.4 MeV, there is a broad resonance in the $^{12}C(\alpha,\gamma)^{16}O$ reaction due to the state at 9.60 MeV in ^{16}O, which has a c.m. width of 510 ± 60 keV (Ajzenberg-Selove 1971). The 7.12-MeV state is 42 keV below the $^{12}C+\alpha$ threshold, so that this state can affect the $^{12}C(\alpha,\gamma)^{16}O$ rate only through the tail of the state, which extends above the $^{12}C+\alpha$ threshold. The extent to which the tail contributes to the cross section depends on the dimensionless reduced alpha-width of the 7.12-MeV state: θ_α^2 .

The strategy of the present experiment is to measure the yield

of gamma rays for a range of alpha energies which extends above and below the resonance corresponding to the 9.60-MeV state in ^{16}O, and which reaches as far below this resonance as it is feasible to measure. Interference of the tail of the 7.12-MeV state in ^{16}O with that of the 9.60-MeV state will cause the shape of the measured excitation function to depart from that due to a single resonance plus possible interference from the tails of higher energy states. If the interference between the 7.12- and 9.60-MeV states is constructive, the yield below the resonance due to the 9.60-MeV state will be larger than that which would be expected if Θ_α^2 were zero. If the interference is destructive, the yield will be smaller, and it will be more difficult experimentally to obtain a value for the alpha width.

Because the gamma-ray detection system does not cover the entire solid angle, it is necessary, in order to determine the total cross section, to know the angular distribution of the gamma rays at each energy. Furthermore, since most theories which will be used to parameterize the data will consider only the 1^- contributions to the cross sections, a knowledge of the angular distributions at various alpha energies will be required in order to determine the relative magnitudes of contributions from other angular momenta.

It was originally expected that the angular distributions below c.m. alpha energies of $\sim$3MeV would be of a pure $\sin^2\theta$ form, characteristic of electric dipole radiation distributions with spinless nuclei in the incident channel. However, measurements made with one detector at 45^o and one at 135^o showed quite early in the experiment that the angular distribution at E_α(c.m.) = 2.4 MeV is asymmetrical

about 90^{o}. This asymmetry indicates interference between states of different parity and has been attributed to the interference of the 2^{+} direct radiative capture process with the 1^{-} resonant process.

Another process which requires investigation is that of cascade radiative decay of the 9.60-MeV state in ^{16}O. This process is not expected to be important at astrophysically interesting energies (see Appendix B). However, the experimental configuration for measuring transitions to the ground state at higher alpha energies is such that cascades are not always separated from ground state transitions. Therefore a correction should be made to allow for them.

There are many other resonant and direct capture processes which are allowed by conservation of angular momentum. None of these transitions is believed to be competitive with 1^{-} resonant capture or 2^{+} direct capture to the ground state of ^{16}O, but a few warrant further thought. A further discussion of this question is given in Appendix B.

II. EXPERIMENTAL METHOD

A. Introduction

The basic components of the experimental configuration are: (1) a bunched and chopped beam of energetic alpha particles, (2) an enriched ^{12}C target, (3) two large NaI(Tℓ) crystals for detection of outgoing gamma rays and (4) the electronic circuits for sorting pulses from the NaI detectors.

The principal difficulties involved in measuring the $^{12}C(\alpha,\gamma)^{16}O$ cross sections at c.m. alpha energies below 3 MeV are low yield (total cross sections of the order of nanobarns) and high background. There are two types of background. The first type, called time-independent, consists of events which are not correlated in time with the incidence of the beam on the target; these events may be caused by cosmic rays, by pile-up of low-energy gamma rays from radioactive elements in the target area, or by neutrons produced at various points along the path of the beam which have been scattered around the target area one or more times. (These neutrons, many of which are produced in the target, will be termed "delayed" neutrons.) The second type of background, called time-dependent, consists of events which are correlated in time with the incidence of the beam on the target. These are events caused by the interaction of an incident alpha particle with some nucleus in the target (or very close to it) followed by immediate detection of a product particle. The primary source of this second type of background is the interaction of the alpha particles with the ^{13}C contaminant in the target, by the

$^{13}C(\alpha,n)^{16}O$ reaction. This reaction produces neutrons (of about 4 MeV for the range of alpha energies considered here) which sometimes produce pulses in the detection system indistinguishable from those of 9-MeV gamma rays. (These neutrons will be termed "prompt" neutrons.)

The experimental configuration described below is thus designed to allow separation of $^{12}C(\alpha,\gamma)^{16}O$ events from most background events, and to facilitate subtraction in the multichannel analyzer spectrum of that background which is not totally separated. The most important technique employed is the time-of-flight method for suppression of prompt-neutron and time-independent background.

The first of the following sections will describe the experimental configuration for measuring the yield at 90^{o} for a range of alpha energies. Following this is a discussion of the modifications required for measurements of angular distributions and cascade radiation.

Yields at 90^{o} have been measured with beams from two different accelerators: the ONR-CIT tandem and the 3 MV generator. Slight differences in experimental configuration will be noted. Only data measured with the use of the tandem accelerator have been included in the analysis of this thesis, since the data needed for normalization of the yields obtained with the 3 MV generator have not yet been measured. The preliminary 3 MV generator data appear to be consistent with the tandem accelerator measurements; the statistical errors are not significantly smaller because of the large background from delayed neutrons which was encountered. Measurements with the 3 MV generator are continuing, and steps are being taken to reduce the neutron background.

The derivation of the "thin-target" alpha energies quoted for the $^{12}C(\alpha,\gamma)^{16}O$ measurements is given in Section III.B. The range of energies considered extends up to the region where contributions to the cross section from the resonance due to the 4^+, 10.34-MeV state in ^{16}O become significant. The region of the narrow resonance at E_α(c.m.) = 2.69 MeV corresponding to the 2^+, 9.85-MeV state in ^{16}O, is excluded.

B. Measurements of Yield at $\Theta = 90^o$

1. Targets: Preparation and Thickness Measurements

It is clearly desirable to have as little ^{13}C as possible in the target. Amorphous carbon, enriched to 99.945% ^{12}C, was obtained from the Oak Ridge National Laboratory. This carbon was converted to carbon dioxide and then to methyl iodide by Dr. Eileen Hess of DHOM Products Ltd. A 3-mil thick, 1-cm by 8-cm tantalum strip was mounted inside a small pyrex tube, with stainless steel end caps sealed by Viton O-rings, in such a way that an electric current could be passed through the strip (Figure 2). The interior of the pyrex tube was evacuated and the methyl iodide was admitted to a pressure of 3 cm Hg. When the strip was heated to a temperature of about 700°C, the methyl iodide decomposed; a layer of elemental carbon was deposited on the strip, and hydrogen and iodine remained as gases. The heating current was left on for about 2 minutes. Then the hydrogen and iodine were pumped out and the process was repeated. About 12 depositions were required to make a carbon layer 180 $\mu g/cm^2$ thick at the center of the strip. The efficiency for conversion of methyl iodide to elemental carbon on the target was about 10%. The final ^{13}C content of the

targets was about 0.1%.

From this 8-cm strip, several targets could be cut, each 1 cm square. These squares were mounted in the back of a rectangular Faraday cup of dimensions 1 cm by 1 cm by 2.5 cm long. In the case of the experimental arrangement on the tandem accelerator, this cup was made entirely of 5-mil tantalum. However, because of the greater amount of heat generated by the higher-intensity beam of the 3 MV generator, it was necessary in this case to clamp the target and Ta backing between two pieces of copper. The copper pieces were then bolted directly to the copper target rod, and cooling was applied to the other end of the target rod by means of air blowing across attached fins. Even with these added precautions, blistering of the carbon layer remains a serious problem.

A strip of natural carbon, of approximately the same thickness as the enriched ^{12}C, was deposited on a Ta backing by the same process of methyl iodide cracking. This target was used for background measurements (see Section II.B.6).

The thicknesses of these targets were determined by measuring the width, due to proton energy loss in the target, of the very sharp resonance in the $^{13}C(p,\gamma)^{14}N$ reaction at E_p(lab) = 1.75 MeV (Figure 3). The enriched ^{12}C targets used had thicknesses between 155 and 191 $\mu g/cm^2$; the natural carbon targets, between 133 and 177 $\mu g/cm^2$. For the range of alpha energies used in the $^{12}C(\alpha,\gamma)^{16}O$ measurements, the enriched ^{12}C target thicknesses correspond to a loss in incident beam energy of approximately 200 keV.

All targets used in the measurements reported here were cut from the same tantalum strip.

It is important to investigate the effect of any target impurities. Thus far, this has been done experimentally only for ^{19}F (see Appendix E).

2. Target Chamber

If the enriched ^{12}C target were placed in a typical target chamber using rubber O-ring seals and oil diffusion pumps, and if the target were bombarded with a beam of high enough intensity to heat the target, then a layer of natural carbon (containing 1.1% ^{13}C) would build up on the target surface in a few hours. This natural carbon layer is produced when hydrocarbons in the vacuum system are cracked by the hot target. In order to prevent this, the target chamber was constructed of stainless steel and was sealed by copper gaskets. An ion pump near the target kept the pressure below 5×10^{-7} torr. The target chamber was isolated from the rubber O-rings and diffusion pumps on the upstream portions of the beam pipe by a liquid-nitrogen cold trap. Thus, most hydrocarbon vapors were condensed before reaching the target chamber.

With this system, the target could be bombarded by a beam of several hundred nanoamps for times accumulating to many weeks with no significant deposition of natural carbon on the target. (The long-term carbon deposition of higher-intensity beams has not yet been determined.)

The target chamber for measurements at 90^{o} consisted of a cross of 1.5" O.D. tubing of wall thickness 1/16" (Figure 4). Downstream from the target position was placed a piece of quartz on which the beam could be viewed. (When a target was placed in the path of the beam, no beam was able to reach the quartz.) Two targets were mounted in the transverse arms of the cross. The copper rods supporting the targets were mounted on bellows to avoid O-rings. Compression of one or the other of the bellows placed the corresponding target in the path of the beam. Of the two targets, one was an enriched ^{12}C target, and the other was a natural carbon target used for background measurements (see Section II.B.6).

It is necessary to avoid collimation or obstruction of the beam too near the target (see Section II.B.4). The collimation closest in position to the target was 75 cm away, at the entrance of the beam to the cold trap. At this point, a circular, 0.8-cm-diameter tantalum collimator was placed, in order to keep the beam from hitting the 1.0-cm-diameter beam tube leading through the cold trap.

The chamber was mounted on the south 20^{o} beam line in the tandem accelerator target area, and on the 0^{o} beam line in the 3 MV generator target area.

3. NaI(Tℓ) Detection System; Efficiency

Gamma rays were detected by two 20.3-cm-diameter by 12.7-cm-long NaI(Tℓ) crystals. Scintillations in the crystals were monitored with 13.3-cm-diameter RCA type 4522 14-stage photomultiplier tubes, one mounted on each crystal. This type of tube was chosen for its fast timing capabilities (see Section II.B.4) and good pulse height

resolution. Sodium iodide was chosen because of its high efficiency for detection of high energy gamma rays. The energy resolution of this system, as measured by the 662-keV line of ^{137}Cs, is 9.6% for one detector (serial no. ED98) and 10.8% for the other (serial no. ED97).

The crystals were shielded with both lead and paraffin to reduce background yield. Approximately 5 cm of lead was placed around the crystals to suppress events caused by cosmic rays or natural radioactivity in the walls of the room. In the case of the measurements made at 90^{o}, 8 or 9 cm of lithium carbonate suspended in paraffin wax was placed between the target and each crystal. This shield reduced the prompt neutron background from the $^{13}C(\alpha,n)^{16}O$ reaction by about 40%. The attenuation of 9-MeV gamma rays (of the order of 20%) was taken into account.

Because of the much higher delayed-neutron backgrounds encountered when using the beam from the 3 MV generator, the crystals were in this case surrounded by 10 cm of borated paraffin placed outside the lead shielding. These shields were constructed of 15% by weight anhydrous boric acid suspended in paraffin, and were surrounded on all sides with polyester plastic to add strength to the structure.

The total efficiency for detection of gamma rays with this system is the product of the following factors: (1) the absorption of gamma rays in the NaI(Tℓ) crystals for the particular geometry involved (given the angular distribution of the gamma rays), (2) the spectrum fraction: that fraction of absorbed gamma rays which is recorded in the portion of the spectrum from which the yield is extracted, and (3) the transmission of gamma rays through any material

which lies between the target and crystals.

Whereas the final value for Θ_α^2 which is to be extracted from the $^{12}C(\alpha,\gamma)^{16}O$ data is approximately linearly sensitive to the absolute scale of the cross sections (see Section III.E), it is much more sensitive to the variation with energy of the cross section, since an attempt is being made to see a small interference effect. It is therefore very important to include, for all of the above factors, their variation with gamma-ray energy.

The efficiency was calculated by the method of Lazar et al. (1956), which requires integration of the absorption over all gamma-ray paths through the crystal and through the absorbing material between the crystal and target. Measured standard spectra are then used to obtain the spectrum fraction. For a detector in the form of a right circular cylinder, the required integrals are of the form:

$$J_n = \int_{\text{crystal}} P_n(\cos\Theta')\, e^{-\mu_1 \ell_1(\Theta')} \left(1 - e^{-\mu_2 \ell_2(\Theta')}\right) \sin\Theta' d\Theta' ,$$

where

Θ' = angle of gamma ray with respect to axis of detector,

$P_n(\cos\Theta')$ = Legendre polynomial, order n,

μ_1 = linear attenuation coefficient for a gamma ray in the absorbing material between the crystal and target,

$\ell_1(\Theta')$ = gamma-ray path length in the absorbing material between the crystal and target,

μ_2 = linear attenuation coefficient for a gamma ray in NaI(Tℓ),

$\ell_2(\Theta')$ = gamma-ray path length in NaI(Tℓ).

These integrals were evaluated for each gamma-ray energy and for n ranging from 0 to 4, in order to take into account the interference of

1^- and 2^+ contributions in the angular distributions of gamma rays from the $^{12}C(\alpha,\gamma)^{16}O$ reaction (computer code RWKJL was used for the numerical integration). The attenuation coefficients μ_1 and μ_2 are functions of the gamma-ray energy. The values for μ_2 are tabulated by Grodstein (1957). Coefficients for intermediate values of the tabulated energies were found by linear interpolation. (For the range of energies corresponding to ground state transitions in ^{16}O for this experiment, this interpolation is between coefficients tabulated at 8, 10, and 15 MeV.) The values of μ_1 for the paraffin shielding which contained lithium carbonate were calculated from the measured density of the shielding and of pure paraffin, and with the cross sections for Compton scattering and pair production for the elements H, Be, C and O (Grodstein 1957). An experimental check of this calculation of μ_1 was made by measuring the yield of 9.17-MeV gamma rays from the reaction $^{13}C(p,\gamma)^{14}N$ at $E_p(lab) = 1.75$ MeV, with and without the paraffin shielding between the crystal and target. The calculated and measured transmissions agreed within 1%. There was a small amount of attenuation of gamma rays in the stainless steel wall of the target chamber and in the stainless steel housing of the NaI(Tℓ) crystal. These attenuations were calculated using the linear attenuation coefficients for iron (Grodstein 1957).

For an angular distribution of the form

$$W(\Theta) = \sum_n a_n P_n(\cos \Theta) ,$$

where Θ is the polar angle, the efficiency for detection of events over the entire solid angle of the detector is given by the product of

the spectrum fraction and the quantity

$$\frac{J_o}{2} \sum_n \frac{a_n}{a_o} \frac{J_n}{J_o} P_n(\cos \Theta_d) ,$$

where Θ_d is the polar angle of the detector axis with respect to the beam direction.

When the $^{12}C(\alpha,\gamma)^{16}O$ yields were extracted from multichannel analyzer spectra, the counts were added over a region extending from $0.8E_\gamma$ to $1.1E_\gamma$. The actual pulse height spectrum for a 9-MeV gamma ray extends to zero pulse height, because of Compton scattering, but the shape at lower energies is obscured because of the large number of low-energy background counts. It is therefore necessary to find the fraction of the counts recorded in the interval $0.8E_\gamma$ to $1.1E_\gamma$. For this purpose standard spectra were measured for gamma rays of three different energies: (1) 6.13 MeV, from the $^{19}F(p,\alpha\gamma)^{16}O$ reaction at $E_p(\text{lab}) = 340$ keV, (2) 9.17 MeV, from the $^{13}C(p,\gamma)^{14}N$ reaction at $E_p(\text{lab}) = 1.75$ MeV, and (3) 11.67 MeV, from the $^{11}B(p,\gamma)^{12}C$ reaction at $E_p(\text{lab}) = 163$ keV. The 9.17-MeV gamma-ray spectrum is shown in Figure 5.

In order to compute the spectrum fraction from these data, it is necessary to know the number of counts in the channel corresponding to zero pulse height. This quantity was calculated by the method of Zerby and Moran (1961), who note that only photons which scatter straight ahead once and then escape, contribute to counts in the zero pulse height channel. The cross section for such an interaction can be calculated from the differential Klein-Nishina formula. After summation over the volume of the crystal, a formula is obtained for f_o,

the fraction of the spectrum in the channel corresponding to near-zero pulse height:

$$f_o = J_o^{-1} \Delta E \int_{\text{crystal}} (2\pi r_o^2 \, m_o c^2 E_\gamma^{-2}) \, D\ell_2(\Theta') e^{-\mu_2 \ell_2(\Theta')} \sin\Theta' d\Theta',$$

where

ΔE = energy width of the zero pulse height channel,

E_γ = gamma-ray energy,

r_o = classical electron radius,

$m_o c^2$ = electron rest mass,

D = electron density in NaI(Tℓ),

and the remaining quantities are defined as in the preceding formula for J_n.

The computer code NTOT was then used to calculate the spectrum fraction. The input was the spectrum, the gamma-ray energy, the value of f_o, the energy calibration for the spectrum, and two points on the spectrum in the region just below $0.8E_\gamma$. If there was cascade radiation in the spectrum, these two points were obtained by drawing a smooth curve underneath the cascade radiation. The code fitted a parabola through these two points and through the measured point at $0.8E_\gamma$. Below this region, a straight line extrapolation was made. An iterative procedure was used to vary the number of counts in the zero pulse height channel until the fraction f_o of the total spectrum was found in that channel. The spectrum fraction is the ratio of the number of measured counts in the region from $0.8E_\gamma$ to $1.1E_\gamma$ to the total number of counts, obtained by adding counts in the linear, parabolic, and measured regions. The results obtained for the three

spectra were as follows:

E_γ	Spectrum Fraction
6.13 MeV	66%
9.17 MeV	65%
11.67 MeV	63%

Spectrum fractions for each gamma-ray energy for the $^{12}C(\alpha,\gamma)^{16}O$ reaction were calculated by linear interpolation between these three values.

An experimental check of the calculated detection efficiencies was made by measuring the absolute efficiency for E_γ = 6.13 MeV, and the ratio of the efficiency at 11.67 MeV to that at 4.44 MeV.

The measurement at E_γ = 6.13 MeV was made by comparing the yield of 6.13-MeV gamma rays from the $^{19}F(p,\alpha\gamma)^{16}O$ reaction at E_p(lab) = 340 keV with the yield of the corresponding alpha particles. The gamma-ray and alpha-particle yields were measured simultaneously. For this reaction at E_p(lab) = 340 keV, the angular distributions of gamma rays and alpha particles are isotropic. The efficiency of the solid state counter used to detect alpha particles was therefore determined simply by the solid angle subtended by the collimator in front of the counter. The efficiency of the gamma-ray detection system is thus

$$\varepsilon_\gamma = \varepsilon_\alpha N_\gamma / N_\alpha$$

where N_γ and N_α are counts and ε_γ and ε_α are efficiencies. The result of this efficiency measurement (accurate to about 3%) was within 6% of the calculated value.

The ratio of 11.67 to 4.44 MeV efficiency was measured with the $^{11}B(p,\gamma)^{12}C$ reaction at E_p(lab) = 163 keV. At this energy, the compound nucleus state in ^{12}C at 16.11 MeV is excited. This state decays primarily by cascading through the 4.44-MeV state, yielding simultaneously a 4.44- and a 11.67-MeV gamma ray. The efficiency ratio is thus

$$\varepsilon_{4.44}/\varepsilon_{11.67} = N_{4.44}/N_{11.67}$$

The measured ratio (accurate to about 3%) was within 4% of the calculated value.

4. Time-of-Flight Technique

The principal means of suppressing the background of prompt neutrons from the $^{13}C(\alpha,n)^{16}O$ reaction consisted of the recording, for each detected event, of the time between the incidence of the beam on the target and the detection of the event by a NaI(Tℓ) crystal. A gamma ray will take 0.3 nsec to travel 10 cm, while a 4-MeV neutron will take 3.7 nsec to go the same distance. Thus, e.g., for a detector positioned 10 cm from the target, the difference in flight time from target to detector would be 3.4 nsec. In order to separate gamma rays and neutrons with this configuration, the system must be capable of resolving times of less than 3 nsec.

Two different accelerators were used for measurements of the $^{12}C(\alpha,\gamma)^{16}O$ yield at 90°. Data in the c.m. alpha energy range of 1.72 to 2.94 MeV were taken with use of the ONR-CIT tandem accelerator. Chopping and bunching techniques were used to produce beam bursts approximately 1.5 nsec wide and separated by 285 nsec (Dietrich 1964, McDonald 1970). The maximum beam intensity attainable was 300 nA. Preliminary

data (the results of which are not reported in this thesis) for c.m. alpha energies from 1.64 MeV to 1.87 MeV, have been obtained with the 3 MV electrostatic generator, with a beam intensity of 2 μA. (Up to 6 μA of beam was available.) The beam from this machine was again bunched and chopped (the bunching was done inside the terminal rather than outside the tank as it was in the case of the tandem accelerator system); beam bursts were about 1.5 nsec wide and 93 nsec apart.

The NaI(Tℓ) crystals were placed 10.76 to 13.30 cm from the target.

In order to monitor the flight time of an outgoing neutron or gamma ray, it was necessary to have an electronic pulse representing the time that the beam pulse arrived at the target and another representing the time of detection of an event in one of the detectors.

The time pulses from the detectors were obtained from the anodes of the photomultiplier tubes. These large negative pulses with rise-times of a few nanoseconds (about 2 volts in magnitude for a gamma-ray energy of 4 MeV, with 2900 volts applied to the resistor chain of the photomultiplier tube) were fed through fast discriminators, and then into the start input of a time-to-amplitude converter.

The time-reference pulses from the target were obtained by amplifying the signals of the beam bursts with a series of three fast, low-noise amplifiers, each having a gain of 8 and a rise-time of 1.2 nsec. These amplifiers were designed and built by Dr. H. B. Mak, on the basis of a circuit of Sherman et al. (1968). The output pulse of the third amplifier was passed through a fast discriminator; it was then fed into the stop input of the time-to-amplitude converter.

Use of a pulse coming directly from the target has distinct advantages compared to earlier experiments where the time-reference pulse was taken from the beam chopper. With the earlier system, it was not possible to change any of the high-energy focusing and steering, as this could change the beam flight-time from the chopper to the target. Furthermore, any drifts in these high-energy components would degrade the time resolution of the system. When the time-reference signal is derived directly from the target it is possible not only to refocus the beam during data accumulation periods (a quite necessary procedure for the long accumulation times required for $^{12}C(\alpha,\gamma)^{16}O$ measurements), but also to change the energy of the beam, without changing the timing of the electronics.

In order to take full advantage of this method of obtaining the time-reference pulses (i.e., from the target), it is necessary to have a reasonably large and steady beam. For time-averaged $^{4}He^{+}$ beams of less than 100 nA, the output of the three fast amplifiers is not large enough to generate a reliable stop pulse. If the beam is unsteady, the time resolution will be degraded because pulses from a momentarily high beam will trigger the fast discriminator earlier than pulses from a momentarily low beam (a time-slewing effect). In order to check the operation of the target time-reference pulse, the output of the corresponding fast discriminator was scaled, and the number of counts was compared with the number of cycles of the chopping and bunching system oscillator, which determined the number of beam bursts in the same period. Whenever the time-averaged beam dropped below 100 nA, all electronic circuits, including the current integration scaler, were

automatically gated off. The two scalers counting stop pulses and oscillator cycles generally agreed within 0.2%.

It is important to note that, since the crystals detect any gamma ray(s) arising from the beam burst on the target in a time-window of only a few nanoseconds, much of the time-independent background is also suppressed by the time-of-flight technique.

The overall time resolution which can be maintained over a period of many hours with this system is about 2.5 nsec, which is somewhat remarkable since NaI(Tℓ) is usually considered to be a "slow" scintillator (1/e light-emission-time = 250 nsec).

5. Electronic Configuration

The complete electronic configuration is shown in Figure 6. The linear signals, which indicate the energy deposited in the crystals, are taken from the ninth dynodes of the photomultiplier tubes. The pulses from each detector are fed through a summing preamplifier and then into a linear amplifier.

The summed outputs of the two fast discriminators receiving time pulses from the photomultiplier anodes and the output of the fast discriminator receiving time-reference pulses from the target, are fed into the start and stop inputs of the time-to-amplitude converter. The output of the time-to-amplitude converter is a linear signal, the magnitude of which indicates the difference in time between the arrival of the beam burst on target and the detection of an event by the crystals.

Pile-up rejection is introduced to reduce background resulting from detection of two or more events of low energy which occur very

closely in time. If two such events are separated by a time of a microsecond or less, the linear signals will sum to one larger signal. The resolving times for the fast discriminators, however, are much less, about 10 nanoseconds. Since the spectrum of events below 3 MeV is not of interest in this experiment, the lower levels on two fast discriminators are set to reject such events. Discriminator output pulses corresponding to energies greater than 3 MeV are stretched to form logic pulses which gate the linear pulses. Thus, for example, two 2-MeV pulses arriving 100 nsec apart would form a 4-MeV pulse in the linear network. However, this pulse would not pass through the linear gate, as there would be no logic pulse from the fast discriminator. The same logic pulses are used to reject coincidences between the two detectors, as a means of reducing cosmic-ray background.

The amplified outputs of dynodes 10 are used only during set-up time and between data-accumulation periods; these signals, kept separate for the two detectors, are converted into logic pulses which allow selection of pulses from one detector or the other for purposes of calibration of the energy scale.

The output of the linear gate and the output of the time-to-amplitude converter (properly delayed) are fed into a multichannel analyzer. A two-dimensional analyzer is used to store events in a 64×64-channel array. One axis corresponds to the energy of the event; the other, to the time of detection of an event, relative to the time that the beam burst arrives at the target. Figure 7 shows an isometric plot of such a spectrum.

6. Procedure for Collecting Data

At the beginning of each set of measurements, the gains of the two detectors were matched, using an $^{241}Am/Be$ source (a compacted mixture of americium oxide with beryllium metal), which produces 4.44-MeV gamma rays from the reaction $^{9}Be(\alpha,n\gamma)^{12}C$ occurring inside the source. In addition, it was necessary to adjust the lengths of the cables leading from the anodes of the two detectors, in order that the electronic pulse travel-time from the cathode of the photomultiplier tube to the input of the time-to-amplitude converter would be the same for both detectors. The $^{13}C(\alpha,n\gamma)^{16}O$ reaction, which produces 6.13-MeV gamma rays at lab alpha energies above 5.1 MeV, provided a convenient means of doing this when using the tandem accelerator. When using the 3 MV generator, the $^{13}C(p,\gamma)^{14}N$ reaction at $E_p(lab) = 1.75$ MeV (yielding 9.17-MeV gamma rays) was used. This reaction was also used to calibrate the time scale, by moving the gamma-ray peak in the spectrum with a calibrated delay cable. The time resolution of the system was checked at this time.

Before (and usually after) measuring the $^{12}C(\alpha,\gamma)^{16}O$ cross section at one or more energies, a data point was measured at $E_\alpha(c.m.) = 2.42$ MeV when using the tandem accelerator, for purposes of normalization. This procedure eliminated possible normalization errors between the measurements at different energies, which were made at different times and with slightly different experimental configurations. Thus, relative errors due to target thickness, beam current integration and positioning of the detectors were eliminated.

The scheme for normalization of data measured with the use of the 3 MV generator is to measure the yield at E_α(c.m.) = 2.18 MeV for each set of measurements. At the time that the measurements of four data points (at c.m. alpha energies of 1.87, 1.80, 1.72 and 1.64 MeV) were made, it was not possible to reach E_α(c.m.) = 2.18 MeV. The yield has been temporarily normalized to the yield of the $^{12}C(p,\gamma)^{13}N$ reaction at E_p(lab) = 1.70 MeV. At a later time this $^{12}C(p,\gamma)^{13}N$ yield can be normalized to the $^{12}C(\alpha,\gamma)^{16}O$ yield at E_α(c.m.) = 2.18 MeV. The results for these four measurements are not included in the analysis of this thesis.

The check measurement at E_α(c.m.) = 2.42 MeV also aided in identifying the region-of-interest of the two-dimensional spectrum (time vs. pulse height), a region otherwise not easily recognizable when making measurements at low alpha energies, because of the very small yield from $^{12}C(\alpha,\gamma)^{16}O$.

Since, in the two-dimensional spectrum, events due to prompt neutrons from the reaction $^{13}C(\alpha,n)^{16}O$ were not totally separated from events due to gamma rays from the reaction $^{12}C(\alpha,\gamma)^{16}O$, it was desirable to determine the time- and energy-dependence of the prompt-neutron background. A natural carbon target of approximately the same thickness as the enriched target used, and made by the same process, was placed in the target chamber. Measurements were made at the same incident energies as the $^{12}C(\alpha,\gamma)^{16}O$ measurements. In most cases, these backgrounds were measured immediately before or after the corresponding $^{12}C(\alpha,\gamma)^{16}O$ measurement.

Accumulated charge was measured with a BNI model 1000 current integrator. A +300V bias was placed in series with the current lead, to avoid loss of secondary electrons from the target.

Checks made on the operation of the electronics included the following: (1) monitoring the gain of each detector periodically by noting the location of the 4.44-MeV gamma rays from an ^{241}Am/Be source, (2) monitoring scalers which recorded the number of logic pulses arising from four different modules of the pile-up and coincidence-rejection electronics, and (3) monitoring scalers which compared the number of stop pulses derived from the target with the number of cycles from the oscillator of the chopping and bunching system.

7. Extraction of Yields

Analysis of the data consists of the following: (1) identification of a rectangular region of the two-dimensional spectrum corresponding to the time of arrival of gamma rays from the target and to the energy of the desired gamma rays ($E_\gamma = 7.16 + E_\alpha$(c.m.) in MeV), (2) addition of counts in that region and subtraction of those due to background, and (3) conversion of the yield to absolute cross section (see Section III.B).

By means of radioactive sources, it was possible to calibrate the energy scale up to 4.44 MeV. Extrapolation of this calibration yielded a first estimate of the energy region of interest. By adding the counts in each time channel over this energy region, a time spectrum was produced, from which the time region corresponding to gamma rays could be identified. It was then possible to iterate: by adding

counts in each energy channel over the identified time region, an energy spectrum of gamma rays was produced (Figure 8) from which a more accurate energy region of interest could be selected. (In the case of the lower α-energy data points, the 9-MeV gamma-ray peak could not be readily identified, and it was necessary to rely on the energy calibration from the normalizing run and from any other higher-energy runs taken at the same time.) Another summation over the proper energy range yielded the final time spectrum, from which the yield was extracted (Figure 9). The same summation was applied to the corresponding spectrum obtained with a natural carbon target. The time-independent background could be subtracted immediately from both time spectra. The neutron background spectrum was then normalized to the ^{12}C spectrum by matching the heights of the prompt neutron peaks. The resulting prompt neutron background was subtracted from the ^{12}C spectrum. The remainder represented gamma rays from the $^{12}C(\alpha,\gamma)^{16}O$ reaction. It was necessary to iterate this subtraction procedure once, as there were, of course, some gamma rays from the $^{12}C(\alpha,\gamma)^{16}O$ reaction in the background spectrum from ^{12}C in the natural carbon target. The errors assigned to the yields were statistical, calculated from standard formulae for combining errors of quantities added and subtracted. An additional statistical error was introduced when normalizing the yield to that at E_α(c.m.) = 2.42 MeV.

C. Measurements of Angular Distributions

Angular distributions were measured on the north 10^o beam line of the tandem accelerator. Gamma rays were detected with two 12.7-cm by 10.2-cm NaI(Tℓ) crystals, placed 10.5 cm from the target, which were

monitored with RCA type 4522 photomultiplier tubes. These crystals were surrounded with about 6 cm of lead. No paraffin shielding was used between the target and detectors.

The target used was the same as that used for many of the 90^{o} excitation function measurements. The target chamber was the same with the exception that the piece of beam tube surrounding the target (a cross in the case of the 90^{o} measurements) was replaced by a tee, in order to provide a more symmetrical attenuation of the outgoing gamma rays. Also, the beam entrance to the tee was narrowed to allow the detectors and shielding to reach backward angles up to 143^{o}.

With this tee, there was no longer a port at the downstream end by means of which to optically align the target with the beam. For this purpose of alignment there was constructed a copper-gasket-sealed flange, on which was mounted a piece of quartz to be placed in the path of the beam. This quartz could be viewed from the top by two prisms (forming a periscope). It was thus possible to line up the center of the chamber by viewing the beam on the quartz. This flange was then removed and replaced by the target-holder. The matching of positions of the target and quartz was done externally with the use of a telescope.

The electronic configuration used for angular distribution measurements was basically the same as that used for the 90^{o} excitation function measurements. The pulses from the two detectors (which were generally at different angles with respect to the beam direction) were separated before being stored in the memory of the two-dimensional multichannel analyzer by means of a routing pulse originating at the

tenth dynode of one of the photomultiplier tubes. The 4096 channels were used to store two separate 32(time) × 64(energy)-channel two-dimensional spectra. To insure that this system produced no artificial asymmetry between the two detectors, the $^{13}C(\alpha,n\gamma)^{16}O$ reaction at E_α(lab) = 6.5 MeV was measured at 90^o with each detector. In addition, the $^{12}C(\alpha,\gamma)^{16}O$ reaction at 90^o was measured with each detector.

The isotropic angular distribution of 8.06-MeV gamma rays from the reaction $^{13}C(p,\gamma)^{14}N$ at E_p = 551 keV was measured with a natural carbon target to check the symmetry of the geometry and detector efficiencies. The yield was independent of angle, within the statistical accuracy of the data (about 3%); no correction to the $^{12}C(\alpha,\gamma)^{16}O$ data was warranted.

As before, neutron background runs were taken with a natural carbon target. With the exception of the measurement at E_α(c.m.) = 2.83 MeV (in which case the yield of neutrons from the reaction $^{13}C(\alpha,n)^{16}O$ is small), these background measurements were made at all angles.

Calibration of the energy scale was checked with the 4.44-MeV gamma rays from an $^{241}Am/Be$ source both before and after moving the detectors, since the presence of a magnet on the ion pump created a non-uniform magnetic field, which caused a slight photomultiplier tube gain shift at backward angles (in spite of magnetic shielding around the magnet and around the photomultiplier tube).

The procedure for extraction of yields from the two-dimensional spectra was identical to that used for the 90^o excitation-function measurements.

D. Measurements of Cascade Radiation

Two different schemes were used in an attempt to measure the production of ^{16}O through de-excitation of the 9.60-MeV state of ^{16}O by gamma decay through a lower excited state. In both schemes, only cascades through the 6.92-MeV (2^+) or the 7.12-MeV (1^-) states were considered. In the first method the yield of 7-MeV gamma rays was extracted from the same $^{12}C(\alpha,\gamma)^{16}O$ spectra from which the 9-MeV yields were extracted. The second method was a rearrangement of the experimental configuration to look for coincidences in the detectors caused by cascading gamma rays.

In all but the lower-energy $^{12}C(\alpha,\gamma)^{16}O$ spectra, a peak in the gamma-ray energy spectrum at 7 MeV could be observed (Figure 8), and the yields of the 7-MeV gamma rays were extracted in the same way as those of the 9-MeV gamma rays. The same energy calibration was used to determine the energy region-of-interest, and time spectra were computed by summing over this region. The corresponding spectra obtained with a natural carbon target were used to determine the shape of the prompt neutron background, as before. It was also necessary to subtract the yield of the lower-energy tail arising from the higher-energy ground-state transition. This was done by using the yields of the higher-energy gamma rays, the experimental 9.17-MeV line shape from the $^{13}C(p,\gamma)^{14}N$ reaction (see Section II.B.3), and a modification of the spectrum fraction code NTOT, in order to determine the fraction of total counts to be expected in the 7-MeV region. Only spectra obtained with the use of the tandem accelerator were analyzed for the 7-MeV gamma-ray yield.

In order to look for coincidences in the detectors caused by two members of a cascade, a 1.6-cm-diameter glass target chamber and an enriched ^{12}C target were placed on the north 10^{o} beam line of the tandem accelerator. The target was bombarded with about 1 μA of D.C. beam. The two 20.3-cm-diameter by 12.7-cm-long NaI(Tl) crystals were each placed 2.7 cm from the target. About 5 cm of lead shielding was placed around the crystals, and two cone-shaped lead shields were placed between the detectors to reduce background of genuine coincidences from backscattering of photons from one crystal to the other.

Two-dimensional spectra were accumulated with a multichannel analyzer. One axis represented the time between two detected events, one detected in each crystal. The second axis represented the energy of any pulse which occurred in coincidence with a pulse with an energy corresponding to the lower-energy gamma ray of the cascade (2.2 to 3.0 MeV, depending on the incident alpha energy).

Yields were measured at c.m. alpha energies of 1.95, 2.18, 2.42, 2.56, and 2.80 MeV. Background measurements were made at the same energies with a natural carbon target. There was also a background measurement made with the beam off. To check the proper operation of the coincidence configuration, a measurement was made at E_{α}(c.m.) = 3.18 MeV , on the resonance due to the 4^{+} state at 10.34 MeV in ^{16}O, which cascades through the 6.92-MeV state.

To extract yields from the two-dimensional spectra, the counts in each energy channel were added over the time region corresponding to real coincidences. A background from random coincidences was subtracted.

Such energy spectra were obtained for the enriched-^{12}C, natural-C, and room-background measurements. The energy spectrum of the room-background measurement was subtracted from those of the enriched ^{12}C and natural-C targets according to accumulated time. The remaining energy spectra from the natural C target were normalized according to accumulated charge, reduced by a factor of 10 (the approximate ratio of ^{13}C in the natural C and enriched ^{12}C targets), and were then subtracted from the enriched-^{12}C spectra. Unfortunately, because of the very poor counting statistics, no 7-MeV peaks could be observed in the resulting energy spectra. In order to extract an upper limit for the yield, counts were summed over a region corresponding to the expected 7-MeV peak. A background yield was extracted by summing over a region of equivalent size, half of the region being above and half below the 7-MeV region. The upper limit was taken as the greater of the following two quantities: (1) the 7-MeV yield, and (2) the 7-MeV yield less this background.

III. RESULTS

A. Cascade Radiation

The upper limits for the yield of coincidences, converted to absolute cross sections, are given in Table 1. The efficiency for detection of these coincidences was taken to be the product of the efficiencies for detecting each member of the cascade. The factor $J_o/2$ was calculated as described in Section II.B.3 (the angular distributions and the angular correlation were assumed to be isotropic for simplicity. This assumption is justified by the large solid angles subtended by the counters). The spectrum fraction for the 7-MeV gamma rays was taken from the measured spectrum of a 6.13-MeV gamma ray (Section II.B.3), and the spectrum fraction for the lower-energy member of the cascade (for a $0.9E_\gamma$ to $1.1E_\gamma$ region) was found by extrapolation of the 4.44-MeV spectrum fraction. The reduction in efficiency which occurs because cascades are not counted if both gamma rays go into the same detector was taken into account.

The yields of 7-MeV gamma rays from the non-coincident measurements, converted to absolute cross sections (assuming an isotropic angular distribution), are also shown in Table 1.

For the higher alpha energies, the cross section for production of 7-MeV gamma rays appears to be larger than the upper limit on the cross section for production of 7-MeV and $\sim$2-MeV gamma rays in coincidence. There are several factors which have not been taken into account in this analysis: the angular correlation, the angular distributions, the effect of possible cascades through the 6-MeV states in

^{16}O. However, none of these factors can explain the large difference between the two sets of results at the higher alpha energies. The data seem to indicate that some of the 7-MeV gamma rays recorded in the "singles" spectra are not in coincidence with a ∿2-MeV gamma ray, which suggests that some of the 7-MeV gamma rays come from impurities in the target.

No attempt will be made to resolve this dilemma in the present work; more measurements of the cascade radiation are clearly needed. However, it is possible to obtain an upper limit to the yield of coincidences for the detector geometry used for the 90^{o} measurements. If both members of the cascade are absorbed by the same detector, they may sum to form a pulse indistinguishable from that of a 9-MeV gamma ray. The analysis of the $^{12}C(\alpha,\gamma)^{16}O$ cross section for radiative capture to the ground state of ^{16}O is then affected. The detection of one member of the cascade in one detector and the other member of the cascade in the other detector may also produce a 9-MeV gamma ray pulse when the two pulses are added. (The 3-MeV discriminator level on the coincidence rejection circuit does not give rejection for coincidences which have a 2-MeV gamma ray as one member. It is only for the very highest alpha energies of the present work that cascade coincidences will be rejected by this circuitry, since the lower-energy gamma ray of the cascade is then about 3 MeV.)

By taking into account the various efficiencies, it can be found that the efficiency for detection of coincidences for the 90^{o} excitation-function geometry is about 6% of that for the geometry used

for measuring coincidences. Thus the corrections to the $^{12}C(\alpha,\gamma)^{16}O$ cross sections for capture to the ground state are, at most, 6% of the cross sections given in Table 1. According to the coincidence measurements, the corrections would be less than 0.5 nb. If the 7-MeV yields from the singles spectra represent true cascade radiation yields, the corrections could be as large as 1.6 nb. Because of the small size of these corrections and because of the uncertainty in the interpretation of the cascade data, no attempt has been made to correct the 90^{o} data at the present time.

B. Conversion of Yield to Absolute Cross Section

In Table 2 are listed the yields extracted from the spectra obtained at 90^{o} and the absolute total cross sections obtained from these yields by assuming that the angular distributions are those of pure electric dipole transitions. Corrections required by the electric quadrupole contributions will be discussed in Sections III.C and III.D.

The conversion from yield to absolute cross section requires a knowledge of the integrated charge, the target thickness (see Section II.B.1), and the efficiency of the detection system (see Section II.B.3). The product of these three factors cannot be specified with a precision better than 10%. However, because the yields are normalized to the yield at E_{α}(c.m.) = 2.42 MeV, relative errors in the above factors are cancelled, and it is only the overall scale factor which is uncertain by 10%. The value of Θ_{α}^{2} derived in the end is only (approximately) linearly dependent on such a scale factor (see Section III.E).

The alpha energies at which the measurements are quoted were derived in the following way. As a first approximation for the effective laboratory alpha energy, the incident laboratory energy minus half the energy loss in the target was calculated. The data were then fitted by the 3-level R-matrix code (see Appendix C). For each data point, the theoretical cross sections were averaged over an energy ranging from the incident laboratory energy to the incident energy minus the total energy loss in the target (using 10 keV steps). The laboratory alpha energy to be quoted for the data point was selected as the energy at which the theoretical cross section was equal to this average cross section. This effective energy was not in most cases different from the center-of-target energy by more than 10 keV. The derived laboratory alpha energy, when converted to c.m. energy, is the energy at which all $^{12}C(\alpha,\gamma)^{16}O$ measurements are quoted in this thesis (unless specifically noted otherwise).

C. Angular Distributions and Extraction of $|A_{2+}|$

Figure 10 shows the results of the yield analysis for the angular distribution measurements. The quoted alpha energies were determined by the method described in Section III.B. Differences between laboratory and c.m. angle were not considered; these differences are at most half of a degree in the present experiments.

The angular distribution data are interpreted as arising from the interference of the 2^+ direct capture process with the 1^- resonant capture process. From the measured angular distributions it is desired

to find the absolute magnitude of the ratio of the 2^+ reaction amplitude (A_{2+}) to the 1^- reaction amplitude (A_{1-}). The angular distribution which arises from the interference of these two contributions will have the shape, for spinless interacting nuclei,

$$W(\theta) = (3|A_{1-}|^2 + 5|A_{2+}|^2)P_o(\cos\theta) + (-3|A_{1-}|^2 + \frac{25}{7}|A_{2+}|^2)P_2(\cos\theta)$$

$$- (\frac{60}{7})|A_{2+}|^2 P_4(\cos\theta) + 6\sqrt{3}\ |A_{1-}||A_{2+}|\ \cos\phi_{12}\left[P_1(\cos\theta) - P_3(\cos\theta)\right],$$

where ϕ_{12} is the phase difference between the two complex amplitudes and the functions $P_n(\cos\theta)$ are Legendre polynomials.

Each measured angular distribution was fitted with the above expression (corrected for the finite solid angle of the NaI(Tl) detector), with $|A_{2+}|/|A_{1-}|$, ϕ_{12}, and a normalizing factor as free parameters. The result was a value for $|A_{2+}|/|A_{1-}|$ for each energy at which an angular distribution was measured. These values are displayed in Table 3. (Lack of sufficient statistical precision in the data prevented the determination of ϕ_{12}.) Because the ratio of amplitudes was not always determined with high precision, and because angular distribution measurements were not possible at low energies, where the cross section is small, it is necessary to obtain a theoretical energy dependence for the 2^+ intensity, in order to determine its contribution at those energies where angular distributions were not measured, and at stellar energies.

The measured energy dependence of $|A_{2+}/A_{1-}|$ is consistent with that to be expected from direct E2 radiative capture, and this model has

been adopted for the 2^+ amplitude.

The theoretical cross section for direct radiative capture has been studied by Tombrello (1961). The differential cross section is given by Fermi's golden rule, where the matrix element for E2 capture is given by

$$M_{E2} = \frac{2}{3}\sqrt{\pi}\left(\frac{\mu_o \hbar C^4}{2\omega}\right)^{1/2} k_\gamma^2 [Z_\alpha (\frac{\mu}{m_\alpha})^2 + Z_C (\frac{\mu}{m_C})^2]$$

$$\times \sum_\kappa D^2_{\kappa p}(\theta_\gamma, \phi_\gamma) \; \langle \phi_f | \; r^2 Y^\kappa_2(\theta,\phi) \; | \phi_i \rangle \; ,$$

where ω, k_γ, and p are the angular frequency, wave number, and state of circular polarization of the gamma ray; $D^2_{\kappa p}$ is a rotation matrix element, and θ_γ and ϕ_γ are the polar and azimuthal angles of the gamma radiation. The charges and masses of the alpha particle and ^{12}C nucleus are Z_α, Z_C and m_α, m_C ; μ is the reduced mass. The functions ϕ_i and ϕ_f are the initial and final wave functions of the system. Since the matrix element for direct capture is dominated by contributions from distances larger than the nuclear radius, the integral was evaluated by ignoring all contributions from the volume inside the nucleus. This approximation is valid as long as there are no nearby 2^+ compound nucleus levels. (Measurements of the $^{12}C(\alpha,\gamma)^{16}O$ cross section near the resonance due to the 2^+, 9.85-MeV state in ^{16}O are excluded here.) The initial and final wave functions outside the nuclear volume can then be approximated as free and bound-state wave functions of the Coulomb potential; no detailed knowledge of the internal wave functions is required. There remains one unknown parameter in the

cross section: the amplitude of the final state wave function, i.e., that of the ground state of ^{16}O, at the nuclear surface. This magnitude is related to the reduced-alpha-width of the ground state of ^{16}O. More detailed discussions of the derivation of the cross section and the numerical evaluation of the matrix element are given by Tombrello (1961) and Parker (1963).

The quantity determined from Tombrello's formula is thus $|A_{2+}|^2/\theta_\alpha^2(g.s.,^{16}O)$, where $\theta_\alpha^2(g.s.,^{16}O)$ is to be found by fitting the quantities $|A_{2+}|^2/|A_{1-}|^2$ obtained from angular distribution measurements. This fitting was done by an iterative procedure, since $|A_{1-}|^2$ was not known at the beginning. Its value was taken for the first iteration to be the total cross section obtained by neglecting 2^+ contributions when deriving the total cross section from the yield at 90^o (see Section III.B). At the end of each iteration, the value of $|A_{2+}|$ from that iteration and the value of $|A_{1-}|$ from the previous iteration could be used to calculate a better angular distribution, and thus a better total cross section. Subtraction of $|A_{2+}|^2$ from this total cross section gave a new value for $|A_{1-}|^2$. After several iterations, the value $\theta_\alpha^2(g.s.,^{16}O) = 0.043 \pm 0.012$ was obtained.

The final values of $|A_{2+}|/|A_{1-}|$ obtained in this way are given in Table 3. The calculated variation of $|A_{2+}|^2$ with alpha energy is shown in Figure 11; values for discrete energies are given in Table 4. The errors quoted for $|A_{2+}|^2$ arise entirely from the uncertainty in $\theta_\alpha^2(g.s.,^{16}O)$.

D. Electric Dipole Contributions to the Total Cross Sections

The two methods of parameterizing the data and extrapolating to lower energies which will be described (Appendices C and D) consider only the E1 contributions to the total cross section. The final numbers desired from the measurements are thus the quantities $|A_{1-}|^2$.

Once the yield at 90^o (expressed in terms of an absolute quantity) and the magnitude of the E2 contribution to the total cross section are determined, it is possible to calculate $|A_{1-}|^2$. The quantities $|A_{1-}|^2$ are shown in Figure 12 and in Table 4. The errors quoted come from the statistical errors in the yield (including that from normalization) and from the uncertainty in the quantity $\Theta_\alpha{}^2(\text{g.s.}, {}^{16}\text{O})$ used in determining the value of $|A_{2+}|^2$. Also given in Table 4 are the quantities $|A_{2+}|^2/|A_{1-}|^2$ and the total cross sections ($\sigma = |A_{1-}|^2 + |A_{2+}|^2$). The quantities $|A_{1-}|^2$ and σ are approximately the same, except at the highest energies considered, since the E2 contribution becomes much smaller than the E1 contribution at low energies (Figure 13).

E. Extrapolation to Lower Energies of the Electric Dipole Contributions

The remaining problem is to determine the extent to which the E1 excitation function departs from that of a single resonance plus an interfering background from the tails of resonances corresponding to higher states.

One theoretical framework for carrying out the extrapolation is to make a 3-level R-matrix parameterization of the cross section (Weisser 1970). The three levels correspond to the 7.12-MeV state,

the 9.60-MeV state, and a fictitious state at 20 MeV, which represents the background from the tails of higher states. A description of this parameterization can be found in Appendix C. Figure 12 shows three fits to the $^{12}C(\alpha,\gamma)^{16}O$ data: (1) the best fit, in which three parameters are free to vary (Θ_α^2 and the gamma widths of the 9.60-MeV and background states), (2) a fit in which Θ_α^2 is constrained to zero and the remaining two parameters are free to vary, and (3) a fit in which Θ_α^2 is constrained to 0.4 and the remaining two parameters are free to vary. Figure 14 shows the same data and the same fits to the data, expressed in terms of the S-factor instead of the total cross section. ($S = \sigma E e^{2\pi\eta}$. See Appendix A.) The S-factor gives the intrinsically "nuclear" dependence of the cross section, as distinct from the kinematic and barrier penetration factors. The χ^2 per degree of freedom for the best fit is 1.4. The S-factor at E_α(c.m.) = 300 keV is found to be $0.20\ ^{+0.14}_{-0.12}$. The result for $\Theta^2_{\alpha,F}$ is $0.14\ ^{+0.10}_{-0.08}$, with statistical errors only. The interference between the levels at 7.12 and 9.60 MeV is constructive.

The value derived for Θ_α^2 is not very sensitive to the absolute value of the cross section. If all of the experimental data points are increased by 20% and fitted again by the 3-level R-matrix theory, $\Theta^2_{\alpha,F}$ is increased by 24%.

Another method of parameterizing the data for extrapolating to lower energies has been developed by Koonin and Tombrello (1972). Contributions from the bound state at 7.12 MeV in ^{16}O are described by a single-level pole; a potential is used to describe the contributions from the 9.60-MeV state, high-lying states and direct capture. A

description of this "hybrid" R-matrix-optical-model parameterization is given in Appendix D. In this case the fit to the $^{12}C(\alpha,\gamma)^{16}O$ data requires the variation of only two parameters. Figure 15 shows two fits to the data: the best fit and a fit in which contributions from the bound state are omitted. Figure 16 shows the best fit expressed in terms of the S-factor. For the best fit, the χ^2 per degree of freedom is 1.3. The S-factor at E_α(c.m.) = 300 keV was found to be $0.16^{+0.15}_{-0.10}$, which gives a value for $\Theta^2_{\alpha,F}$ of $0.11^{+.11}_{-.07}$, and the interference was again found to be constructive between the levels.

For comparison only, the data of Jaszczak et al. (1970,1970a) are shown in Figure 17, along with the 3-level R-matrix fit of the Caltech data. The two sets of measurements do not agree, for reasons which are not apparent. The 3-level R-matrix parameterization does not fit the Jaszczak data well; the Jaszczak data give a χ^2 per degree of freedom of 8 and a range for $\Theta^2_{\alpha,F}$ extending from 0 to above 1.

The value for $\Theta^2_{\alpha,F}$ obtained from the present Caltech $^{12}C(\alpha,\gamma)^{16}O$ data is in qualitative agreement with those values obtained by previous, less direct methods (see Sections I.B and I.C.) However, not enough data have been acquired yet at the lower alpha energies to determine the value of $\Theta^2_{\alpha,F}$ with high precision. It can be seen from Figure 14 that measurements with about 30% accuracy are required at E_α(c.m.) = 1.4 MeV (where the total cross section is expected to be approximately 0.3 nb) in order to obtain $\Theta^2_{\alpha,F}$ with an uncertainty of about 30%.

IV. DISCUSSION

A. Astrophysical Significance

Although this experiment has not yet succeeded in placing very narrow limits on the value of $\Theta^2_{\alpha,F}$, it is of interest to investigate the range of X_C, the mass fraction of ^{12}C, at the end of helium burning as determined by the presently achieved measurements of $\Theta^2_{\alpha,F}$.

Arnett (1972), by considering the evolution of stars composed initially of pure helium in the mass range $2 < M_\alpha/M_\odot < 100$, found X_C at the end of helium burning to decrease approximately linearly with increasing $\log M_\alpha$ and $\log \Theta^2_{\alpha,F}$:

$$X_C = 0.31 - 0.667 \log (M_\alpha/M_\odot) - 0.267 \log \Theta^2_{\alpha,F} .$$

Deinzer and Salpeter (1964) performed similar calculations, and considered lower masses as well. In Figure 18, the mass fraction of ^{12}C at the end of helium burning is shown as a function of the mass of the helium star for three different values of $\Theta^2_{\alpha,F}$: the value which best represents the $^{12}C(\alpha,\gamma)^{16}O$ experimental data and the two values which are one standard deviation above and below the best value. The values of X_C for $2 < M_\alpha/M_\odot < 100$ are taken from the above formula of Arnett. The shape of the function for $M_\alpha/M_\odot < 2$ is obtained from the values of Deinzer and Salpeter for $\Theta^2_{\alpha,F} = 0.1$. Their values are normalized to those of Arnett at $M_\alpha/M_\odot = 2$ (a 10% correction), and scaled with $\Theta^2_{\alpha,F}$ in the same way as those of Arnett--according to $\log \Theta^2_{\alpha,F}$.

The helium stars of these calculations are thought to be good representations of the helium cores of real stars, since the temperature

and pressure at the hydrogen burning shell are small compared with those inside the core. Arnett (1972) gives the following equivalent total masses $M/M_\odot$ corresponding to the core masses $M_\alpha/M_\odot$:

$M_\alpha/M_\odot$	$M/M_\odot$
2	about 7 to 10
4	about 15
8	20 to 24
16	34 to 40
32	70 to 80
64	110 to 125

These values can be used to scale the abscissa of the plot of Figure 18 in terms of the total mass of the star.

These values of X_C emphasize the need to acquire better $^{12}C(\alpha,\gamma)^{16}O$ data in order to obtain a more precise value of $\Theta^2_{\alpha,F}$. For example, at $M_\alpha/M_\odot = 2$, the range of X_C which is within one standard deviation of the best current value of $\Theta^2_{\alpha,F}$ extends from 0.2 to 0.7.

B. The $C^{12}(\alpha,\gamma)^{16}O$ Experiment of the Future

The improvement in the experimental configuration which would apparently produce the most rapid gain at the present stage of development, is the reduction of the amount of ^{13}C in the enriched ^{12}C target. This would reduce the number of prompt neutrons coming from the target, and thus allow the detectors to be placed a little closer to the target. The solid angle would be increased and the error arising from background subtraction would then be decreased. Since the primary source of time-independent background with the 3-MV accelerator seems

to be delayed neutrons due to the ^{13}C in the target, a considerable reduction of time-independent background would also result from reducing the target ^{13}C content.

With the present method of making targets, it is found that a factor of two in isotopic purity is lost when converting the ORNL amorphous carbon to the final carbon target. Thus in order to make a target with much lower ^{13}C content, it is necessary to do both of the following: (1) obtain ^{12}C of higher isotopic purity, and (2) improve the target-making procedure in order to eliminate as far as possible the introduction of natural carbon. It is not clear where and when the natural carbon is being introduced during the present target-making procedure. It has been suggested by Dr. George Rossman that use of the reducing agent, lithium aluminum hydride, to convert CO_2 to CH_3OH in the chemical processing could introduce natural carbon, since the best commercially available $LiAlH_4$ is known to be contaminated with carbonates. The possibility of introducing natural carbon during the final stage of cracking the methyl iodide could be largely eliminated by improving the methyl-iodide cracking chamber.

Highly enriched ^{12}C, containing perhaps less than 1 part per 20,000 ^{13}C, is shortly to be shipped to the Kellogg Radiation Laboratory from the Los Alamos National Laboratory. After some work devoted to improving the present target-making procedure, more data at lower alpha energies should be forthcoming.

Use of only 2 μA out of the possible 6 μA or more of bunched and chopped beam available from the 3 MV generator was necessary to minimize blistering of the carbon on the target. With improvement of the

target cooling, it might be possible to utilize more of the beam available from the 3 MV generator. If many targets were available, the bombarded target could be changed often, before damage from the beam became excessive.

The large time-independent background due to delayed neutrons encountered on the 3 MV generator beam line is partly due to the proximity of the target and detectors to the accelerator and to the wall. With a major expenditure of effort, it might be possible to obtain a longer beam line in a different direction in the present target room. (With a still larger amount of effort, it might be possible to move the wall!)

With the introduction of a new high-intensity ion source currently being built by Dr. H. B. Mak for the tandem accelerator, it may be possible to obtain large enough chopped and bunched beams from that generator. Because of the more spacious target area, there is less of a problem arising from the delayed return of neutrons originally produced at the target or along the beam line.

When the limits of beam intensity and reduction of neutron background are reached, it might be possible to gain a small amount more by introducing anti-coincidence shielding in order to reduce cosmic-ray background.

A worthwhile investigation would be an attempt to measure the $^{12}C(\alpha,\gamma)^{16}O$ yield by using a ^{12}C beam and a ^{4}He gas target. This would eliminate the neutron background from the $^{13}C(\alpha,n)^{16}O$ reaction. Detectors could then be placed very close to the target. Time-independent background could be a problem, but this could possibly be dealt with

if a high-intensity chopped and bunched beam of ^{12}C could be obtained, and if the detectors could be shielded sufficiently.

The main object of future measurements should obviously be to obtain measurements of the yield at lower alpha energies. It might also be possible to obtain the E1 contributions to the total cross section at slightly higher energies than those reported here. However, this would have to be done by making careful angular distribution measurements, since the 2^+ direct capture process increases with increasing energy, and since the low-energy tail of the resonance at E_α(c.m.) = 3.18 MeV, due to the 4^+ state at 10.34 MeV in ^{16}O, soon becomes the dominant contribution to the cross section. Measurement of the E1 contribution above this resonance, in addition to being rather difficult, may not be as useful as one might imagine because of the increasing contributions from the tails of resonances corresponding to the many higher 1^- states in ^{16}O.

For the sake of refinement of the understanding of the reaction mechanisms of the $^{12}C(\alpha,\gamma)^{16}O$ reaction, it would be desirable to have measurements of angular distributions at lower alpha energies. Further measurements of cascade radiation should be made, with a consideration of the 6-MeV states as well as the 7-MeV states.

In order to obtain absolute confidence in measured cross sections in the range of tenths of nanobarns, it is necessary to know the content of any target impurity (in the carbon or in the tantalum backing) and to know the alpha-particle capture cross sections for all stable isotopes of the impurity element. Because of Coulomb barrier effects, only light nuclei need be considered. There are many light nuclei which are

energetically capable of capturing an alpha particle and emitting gamma rays of 9 MeV energy or more. Thus far, only the effect of ^{19}F has been investigated (Appendix E).

Perhaps by the time all of these investigations are complete, large, high-efficiency, high-resolution germanium crystals will become available, and measurements of very small capture cross sections will become trivial.

APPENDIX A

Astrophysical Reaction Rate Formulae for the $^{12}C(\alpha,\gamma)^{16}O$ Reaction

In this section we derive the formula for the rate of the $^{12}C(\alpha,\gamma)^{16}O$ reaction in the interior of a star in terms of the quantity $\Theta^2_{\alpha,F}$. The derivation follows that of Fowler (1967) and Clayton (1968).

The $^{12}C(\alpha,\gamma)^{16}O$ reaction rate per unit volume can be expressed in terms of the cross section, the flux of alpha particles, and the number density of ^{12}C nuclei n_{12_C}. The flux of alpha particles for a given relative velocity v is the product of the number density of alpha particles n_α and the velocity v. Since there is a spectrum of relative velocities $\phi(v)$, where $\int \phi(v)dv = 1$, it is necessary to integrate over all possible relative velocities. The reaction rate per unit volume is

$$P = n_\alpha n_{12_C} \int_0^\infty v\sigma(v)\ \phi(v)dv = n_\alpha n_{12_C} \langle\sigma v\rangle \quad .$$

The quantities n_α and n_{12_C} can be expressed in terms of the atomic mass fractions X_α and X_C, the matter density ρ, and Avogadro's number N_A:

$$n_\alpha = \rho N_A X_\alpha / A_\alpha \quad ,$$

$$n_C = \rho N_A X_C / A_C \quad .$$

(Superscripts "12" have been dropped.) A_α and A_C are atomic masses. The reaction rate is now

$$P = \rho^2 N_A{}^2 \frac{X_\alpha X_C}{A_\alpha A_C} \langle\sigma v\rangle \quad .$$

The function $\phi(v)$, giving the distribution of relative velocities, is

assumed to be the Maxwell-Boltzmann distribution,

$$\phi(v)dv = \left(\frac{\mu}{2\pi kT}\right)^{3/2} \exp\left(-\frac{\mu v^2}{2kT}\right) 4\pi v^2 dv \quad ,$$

where μ is the reduced mass, k is Boltzmann's constant, and T is the absolute temperature of the matter.

For temperatures characteristic of helium burning, the average kinetic energies are orders of magnitude smaller than the Coulomb barrier between the particles. The particles with the best chance of penetrating the Coulomb barrier are those having the largest energy; however, because of the velocity distribution $\phi(v)$, the number of such particles decreases with increasing energy. There is some effective interaction energy for which there is a maximum probability of interaction. This will be shown mathematically below.

In order to evaluate the integral in the rate formula, it is necessary to know the cross section for the reaction. This cross section can be expressed as a product of three energy-dependent factors: (1) an exponential factor $e^{-2\pi\eta}$ which gives the probability of penetration through the Coulomb barrier, (2) a factor $1/E$ which is characteristic of any quantum-mechanical interaction between two particles, and (3) a factor $S(E)$ which depends on nuclear properties and is (hopefully) only weakly dependent on energy. We thus have

$$\sigma(E) = \frac{S(E)}{E} \exp(-2\pi\eta) \quad ,$$

where

$$\eta = Z_\alpha Z_C \, e^2/\hbar v$$

and the quantities Z are atomic numbers. Since there are no

resonances closer to the range of effective interaction energies for the $^{12}C(\alpha,\gamma)^{16}O$ reaction than the 7.12-MeV state, $S(E)$ is approximately constant within this range.

Expressed in terms of center-of-mass energy, the integral becomes

$$\langle\sigma v\rangle = \left(\frac{8}{\mu\pi}\right)^{1/2} \frac{1}{(kT)^{3/2}} \int_0^\infty S(E) \exp\left(-\frac{E}{kT} - bE^{-1/2}\right) dE \quad ,$$

where

$$b = 31.28\ Z_\alpha Z_C\ A^{1/2}\ keV^{1/2} \quad ,$$

$$A = \frac{A_\alpha A_C}{A_\alpha + A_C} \quad .$$

The integrand is small for large values of E, because of the factor $\exp(-E/kT)$, and is small for small values of E, because of the factor $\exp(-bE^{-1/2})$. For intermediate values of E, the integrand has a maximum value, as noted above.

An approximate value for the integral can be obtained by replacing $S(E)$ with S_{eff}, the value of the S-factor at the energy E_o for which the exponential factor has a maximum, and by replacing the exponential factor by a Gaussian function (the method of steepest descent). The effective interaction energy is given by

$$E_o = (bkT/2)^{2/3} = 0.9226\ T_9^{2/3}\ MeV \quad ,$$

where T_9 is the temperature expressed in units of $10^9\ ^oK$. For temperatures typical of helium burning ($T \simeq 2 \times 10^8\ ^oK$), E_o is about 300 keV. The resulting rate is

$$P = \left[\rho^2 N_A^2 \frac{X_\alpha X_C}{A_\alpha A_C} \left(\frac{8}{\mu\pi}\right)^{1/2} \frac{1}{(kT)^{3/2}}\right] S_{eff} \left[e^{-3E_o/kT} \sqrt{\pi} \frac{2}{\sqrt{3}} (E_o kT)^{1/2}\right]$$

$$= 1.56 \times 10^{32} \rho^2 X_\alpha X_C S_{eff} T_9^{-2/3} \exp(-32.12 T_9^{-1/3}) \quad .$$

Since the major contribution to S_{eff} comes from the tail of the bound, 7.12-MeV state in ^{16}O, the value of S_{eff} can be obtained approximately by extrapolating a Briet-Wigner resonance shape into the positive-energy region (Fowler 1967):

$$S_{eff} = 2.67 \times 10^6 \frac{\Gamma_\gamma}{(E_o + |E_r|)^2} \Theta_{\alpha,F}^2 \quad \text{MeV-barns} \quad ,$$

where Γ_γ is the measured radiation width in MeV of the 7.12-MeV state in ^{16}O, $|E_r|$ is the binding energy of the same state in MeV, and $\Theta_{\alpha,F}^2$ is the dimensionless reduced-alpha-width of that state. Inserting the values $\Gamma_\gamma = 62 \times 10^{-9}$ MeV (Swann 1970) and $|E_r| = 0.042$ MeV (Ajzenberg-Selove 1971) gives

$$S_{eff} = \frac{0.166}{(E_o(\text{MeV}) + 0.042)^2} \Theta_{\alpha,F}^2 \quad \text{MeV-barns}$$

$$= 0.166 \ (0.9226 T_9^{2/3} + 0.042)^{-2} \ \Theta_{\alpha,F}^2 \ \text{MeV-barns} \ .$$

Because there is some confusion in the definition of the dimensionless reduced-alpha-width of the 7.12-MeV state when the $^{12}C(\alpha,\gamma)^{16}O$ measured cross sections are parameterized by multilevel formulae, the quantity $\Theta_{\alpha,F}^2$ is obtained by calculating the S-factor with the chosen parameterization at E_α(c.m.) = 300 keV, and then determining what

value of Θ_α^2 would give that value of the S-factor with the single-level formula given above. The quantity $\Theta_{\alpha,F}^2$ is thus defined as

$$\Theta_{\alpha,F}^2 = \frac{(0.342)^2}{0.166} S(300 \text{ keV}) = 0.705\ S(300 \text{ keV}) \quad ,$$

where S is expressed in units of MeV-barns. With this definition, the stellar reaction rate can be calculated in terms of the above simple formula for S_{eff} .

The final formula for the reaction rate per unit volume becomes

$$P = 3.04 \times 10^{31}\ \rho^2 X_\alpha X_C\ T_9^{-2}(1+0.046T_9^{-2/3})^{-2}\ \exp(-32.12T_9^{-1/3})\Theta_{\alpha,F}^2 \quad ,$$

where P has units of reactions $cm^{-3}sec^{-1}$; ρ , of g cm^{-3}; T_9 , of 10^9 ^oK.

APPENDIX B

Direct and Resonant Capture Processes in the $^{12}C(\alpha,\gamma)^{16}O$ Reaction

In the text of this thesis, it has been assumed that the primary contribution to the $^{12}C(\alpha,\gamma)^{16}O$ cross section at c.m. alpha energies of the order of 300 keV comes from the tail of the bound state at 7.12-MeV in ^{16}O, and that ground state transitions are the most important. Furthermore, when interpreting the cross sections measured in the region of the resonance corresponding to the 9.60-MeV state in ^{16}O, it has been assumed that the primary contribution to the cross section in this energy range comes from the E1 resonant capture to the ground state of ^{16}O. The interpretation of the data in this range has taken into consideration the resonant capture of alpha particles through the 1^- state at 9.60 MeV, the tails of higher 1^- states and the tail of the 1^- state at 7.12 MeV, and the E2 direct capture of alpha particles, all transitions being to the ground state of ^{16}O. In the case of the analysis by Koonin and Tombrello (1972; see Appendix D), the E1 extranuclear contribution is included. In the case of the R-matrix fit, E1 direct capture is partially included, since it would affect the empirically-determined parameters of the (fictitious) distant background state. There are many more processes, both resonant and direct, which are allowed by conservation of angular momentum and parity. Those of lowest angular momenta are listed in Table 5. The cross section for radiative capture is generally calculated from first order perturbation theory. This calculation requires integration over all of configuration space of the product of the final wave function (that of a bound state), the interaction Hamiltonian, and an initial wave function (that

of a scattering state). That part of the interaction matrix element which comes from integration over the nuclear volume will be referred to as the resonant amplitude, whereas that part which comes from integration over the space outside the nuclear volume will be called the direct capture amplitude. The resonant and direct capture amplitudes for a given transition are, of course, coherent, since they are parts of the same matrix element. The division of the capture process into resonant and direct capture processes is somewhat arbitrary; however, such a division is useful, because the dependence on alpha energy is quite different for the two parts, and it is sometimes possible to ignore one or the other in certain energy ranges.

For a consideration of the relative magnitudes of the various direct and resonant capture processes, it is essential to consider both the astrophysical range of energies and the range of energies covered by the experimental measurements. It is first of all necessary to determine the dominant mechanism at astrophysical energies; then, if the value of the cross section at these energies is to be determined by extrapolation, that extrapolation must come from measurements of the same mechanism. If other processes contribute to the cross sections measured at higher energies, these must either be subtracted or taken into account in the parameterization.

For a consideration of the magnitudes of the contributions of the various resonant and direct captures, it will be useful to compare the S-factors to the S-factor of the process believed to be dominant: the E1 capture to the ground state of ^{16}O. The S-factor for the astrophysical region, according to the analysis of this work, is

S(300 keV,c.m.) ≃ 0.06 to 0.3 MeV-barns. The S-factors for the measured energy region range from S(1.8 MeV,c.m.) ≃ 0.02 and S(3.0 MeV,c.m.) ≃ 0.003 to S(2.4 MeV,c.m.) ≃ 0.07 MeV-barns.

Resonant capture cross sections contain the factor E_γ^{2L+1}, where E_γ is the energy of the emitted gamma ray, and L is the order of the multipole radiation. For a given multipole order L, the cross section for resonant capture leading to an excited state in ^{16}O is smaller than that for resonant capture to the ground state by the factor $[\frac{E_{es}}{E_{gs}}]^{2L+1}$, where E_{es} is the gamma-ray energy of the continuum to excited state transition, and E_{gs} is the gamma-ray energy of the continuum to ground state transition. (There are, of course, other energy dependent factors still to be considered.) For the astrophysically interesting alpha energy of 300 keV (c.m.), and for the energy of the resonance corresponding to the 9.60-MeV state in ^{16}O, E_α(c.m.) = 2.4 MeV, these factors are as follows:

L	excitation energy (MeV)	$(E_{es}/E_{gs})^{2L+1}$(300 keV)	$(E_{es}/E_{gs})^{2L+1}$(2.4 MeV)
1	6.05	7×10^{-3}	5×10^{-2}
1	6.13	6×10^{-3}	5×10^{-2}
1	6.92	4×10^{-4}	2×10^{-2}
1	7.12	1×10^{-4}	2×10^{-2}
2	6.05	2×10^{-4}	7×10^{-3}
2	6.13	2×10^{-4}	6×10^{-3}
2	6.92	2×10^{-6}	2×10^{-3}
2	7.12	2×10^{-7}	1×10^{-3}

The smallness of the ratios for E_α(c.m.) = 300 keV indicates that cross sections for resonant captures to excited states are likely to be much smaller than those for captures to the ground state. The

experimental configuration used for measuring the $^{12}C(\alpha,\gamma)^{16}O$ cross section is not highly sensitive to the cascade radiation yield. Since the transition yields were extracted from the region of the full-energy peak in the pulse height spectrum ($\sim$9 MeV), cascade radiation contributes to the measured yield only when both members of the cascade are absorbed by the NaI(Tl) crystals and the energy deposited is summed. The efficiency for detecting both members of the cascade is only 6% of that for detecting a single 9-MeV gamma ray (see Section III.A). The effective ratios for E_α(c.m.) = 2.4 MeV are thus the product of the above listed ratios and the efficiency ratio 0.06.

In the case of the direct capture process (Tombrello 1961), the factor E_γ^{2L+1} also appears in the formula for the cross section, but its effect is partially cancelled by the energy dependence of the radial integral. However, it is to be expected that the cross section for direct capture to an excited state is not much larger than that for direct capture to the ground state in the case of the ^{16}O nucleus, since the reduced-alpha-widths of the excited states are not expected to be as much as 10 times larger than the reduced-alpha-width of the ground state. These widths have been measured by Loebenstein et al. (1967) and by Pühlhofer et al. (1970). A value for the reduced-alpha-width of the ground state of ^{16}O has also been derived indirectly in the present work (see Section III.C).

It is thus first of all important to consider the cross sections for capture leading to the ground state of ^{16}O; if these are found to be small, then it is unlikely that the captures to excited states will be large.

The E0 transition from the s, p, or d plane-wave states is not expected to make a significant contribution to the cross section; it is believed that these transitions proceed primarily by pair emission. Neglect of pair emission is supported by the measurement of the lifetime of the 0^+, 6.05-MeV state in ^{16}O, which is found to be four orders of magnitude larger than the lifetimes of the 6.92- and 7.12-MeV gamma-ray-emitting states (Ajzenberg-Selove 1971).

Calculations have been performed for contributions to the ground-state gamma cross section from the tails of the following natural-parity states in ^{16}O:

6.13 MeV	3^-
6.92 MeV	2^+
9.85 MeV	2^+
10.34 MeV	4^+
11.52 MeV	2^+
12.44 MeV	1^-
13.09 MeV	1^-

These cross sections were calculated with the use of a single-level formula which included the energy dependence of the gamma-ray and alpha widths and the level shift. The energy and width parameters were taken from the compilation of Ajzenberg-Selove (1971). The S-factor for the tail of the 6.13-MeV state at 300 keV (c.m.) is 10^{-7} MeV-barns, for $\Theta_\alpha^2(6.13\text{-MeV}, ^{16}O) = 1$; this contribution is negligible. The contribution for the 6.92-MeV state is 0.09 MeV-barns for $E_\alpha(\text{c.m.}) = 300$ keV and $\Theta_\alpha^2(6.92\text{-MeV}, ^{16}O) = 1$. The reduced-alpha-width of the 6.92-MeV state is expected to be somewhat smaller than 1, although its value is highly uncertain. It is important to note that

if the reduced-alpha-width of the 6.92-MeV state were 10 times larger than that of the 7.12-MeV state, then the contributions of the two states would be roughly equivalent at E_α(c.m.) = 300 keV. This is not very far outside the range of errors in the determination of the two reduced widths. Significant contributions to the cross section from the 9.85-MeV state are restricted to a very narrow range of alpha energies; this range has been omitted in the analysis of the $^{12}C(\alpha,\gamma)^{16}O$ cross section. Contributions from higher states considered are not significant as long as the two higher 1^- resonances interfere destructively in the region outside the two resonances.

A separation of direct and resonant capture contributions of the p plane-wave initial state is not physically meaningful, since contributions to the interaction matrix element from the nuclear volume are significant at all energies under consideration, and the direct and resonant amplitudes are coherent. Werntz (1970) calculated the two E1 amplitudes for transition to the ground state and found the square of the magnitude of the extranuclear amplitude to be three orders of magnitude smaller than the square of the amplitude arising from the nuclear volume.

Tombrello (1971) and Werntz (1970) have both considered the E2 capture to the ground state from the $\ell = 2$ plane-wave state. This capture has been taken into account in extracting the E1 contribution to the cross section for the 2.4 MeV (c.m.) region (see Section III.C), and has been shown to be negligible in the 300 keV (c.m.) region (see Section III.D and Figure 13). Werntz considered in addition the interference of this E2 direct capture with the resonant capture through the

2^+, 9.85-MeV state in ^{16}O. Such an interference effect can extend well beyond the width of the resonance, and may be significant in the cases of the angular distributions measured at E_α(c.m.) = 2.56 and 2.83 MeV. However, because the sign of the interference is uncertain, this interference has not been taken into account in the analysis of the experimental data. If more precise angular distributions can be measured, it may be possible to determine the sign of this interference; a more accurate analysis could then be made. From the analysis of Section III.D, the ratio of the E2 direct capture to the ground state, to the E1 resonant capture to the ground state at E_α(c.m.) = 300 keV is about 1×10^{-2}, which justifies the neglect of the E2 direct capture at astrophysical energies.

Of the direct captures to excited states in ^{16}O from s and d plane-wave initial states, the one which is most likely to contribute significantly is that of the E1 capture to the 7.12-MeV state, from the s plane-wave initial state. Both Tombrello (1970) and Werntz (1970) considered this capture. Werntz found this cross section to be negligible. Tombrello finds the values $S(300\ \text{keV,c.m.}) \lesssim 200p^2\ \theta_\alpha^2(7.12\text{-MeV},{}^{16}O)$ MeV-barns and $S(2.4\ \text{MeV, c.m.}) \lesssim 60p^2\ \theta_\alpha^2(7.12\text{-MeV},{}^{16}O)$ MeV-barns, where p is the effective dipole moment of the system.

The remaining problem is to determine the value of p^2. Deviations from integral masses give a lower limit for p^2 of 4×10^{-7}. Estimates of isospin mixing of a $T = 1$ isospin component into the 7.12-MeV state give $p^2 \sim 10^{-4}$. Such an estimate is consistent with the dipole strength of the 7.12-MeV state obtained from measurement of the radiative width (Swann 1970). This value for p^2

would give the above S-factors negligible values. A consideration of typical dipole moments in other self-conjugate nuclei compared to typical dipole moments in non-self-conjugate nuclei suggests that p^2 might be between 10^{-3} and 10^{-2}. In the unlikely event that p^2 were as high as 10^{-2}, then the S-factor for E1 direct capture to the 7.12-MeV state of ^{16}O would be roughly equivalent to that for E1 capture to the ground state. It is more likely that the contribution is at least a few times smaller.

Another direct capture cross section considered by Tombrello (1971) is that of E2 capture to the 6.92-MeV state, from the s plane-wave state. This S-factor is expected to be three orders of magnitude smaller than that of E1 capture to the ground state.

APPENDIX C

Three-Level R-Matrix Fit to the $^{12}C(\alpha,\gamma)^{16}O$ Data

Weisser, Morgan and Thompson (1970) have parameterized the $^{12}C(\alpha,\gamma)^{16}O$ measured excitation function (E1 contributions only) with a 3-level R-matrix formula (Lane 1958). The three levels are located at ^{16}O excitation energies of 7.12 MeV, 9.60 MeV, and 20 MeV (the latter is a fictitious level added to account for background strength from the tails of high-energy, broad 1^- levels). The expression for the cross section is

$$\sigma = \frac{3\pi}{k^2} \left| \sum_{\lambda',\lambda=1}^{3} \Gamma_{\lambda\alpha}^{1/2} \Gamma_{\lambda'\gamma}^{1/2} [(E_\lambda - E)\delta_{\lambda\lambda'} + \Delta_{\lambda\lambda'} - \frac{i}{2} \Gamma_{\lambda\alpha}^{1/2} \Gamma_{\lambda'\alpha}^{1/2}]^{-1} \right|^2 ,$$

where

k = wave number of the relative motion of the ^{12}C nucleus and alpha particle,

$\Gamma_{\lambda\alpha}$ = alpha width of level λ, which is twice the product of the $\ell = 1$ penetration function and the reduced-alpha-width,

$\Gamma_{\lambda\gamma}$ = gamma width of level λ, which contains the cubic energy dependence for electric dipole radiation,

E_λ = eigen-energy of level λ,

$\Delta_{\lambda\lambda'}$ = level-shift matrix, a function of the reduced-alpha-widths, a boundary condition number and an $\ell = 1$ shift function.

There are, in this formula, nine parameters to be determined; three for each level: a reduced-alpha-width, a gamma width, and a position of the level. Two of the parameters describing the 7.12-MeV level are determined from other experimental measurements: the gamma

width, measured by resonance fluorescence techniques to be 62 ± 5 meV (Swann 1970), and the energy of the state--42 keV below the $^{12}C+\alpha$ threshold (Ajzenberg-Selove 1971). A third parameter, the position of the background level, was taken to be 20 MeV excitation in ^{16}O; variation of this position over a broad range about 20 MeV showed that the results of the fit were insensitive to the exact position. Three more parameters, the position and the reduced-alpha-width of the 9.60-MeV level and the reduced-alpha-width of the background level, were obtained by fitting the p-wave phase shifts obtained from the $^{12}C(\alpha,\alpha)^{12}C$ elastic scattering data (Jones 1962, Clark 1968), with the 3-level R-matrix formula for 1^- phase shifts. This leaves three parameters to be determined by fitting the $^{12}C(\alpha,\gamma)^{16}O$ data: the gamma widths of the 9.60-MeV and background levels and the desired reduced-alpha-width of the 7.12-MeV level. The final result was found to be insensitive to the exact values of the boundary condition number and the interaction radius.

The fitting procedure was iterative: with a set of initial values for the parameters, the p-wave elastic scattering phase shifts were fitted; with the new values for three of the parameters, the measured $^{12}C(\alpha,\gamma)^{16}O$ cross sections (1^- contributions only) were fitted. This process was repeated, with the inclusion each time of the best parameter values from the previous fit.

The final parameters were used to calculate the S-factor at 300 keV c.m. alpha energy. From this, the value of $\Theta^2_{\alpha,F}$ was derived, as described in Appendix A.

APPENDIX D

"Hybrid" R-Matrix-Optical-Model Fit to the $^{12}C(\alpha,\gamma)^{16}O$ Data

Koonin and Tombrello (1972) have developed a "hybrid" R-matrix-optical-model parameterization of the $^{12}C(\alpha,\gamma)^{16}O$ cross section. Two parameters are varied in fitting the data. The formula for the $^{12}C(\alpha,\gamma)^{16}O$ cross section is

$$\sigma = \frac{6\pi}{k^2} P \left| \frac{R_{\alpha\gamma}}{1 - (S+iP) R_{\alpha\alpha}} \right|^2 ,$$

where

k = wave number of the relative motion of the ^{12}C nucleus and alpha particle,

P = penetration function for $\ell = 1$,

S = shift function for $\ell = 1$,

$R_{\alpha\gamma}$ = capture R-function of R-matrix theory,

$R_{\alpha\alpha}$ = elastic scattering R-function of R-matrix theory.

The R-functions are split into two parts:

$$R_{\alpha\alpha} = R_{\alpha\alpha}^{(0)} + R_{\alpha\alpha}^{(7.12)} ,$$

$$R_{\alpha\gamma} = R_{\alpha\gamma}^{(0)} + R_{\alpha\gamma}^{(7.12)} .$$

The superscript "7.12" refers to the 7.12-MeV state in ^{16}O; the superscript "0" includes the 9.60-MeV level, high-lying levels, and direct capture (extra-nuclear) processes.

The $R_{\alpha\alpha}^{(7.12)}$ and $R_{\alpha\gamma}^{(7.12)}$ bound state contributions to the R-functions are treated in the manner of R-matrix theory (Lane 1958). These quantities are described in terms of a pole associated with the

7.12-MeV level, where the gamma width and position are determined from experimental data (Swann 1970, Ajzenberg-Selove 1971) and the reduced-alpha-width is to be determined by fitting the $^{12}C(\alpha,\gamma)^{16}O$ data. The functions $R_{\alpha\alpha}^{(0)}$ and $R_{\alpha\gamma}^{(0)}$, which represent contributions to the R-functions from the 9.60-MeV level, high-lying levels and direct capture, are treated in the manner of optical-model theory. These functions are generated by a potential acting between the ^{12}C nucleus and alpha particle, with $R_{\alpha\gamma}^{(0)}$ being scaled by an effective dipole strength, which is the second parameter varied in the fit to the $^{12}C(\alpha,\gamma)^{16}O$ data. The potential consists of a Coulomb potential (that of a uniformly charged sphere) and a truncated real Woods-Saxon potential. The point of truncation gives the channel radius used in the R-matrix expression; fits were performed for a range of these radii, and that value was chosen which gave the best fit. The parameters describing the potential were adjusted to give a best fit to the p-wave phase shifts of the $^{12}C(\alpha,\alpha)^{12}C$ elastic scattering data (Jones 1962).

APPENDIX E

Measurement of the Yield of the $^{19}F(\alpha,\gamma)^{23}Na$ Reaction and of ^{19}F Target Content

When an enriched ^{12}C target from one particular tantalum strip was bombarded with alpha particles of c.m. energy 2.4 MeV, it was found that the yield of 9-MeV gamma rays was about 40% too high, and that there were events in the spectrum corresponding to gamma rays of energies higher than 9 MeV. Targets from this strip were consequently not used in measuring the $^{12}C(\alpha,\gamma)^{16}O$ cross sections. However, since an impurity was evidently present, it was desirable to investigate its identity and to check the other targets which were used for $^{12}C(\alpha,\gamma)^{16}O$ measurements for the same impurity.

The isotope ^{19}F, which can produce high-energy gamma rays by the reaction $^{19}F(\alpha,\gamma)^{23}Na$, was suspected because of the possible presence of a fluorine compound in the chemical apparatus used to convert amorphous carbon to methyl iodide, just prior to its use for ^{12}C. Also, it was noted that the yield of 6-MeV gamma rays was abnormally high in the spectra obtained when bombarding the target with protons in order to measure the target thickness; this 6-MeV gamma-ray yield was attributed to the well-known $^{19}F(p,\alpha\gamma)^{16}O$ reaction. The compound nucleus ^{23}Na of the $^{19}F(\alpha,\gamma)^{23}Na$ reaction is excited to energies of 12.4 to 13.8 MeV for the range of alpha energies in which the $^{12}C(\alpha,\gamma)^{16}O$ measurements were made, so that ground state transitions produce gamma rays of about 13 MeV. The low-energy tail of a 13-MeV gamma-ray energy spectrum (arising mainly from Compton scattering) can

produce pulses in the 9-MeV gamma-ray region. In addition, there are several states in ^{23}Na at excitation energies of a few MeV; cascades through these states can result in a yield of 9-MeV gamma rays.

Two quantities are required in order to calculate the effect of a ^{19}F impurity in the target: (1) the amount of ^{19}F in the target, and (2) the cross section for production of 9-MeV gamma rays from the capture of alpha particles by ^{19}F.

Measurements of ^{19}F content were made for two enriched ^{12}C targets: the target which was used for most of the measurements considered in the present work (henceforth referred to as target A) and the target for which the 9-MeV gamma-ray yield from alpha particle bombardment was found to be too high (henceforth referred to as target B). The ^{19}F contents of these targets were determined by measuring the yield of 6.13-MeV gamma rays from the $^{19}F(p,\alpha\gamma)^{16}O$ reaction at $E_p(lab) = 872$ keV, at which energy there is a strong, narrow ($\Gamma_{lab} = 4.7$ keV), isolated resonance (Ajzenberg-Selove 1972). The yields were measured for a range of incident energies extending from just below 872 keV to that energy plus the proton energy loss in the target. It was thus possible to obtain the magnitude of the ^{19}F content as a function of depth in the target. This measurement was also performed for a 20 $\mu g/cm^2$ CaF_2 target. All measurements were made with the same experimental configuration. The results are shown in Figure 19. For both ^{12}C targets, there is a minimum in the ^{19}F content halfway through the target. Target B has roughly 60 times the ^{19}F content of target A, and $\sim$0.5% of that of a thick CaF_2 target.

The yields for the $^{19}F(\alpha,\gamma)^{23}Na$ reaction were measured by the same technique as that by which the $^{12}C(\alpha,\gamma)^{16}O$ yields were measured. Gamma rays were detected with two 20.3-cm-diameter by 12.7-cm-long NaI(Tl) crystals, and time-of-flight technique was employed to suppress prompt-neutron and time-independent background. A 20 $\mu g/cm^2$ CaF_2 target evaporated onto a tantalum backing (the same target that was used to make the ^{19}F content measurement) was supported in the target chamber used for the $^{12}C(\alpha,\gamma)^{16}O$ angular distribution measurements, on the north 10^o beam line of the tandem accelerator. The target thickness is uncertain by $\sim$20%; its value was obtained from the thickness monitor in the evaporation chamber. Events were stored in a two-dimensional multichannel analyzer. Data were accumulated for lab alpha energies ranging from 2.7 to 4.0 MeV. In Figure 20 the yields of gamma rays of energy corresponding to the ground state transition in ^{23}Na are shown. For the alpha energies studied, these gamma-ray energies range from 12.7 to 13.8 MeV. The yields which are of interest for the $^{12}C(\alpha,\gamma)^{16}O$ study are the yields from the $^{19}F(\alpha,\gamma)^{23}Na$ reaction of gamma rays of energy corresponding to the ground state transition in ^{16}O for the particular lab alpha energy. These yields are displayed in Figure 21.

By combination of the ^{19}F content data and the $^{19}F(\alpha,\gamma)^{23}Na$ data, it was possible to obtain for each of the targets A and B the yield of 9-MeV gamma rays from the $^{19}F(\alpha,\gamma)^{23}Na$ reaction due to the ^{19}F impurity content of the target. This yield for 1 μC of integrated charge and for an incident lab alpha energy $E_\alpha(inc)$ was estimated by the formula

$$[\alpha,\gamma]^{^{12}C}_{E_\alpha(\text{inc})} = \sum_i [\alpha,\gamma]^{CaF_2}_{E_\alpha(i)} \frac{[p,\alpha\gamma]^{^{12}C}_{E_p(i)}}{[p,\alpha\gamma]^{CaF_2}_{872\ \text{keV}}} ,$$

where the target thickness is divided into about 15 intervals in depth and a sum is carried out over these intervals, and where

$[\alpha,\gamma]^{CaF_2}_{E_\alpha(i)}$ = yield of 9-MeV gamma rays from a CaF_2 target from the $^{19}F(\alpha,\gamma)^{23}Na$ reaction for 1 μC of integrated charge, evaluated at an alpha energy of $E_\alpha(\text{inc})$ less the loss of alpha particle energy in penetrating to the depth of interval i ; the yield is scaled to a CaF_2 target thickness of that of interval i ,

$[p,\alpha\gamma]^{^{12}C}_{E_p(i)}$ = yield of 6.13-MeV gamma rays from a ^{12}C target from the $^{19}F(p,\alpha\gamma)^{16}O$ reaction for 1 μC of integrated charge, evaluated at a proton energy of 872 keV plus the loss of proton energy in penetrating to the depth of interval i ,

$[p,\alpha\gamma]^{CaF_2}_{872\ \text{keV}}$ = yield of 6.13-MeV gamma rays from a thick CaF_2 target from the $^{19}F(p,\alpha\gamma)^{16}O$ reaction for 1 μC of integrated charge, evaluated at the energy corresponding to maximum yield.

(All energies are lab energies in this formula.) It is assumed that the efficiency for detection of the yields $[\alpha,\gamma]^{^{12}C}$ and $[\alpha,\gamma]^{CaF_2}$ and of the yields $[p,\alpha\gamma]^{^{12}C}$ and $[p,\alpha\gamma]^{CaF_2}$ are the same; a correction is to be made if this is not true. Because the $^{19}F(p,\alpha\gamma)^{16}O$ yield measured with the 20 μg/cm^2 CaF_2 target was not a thick-target yield, as required for determination of the quantity $[p,\alpha\gamma]^{CaF_2}$, it was necessary to correct the measured peak yield. Fowler et al. (1948)

derive the following relationship between the maximum yield of a thin target $Y_{max}(\xi)$, where ξ is the target thickness in energy units, and the maximum yield of a thick target $Y_{max}(\infty)$

$$\frac{Y_{max}(\xi)}{Y_{max}(\infty)} = \frac{2}{\pi} \tan^{-1} \frac{\xi}{\Gamma} \quad ,$$

where Γ is the width of the resonance. For this measurement, $\xi \simeq 4$ keV and $\Gamma = 4.7$ keV , so that

$$Y_{max}(\infty) \simeq 2.2\ Y_{max}(\xi) \quad .$$

The results of this evaluation for target A are given in Table 6. For comparison, the measured yields of 9-MeV gamma rays from the $^{12}C(\alpha,\gamma)^{16}O$ reaction are given. The effect of the ^{19}F impurity is seen to be small, but not completely negligible. Since the yield of the $^{19}F(\alpha,\gamma)^{23}Na$ reaction has not been measured over the full range of alpha energies for which the $^{12}C(\alpha,\gamma)^{16}O$ yield has been measured, it is not possible at present to obtain corrections at all energies. For this reason, the correction has not been applied to the $^{12}C(\alpha,\gamma)^{16}O$ results given in Section III. Although the correction would be smaller than the statistical error assigned to the $^{12}C(\alpha,\gamma)^{16}O$ yield, the effect cannot be neglected in the final analysis, because there is an energy dependence. In order to obtain a preliminary evaluation of the effect of the ^{19}F impurity yield on the derived parameter $\Theta^2_{\alpha,F}$, the $^{19}F(\alpha,\gamma)^{23}Na$ yields of Table 6 were subtracted from those for the $^{12}C(\alpha,\gamma)^{16}O$ reaction (no corrections being attempted for the lower-energy points), and the data were fitted again with the 3-level R-matrix

formula (Appendix C); the value of $\Theta^2_{\alpha,F}$ decreased by only 5%. A completely reliable correction, however, can only be presented when the $^{19}F(\alpha,\gamma)^{23}Na$ yields have been measured at lower alpha energies.

It can be seen from the yields given in Table 6 that the much higher (about 60 times higher) ^{19}F content of target B would have a disastrous effect on the shape of the 9-MeV gamma-ray excitation function. The $^{19}F(\alpha,\gamma)^{23}Na$ yield for target B is of the right order of magnitude to account for the 40% increase in the 9-MeV gamma-ray yield which was originally observed for this target.

REFERENCES

Adams, A., M. H. Shapiro, C. A. Barnes, E. G. Adelberger and W. M. Denny 1968, Bull. Am. Phys. Soc. 13, 698.

Ajzenberg-Selove, F. 1971, Nuc. Phys. A166, 1.

Ajzenberg-Selove, F. 1972, Nuc. Phys. A190, 1.

Arnett, W. David 1969, Ap. and Space Sci. 5, 180.

Arnett, W. David 1971, private communication.

Arnett, W. David 1972, Ap. J. 176, 681.

Barker, F. C. 1971, Aust. J. Phys. 24, 777.

Barnes, C. A. and William A. Fowler 1970, unpublished work.

Barnes, C. A. 1971, Advances in Nuclear Physics 4, 133.

Brown, G. E. and A. M. Green 1965, Phys. Letters 15, 168.

Brown, G. E. and A. M. Green 1966, Nuc. Phys. 75, 401.

Cameron, A.G.W. 1968, Origin and Distribution of the Elements, edited by L. H. Ahrens, Pergamon Press (New York), page 125.

Clark, G. J., D. J. Sullivan and P. B. Treacy 1968, Nuc. Phys. A110, 481.

Clark, G. J., 1969, Aust. J. Phys. 22, 289.

Clayton, Donald D. 1968, Principles of Stellar Evolution and Nucleosynthesis, McGraw-Hill, Inc. (New York).

Deinzer, W. and E. E. Salpeter 1964, Ap. J. 140, 499.

Dietrich, F. S. 1964, Ph.D. Thesis, California Institute of Technology.

Ewen, Klaus 1970, Ph.D. Thesis, Universität zu Köln.

Fowler, William A., C. C. Lauritsen and T. Lauritsen 1948, Rev. Mod Phys. 20, 236.

Fowler, William A., Georgeanne R. Caughlan and Barbara A. Zimmerman 1967, Ann. Rev. Astron. and Astrophys. 5, 525.

Fowler, William A. 1968, Origin and Distribution of the Elements, edited by L. H. Ahrens, Pergamon Press (New York), page 3.

Grodstein, G. W. 1957, NBS Circular 583.

Gunn, J. E. and J. P. Ostriker 1970, Ap. J. 160, 979.

Hättig, H., K. Hünchen, P. Roth and H. Wäffler 1969, Nuc. Phys. A137, 144.

Jaszczak, Ronald J., John H. Gibbons and R. L. Macklin 1970, Phys. Rev. C2, 63.

Jaszczak, Ronald J. and R. L. Macklin 1970a, Phys. Rev. C2, 2452.

Jones, C. Miller, G. C. Phillips, R. W. Harris and E. H. Beckner 1962, Nuc. Phys. 37, 1.

Koonin, S. E. and T. A. Tombrello 1972, to be published.

Lane, A. M. and R. G. Thomas 1958, Rev. Mod. Phys. 30, 257.

Larson, J. D. and R. H. Spear 1964, Nuc. Phys. 56, 497.

Larson, J. D. 1965, Ph.D. Thesis, California Institute of Technology.

Lazar, N. H., R. C. Davis and P. R. Bell 1956, Nucleonics 14(#4), 52.

Loebenstein, H. M., D. W. Mingay, H. Winkler and C. S. Zaidins, 1967 Nuc. Phys. A91, 481

McDonald, A. B. 1970, Ph.D. Thesis, California Institute of Technology.

Paczyński, B. 1970, Acta Astr. 20, 47.

Paczyński, B. 1971, Acta Astr. 21, 271.

Parker, P.D.M. 1963, Ph.D. Thesis, California Institute of Technology

Pühlhofer, F., H. G. Ritter and R. Bock 1970, Nuc. Phys. A147, 258.

Schwarzschild, M. and R. Härm 1967, Ap. J. 150, 961.

Sherman, I. S., R. G. Roddick and A. J. Metz 1968, IEEE Trans. Nucl. Sci. NS-15, 500.

Smith, R. L. and I.-J Sackmann 1972, preprint.

Stephenson, G. J., Jr. 1966, Ap. J. 146, 950.

Swann, C. P. 1970, Nuc. Phys. A150, 300.

Tombrello, T. A. and G. C. Phillips 1961, Phys. Rev. 122, 224.

Tombrello, T. A. 1970, private communication.

Tombrello, T. A. 1971, private communication.

Weigert, A. 1966, Zeitschrift für Astrophysik 64, 395.

Weisser, D. C., J. F. Morgan and D. R. Thompson 1970, internal report.

Werntz, Carl 1970, private communication.

Werntz, Carl 1971, Phys. Rev. C4, 1591.

Wheeler, J. Craig, Zalman Barket and Jean-Robert Buchler 1970, Ap. J. 162, L129.

Zerby, C. D. and H. S. Moran 1961, Nuc. Instr. and Meth. 14, 115.

TABLE 1

Yields of 7-MeV Single Gamma Rays and Yields of Coincidences

The quantities in Column 2 were extracted from the two-dimensional spectra; it is possible that some of this yield is produced by impurities in the target. The upper limits listed in Column 3 were obtained by observing coincidences between 7-MeV and ∿2-MeV gamma rays. For additional details, see pages 41 to 43.

E_{α} (lab) MeV	7-MeV Gamma-Ray Yield nb	Yield of Coincidences nb
2.31	< 4	
2.39	< 1	
2.49	1 ± 1	
2.61	2.1 ± 1.2	< 3
2.71	3.7 ± 1.2	
2.77	3.4 ± 1.2	
2.82	4.4 ± 1.4	
2.87	4.6 ± 1.4	
2.91	8.0 ± 1.3	< 1
3.01	12.4 ± 1.8	
3.09	17.6 ± 2.5	
3.23	15.2 ± 3.0	< 5
3.32	17.4 ± 2.8	
3.42	14.0 ± 2.2	< 2
3.71	16.8 ± 1.0	
3.77		< 8
3.82	18.9 ± 0.9	
3.92	25.9 ± 0.9	

TABLE 2

$^{12}C(\alpha,\gamma)^{16}O$ Yields from Measurements at 90^{o}

Column 3 gives the number of counts, per mC of integrated charge, extracted from the spectra measured at 90^{o}. In order to relate these yields to absolute quantities, there is given in Column 4 the total cross section which would result if the angular distributions of gamma rays were those of pure electric dipole transitions. For additional details, see pages 43 and 44.

E_{α}(c.m.) MeV	E_{α}(lab) MeV	Yield counts/mC	$\sigma(1^{-})$ nb
1.73	2.31	9.1 ± 2.8	1.8 ± 0.6
1.79	2.39	10.8 ± 2.1	2.2 ± 0.4
1.87	2.49	16.9 ± 2.7	3.4 ± 0.5
1.96	2.61	20.3 ± 2.8	4.1 ± 0.6
2.03	2.71	36.3 ± 2.8	7.3 ± 0.6
2.08	2.77	46.9 ± 3.0	9.4 ± 0.6
2.11	2.82	72.6 ± 3.4	14.5 ± 0.7
2.15	2.87	82.5 ± 6.6	16.5 ± 1.3
2.18	2.91	99.8 ± 3.8	19.9 ± 0.8
2.26	3.01	147.1 ± 5.1	29.4 ± 1.0
2.32	3.09	201.4 ± 6.6	40.1 ± 1.3
2.42	3.23	190.0 ± 8.0	37.8 ± 1.6
2.49	3.32	161.1 ± 5.9	32.1 ± 1.2
2.56	3.42	110.8 ± 6.6	22.0 ± 1.3
2.78	3.71	50.2 ± 2.8	10.0 ± 0.6
2.86	3.82	42.6 ± 2.5	8.5 ± 0.5
2.94	3.92	39.1 ± 2.3	7.8 ± 0.5

TABLE 3

Quantities $|A_{2+}|/|A_{1-}|$

Obtained from Angular Distribution Measurements

The quantities in Column 2 are obtained by fitting the measured angular distributions. The quantities in Column 3 are obtained from Tombrello's (1961) formula for the direct capture cross section, using $\Theta_\alpha^2(g.s., {}^{16}O) = 0.043 \pm 0.012$ to achieve consistency with these measured values and with the yields measured at $\Theta = 90^\circ$. For additional details, see pages 44 to 47.

E_α(c.m.) in MeV	$\lvert A_{2+}\rvert/\lvert A_{1-}\rvert$ measured	$\lvert A_{2+}\rvert/\lvert A_{1-}\rvert$ calculated
2.18	0.10 ± 0.10	0.19
2.42	0.14 ± 0.05	0.19
2.56	0.36 ± 0.06	0.29
2.83	0.58 ± 0.05	0.56

TABLE 4

E1 and E2 Contributions to the $^{12}C(\alpha,\gamma)^{16}O$ Total Cross Section

The quantities in Column 2 are obtained from Tombrello's (1961) formula for the 2^+ direct capture cross section, using $\Theta_\alpha^2(g.s.,{}^{16}O) = 0.043 \pm 0.012$. The values $|A_{1-}|^2$ are obtained from the yield at 90°, the detection efficiency, and the values $|A_{2+}|^2$. The quantity σ is the total cross section, the sum of $|A_{1-}|^2$ and $|A_{2+}|^2$. For additional details, see pages 46 to 48.

E_α(c.m.) MeV	$\lvert A_{2+}\rvert^2$ calc nb	$\lvert A_{1-}\rvert^2$ nb	$\lvert A_{2+}\rvert^2$calc/$\lvert A_{1-}\rvert^2$	σ nb
1.73	0.15	1.8 ± 0.6	0.08	1.9
1.79	0.18	2.1 ± 0.4	0.09	2.3
1.87	0.24	3.3 ± 0.5	0.07	3.5
1.96	0.33	3.9 ± 0.6	0.08	4.2
2.03	0.42	7.1 ± 0.6	0.06	7.5
2.08	0.49	9.2 ± 0.6	0.05	9.7
2.11	0.54	14.3 ± 0.7	0.04	14.8
2.15	0.61	16.2 ± 1.3	0.04	16.8
2.18	0.66	19.6 ± 0.8	0.03	20.3
2.26	0.80	29.0 ± 1.0	0.03	29.8
2.32	0.94	39.7 ± 1.3	0.02	40.6
2.42	1.22	37.3 ± 1.6	0.03	38.5
2.49	1.43	31.5 ± 1.2	0.05	32.9
2.56	1.68	21.3 ± 1.3	0.08	23.0
2.78	2.61	9.2 ± 0.6	0.28	11.8
2.86	3.03	7.7 ± 0.5	0.39	10.7
2.94	3.46	7.1 ± 0.4	0.49	10.6

TABLE 5

$^{12}C(\alpha,\gamma)^{16}O$ Capture Transitions

The various capture processes by which the $^{12}C(\alpha,\gamma)^{16}O$ reaction may proceed are listed for the plane-wave states of lowest angular momenta. For additional details, see pages 62 to 69.

Initial plane-wave state	Order of multipole radiation	Final bound state in ^{16}O
s	E0	ground state
		6.05-MeV
	E1	7.12-MeV
	E2	6.92-MeV
p	E0	7.12-MeV
	E1	ground state
		6.05-MeV
		6.92-MeV
	E2	6.13-MeV
		7.12-MeV
d	E0	6.92-MeV
	E1	6.13-MeV
		7.12-MeV
	E2	ground state
		6.05-MeV
		6.92-MeV

TABLE 6

Yield of 9-MeV Gamma Rays from the ^{19}F Impurity in an Enriched ^{12}C Target

The second column gives the yield of 9-MeV gamma rays from enriched ^{12}C target A which are produced by the $^{19}F(\alpha,\gamma)^{23}Na$ reaction. The values are obtained from measurements of the ^{19}F content of the target and from measurements of the $^{19}F(\alpha,\gamma)^{23}Na$ yield from a CaF_2 target. For comparison, the $^{12}C(\alpha,\gamma)^{16}O$ yields from Table 2 are given. For additional details, see pages 74 to 79.

Lab incident energy MeV	$^{19}F(\alpha,\gamma)^{23}Na$ yield counts/mC	$^{12}C(\alpha,\gamma)^{16}O$ yield counts/mC
2.9	0.5	73 ± 3
2.95	0.3	82 ± 7
3.0	0.3	100 ± 4
3.1	0.1	147 ± 5
3.2	0.3	201 ± 7
3.3	0.6	190 ± 8
3.4	0.6	161 ± 6
3.5	0.6	111 ± 7
3.79	1.5	50 ± 3
3.9	0.7	43 ± 3
4.0	0.5	39 ± 2

Figure 1

Energy Level Diagram of the ^{16}O Nucleus (Ajzenberg-Selove 1971). For details, see pages 8, 9, and 12.

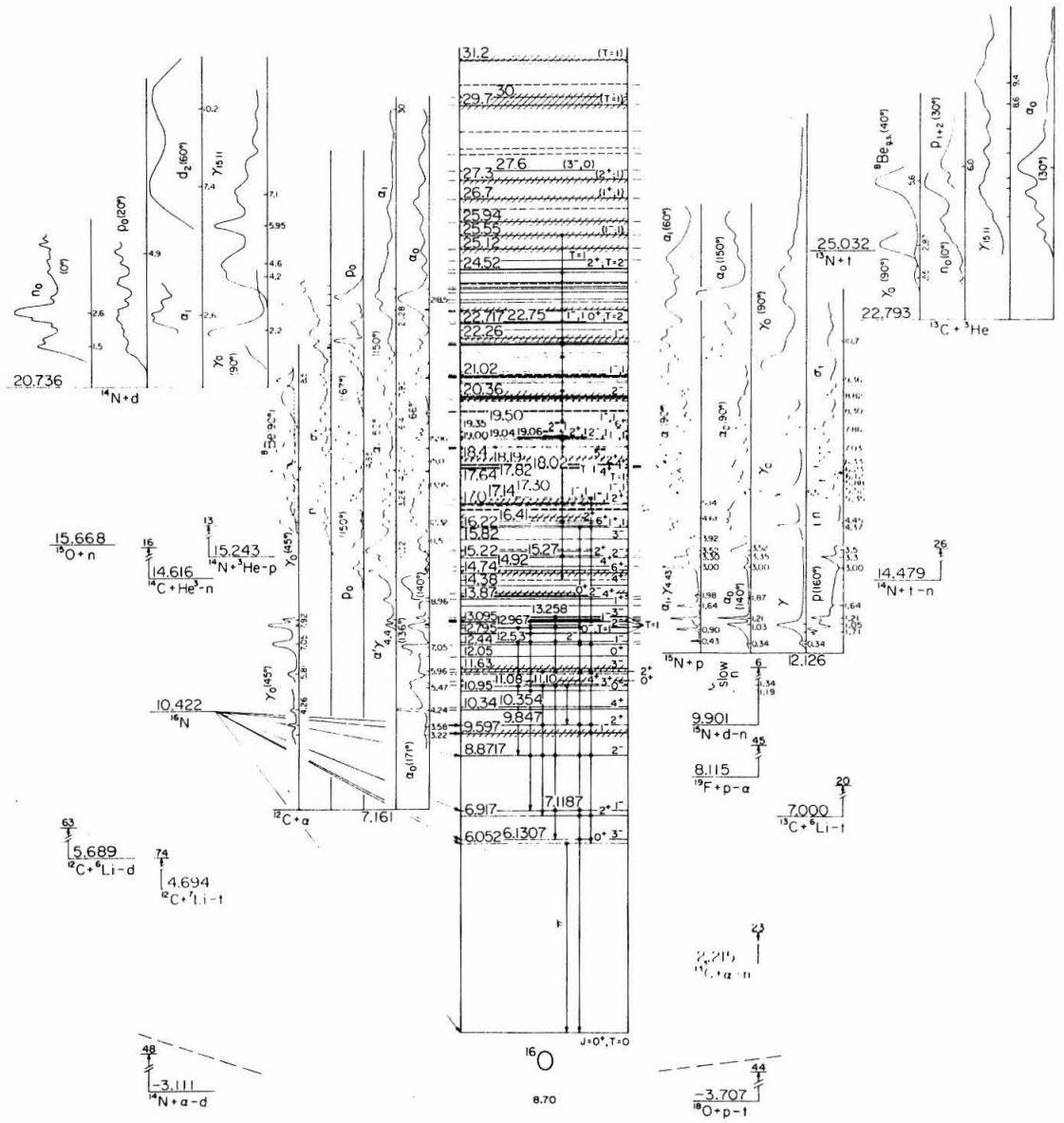
20.736
14N+d
15.668
15O+n
14.616
14C+He3-n
15.243
14N+3He-p
10.422
16N
5.689
12C+6Li-d
4.694
12C+7Li-t
-3.111
14N+α-d
12C+α
7.161
31.2
29.7
27.3
27.6
26.7
25.94
25.55
25.12
24.52
22.71
22.75
22.26
21.02
20.36
19.50
19.35
19.04
19.06
18.4
18.1
18.0
17.64
17.82
17.14
17.30
16.22
16.41
15.82
15.22
15.27
14.74
14.92
14.38
13.87
13.258
12.967
12.795
12.44
12.53
12.05
11.63
11.08
11.10
10.95
10.34
10.354
9.847
9.597
8.8717
7.1187
6.917
6.052
6.1307
16O
J=0+,T=0
8.70
25.032
13N+t
22.793
13C+3He
14.479
14N+t-n
15N+p
12.126
9.901
13N+d-n
8.115
19F+p-α
7.000
13C+6Li-t
-3.707
18O+p-t

Figure 1.

Figure 2

Schematic Diagram of Apparatus for Making Enriched ^{12}C Targets

This chamber is used to crack ^{12}C-enriched methyl iodide. Elemental ^{12}C is deposited on the tantalum strip supported in the center of the pyrex tube. A weight, with flexible coupling to the bottom end cap, is suspended from this strip to take up length in the strip gained from heat expansion. The apparatus is water cooled (not shown). For additional details, see pages 17 and 18.

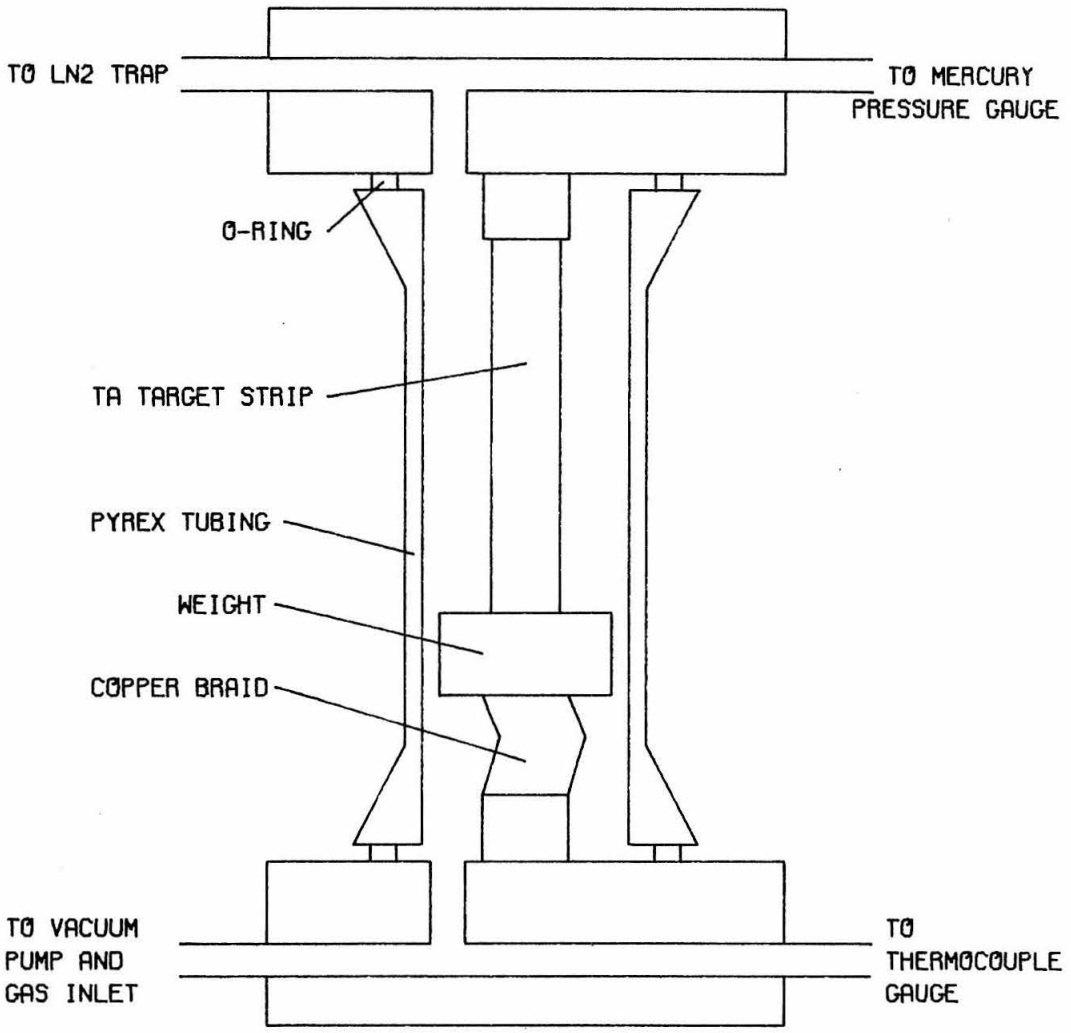
TØ LN2 TRAP
TØ MERCURY PRESSURE GAUGE
Ø-RING
TA TARGET STRIP
PYREX TUBING
WEIGHT
CØPPER BRAID
TØ VACUUM PUMP AND GAS INLET
TØ THERMØCØUPLE GAUGE

Figure 2.

Figure 3

Target Thickness Determination by the $^{13}C(p,\gamma)^{14}N$ Reaction

Both plots show the yield, as a function of incident laboratory proton energy, of 9.17-MeV gamma rays from the $^{13}C(p,\gamma)^{14}N$ reaction. The width of the resonance which rises at E_p(lab) = 1.75 MeV is primarily due to proton energy loss in the target and is a measure of the target thickness which can be determined with the use of energy loss tables. The top plot shows a measurement made with an enriched ^{12}C target. The structure in the region of maximum yield indicates that ^{13}C is not uniformly distributed in the target. The bottom plot shows a measurement made with a natural carbon target. In this case, such structure does not exist. For additional details see page 18.

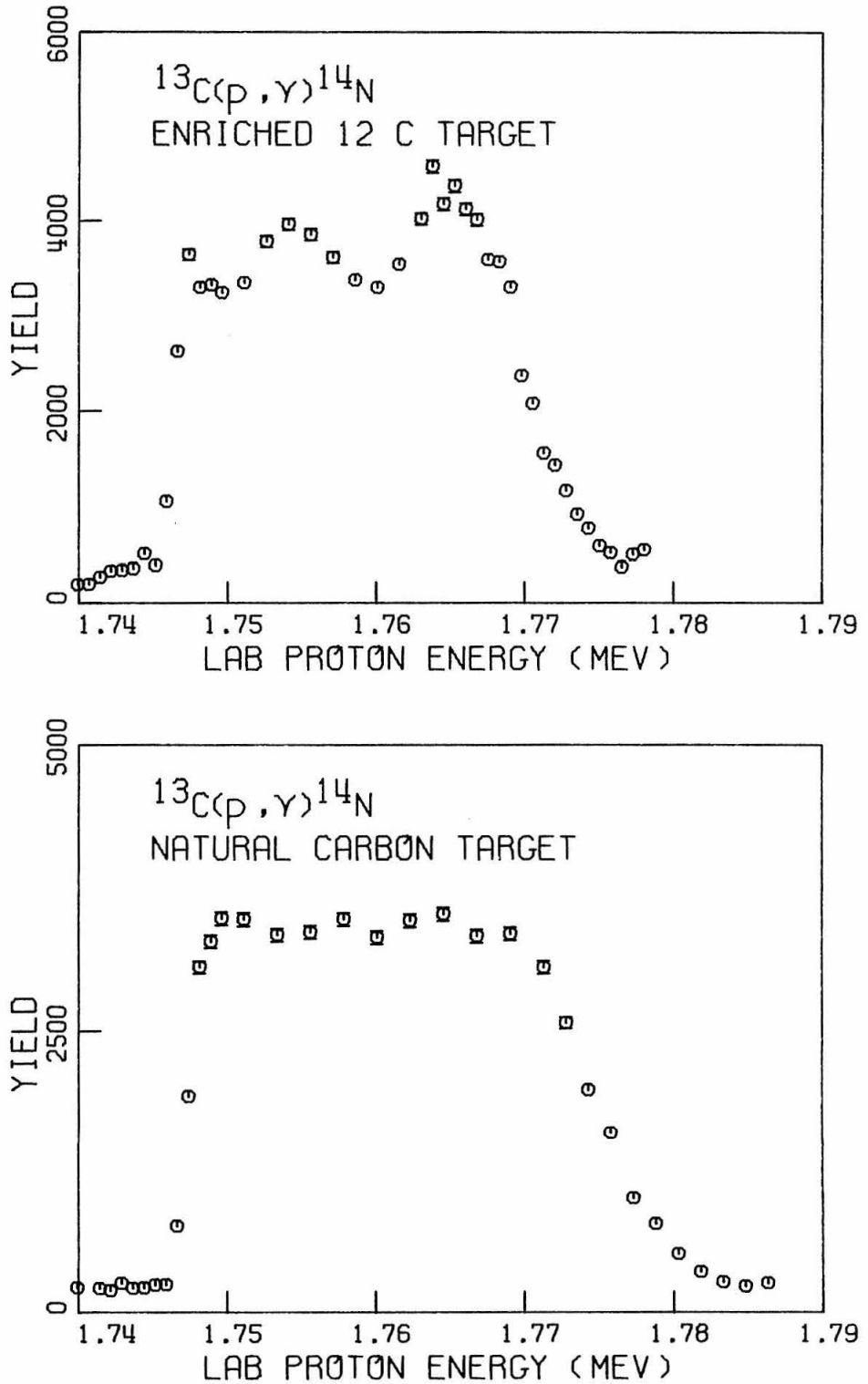
$^{13}C(p,\gamma)^{14}N$
ENRICHED 12 C TARGET
YIELD
0
2000
4000
6000
1.74
1.75
1.76
1.77
1.78
1.79
LAB PROTON ENERGY (MEV)
$^{13}C(p,\gamma)^{14}N$
NATURAL CARBON TARGET
YIELD
0
2500
5000
1.74
1.75
1.76
1.77
1.78
1.79
LAB PROTON ENERGY (MEV)

Figure 3.

Figure 4

Schematic Diagram of the Target and Detection System

The top diagram shows a vertical section of the target chamber and vacuum system (not to scale). In order to minimize deposit of natural carbon on the enriched ^{12}C target, copper gasket vacuum seals are used at all points downstream from the cold trap. For additional details see pages 19 and 20.

The bottom diagram shows the detector geometry and the lead shielding (not to scale). For additional details see pages 20 and 21.

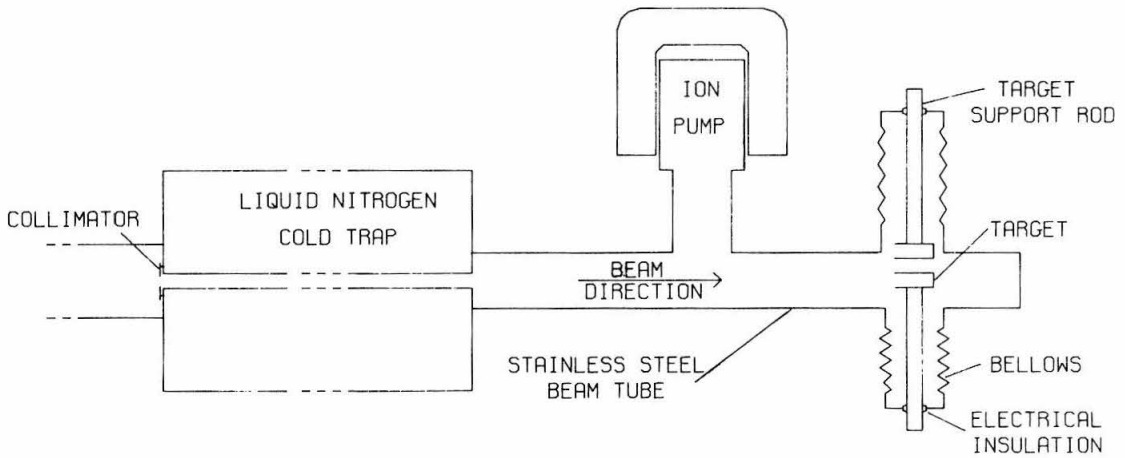
ION
PUMP
TARGET
SUPPORT ROD
LIQUID NITROGEN
COLD TRAP
COLLIMATOR
TARGET
BEAM
DIRECTION
STAINLESS STEEL
BEAM TUBE
BELLOWS
ELECTRICAL
INSULATION

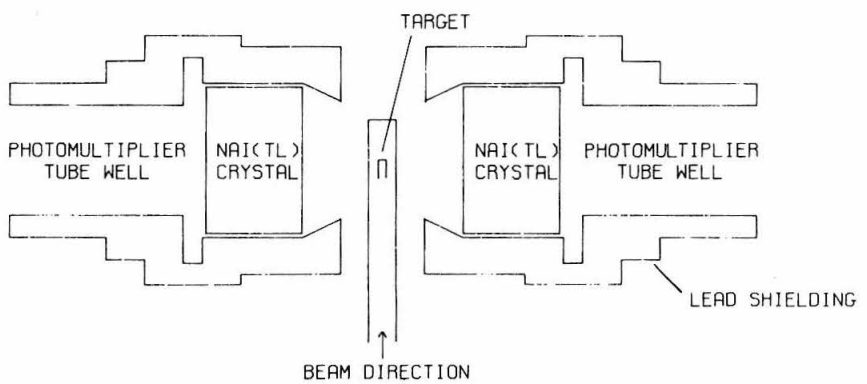
TARGET
PHOTOMULTIPLIER
TUBE WELL
NAI(TL)
CRYSTAL
NAI(TL)
CRYSTAL
PHOTOMULTIPLIER
TUBE WELL
LEAD SHIELDING
BEAM DIRECTION

Figure 4.

Figure 5

9.17-MeV Standard Spectrum for a 20.3-cm by 12.7-cm NaI(Tl) Crystal

This energy spectrum was measured with the reaction $^{13}C(p,\gamma)^{14}N$ at E_p(lab) = 1.75 MeV. An enriched ^{13}C target was used. The solid curve represents the extrapolation to the zero pulse height channel required for calculation of the spectrum fraction. For additional details, see pages 24 to 26.

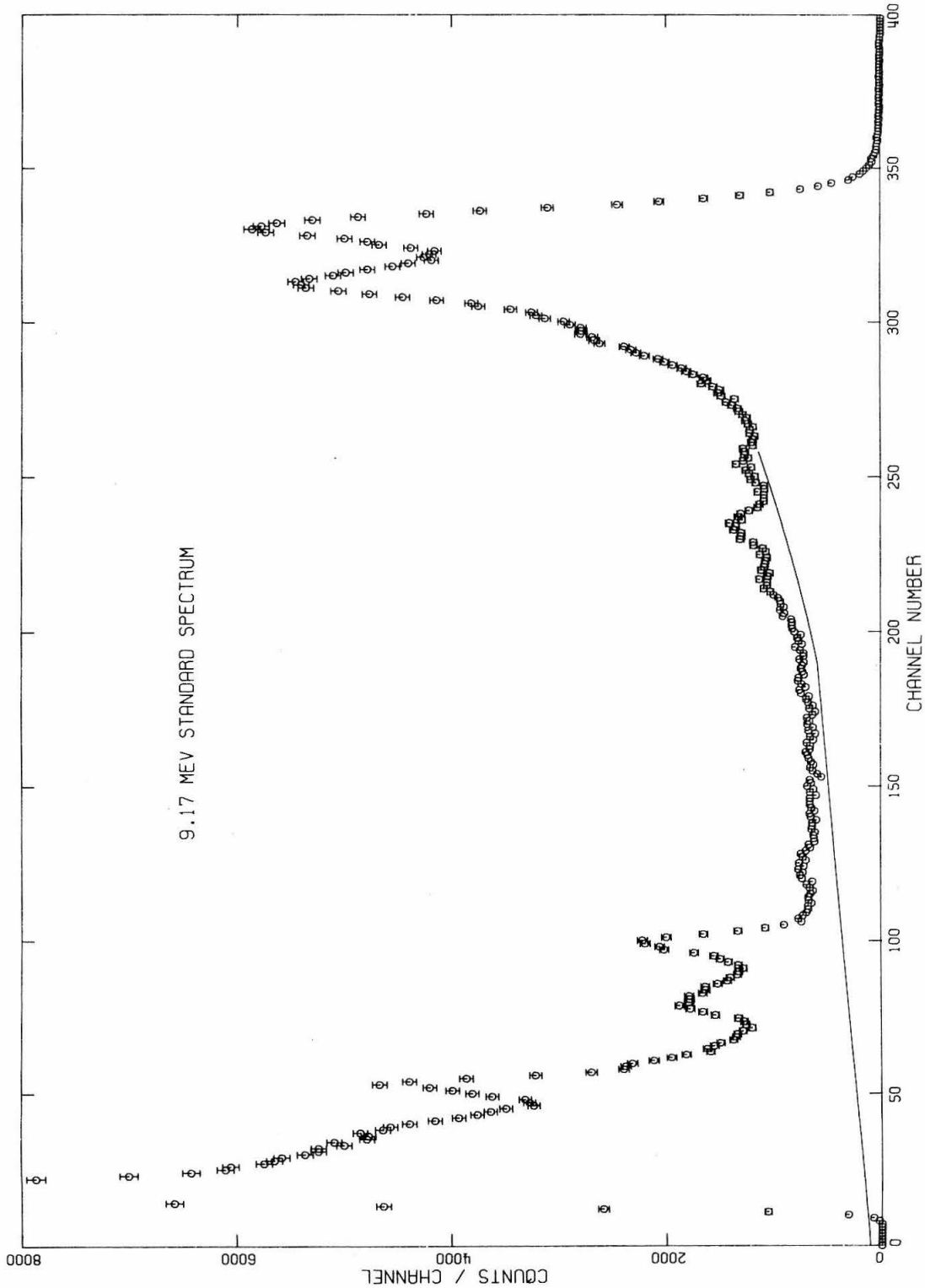
9.17 MEV STANDARD SPECTRUM
COUNTS / CHANNEL
CHANNEL NUMBER
0
2000
4000
6000
8000
0
50
100
150
200
250
300
350
400

Figure 5.

Figure 6

Electronic Configuration Used for Measurements of $^{12}C(\alpha,\gamma)^{16}O$ Yield at 90^{o}

For details, see pages 28, 30, and 31.

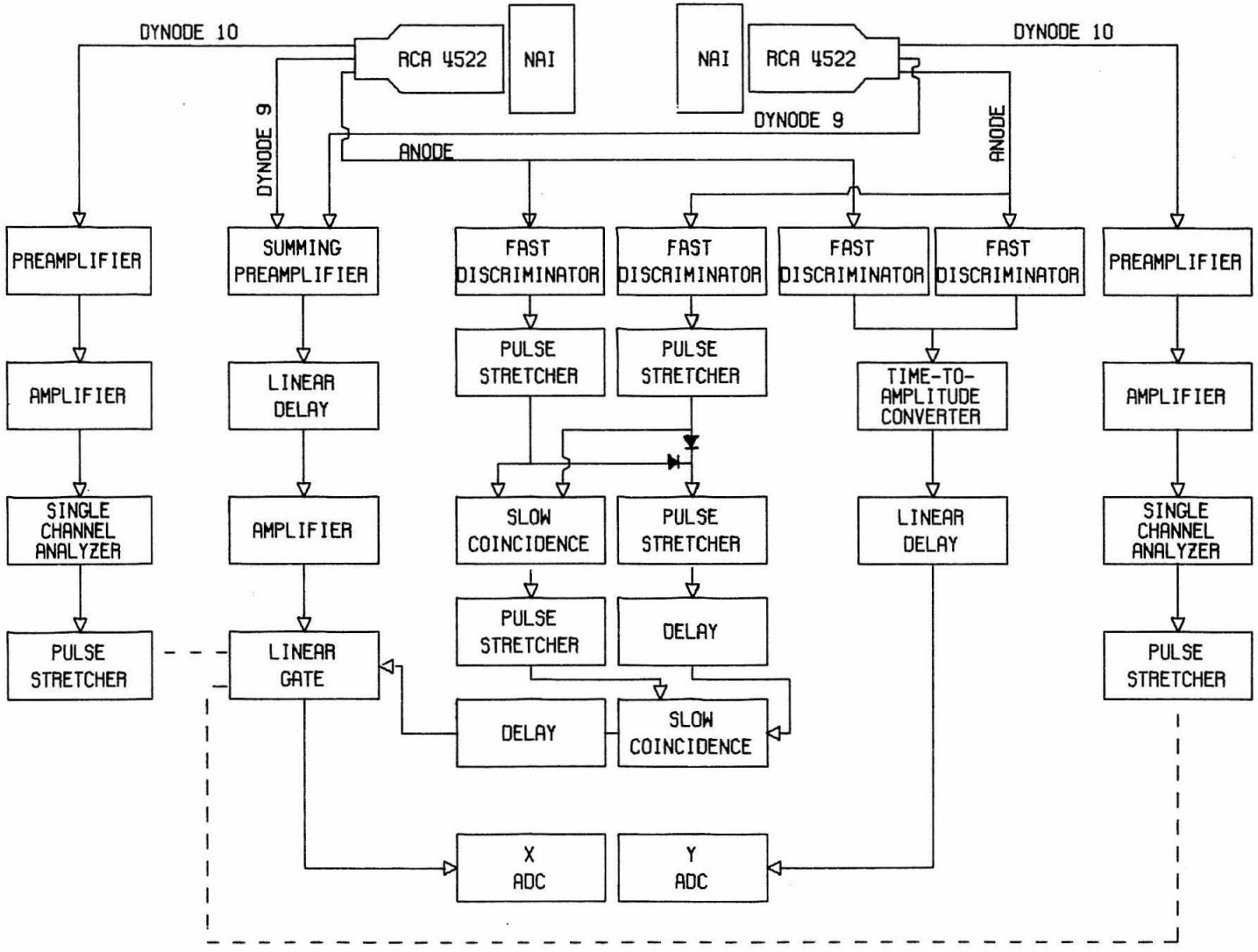
DYNODE 10
RCA 4522
NAI
NAI
RCA 4522
DYNODE 10
DYNODE 9
DYNODE 9
ANODE
ANODE
PREAMPLIFIER
SUMMING PREAMPLIFIER
FAST DISCRIMINATOR
FAST DISCRIMINATOR
FAST DISCRIMINATOR
FAST DISCRIMINATOR
PREAMPLIFIER
AMPLIFIER
LINEAR DELAY
PULSE STRETCHER
PULSE STRETCHER
TIME-TO-AMPLITUDE CONVERTER
AMPLIFIER
SINGLE CHANNEL ANALYZER
AMPLIFIER
SLOW COINCIDENCE
PULSE STRETCHER
LINEAR DELAY
SINGLE CHANNEL ANALYZER
PULSE STRETCHER
LINEAR GATE
PULSE STRETCHER
DELAY
PULSE STRETCHER
DELAY
SLOW COINCIDENCE
X ADC
Y ADC

Figure 6.

Figure 7

Isometric Plot of a $^{12}C(\alpha,\gamma)^{16}O$ Two-Dimensional Multichannel Analyzer Spectrum

This spectrum was measured at E_α(c.m.) = 2.42 MeV, at the peak of the resonance due to the 9.60-MeV state in ^{16}O. The 9.60-MeV region in the spectrum is about three quarters of the distance from left to right. The gamma-ray region is roughly in the center of the vertical scale; the prompt-neutron region is at the bottom. For additional details, see page 31.

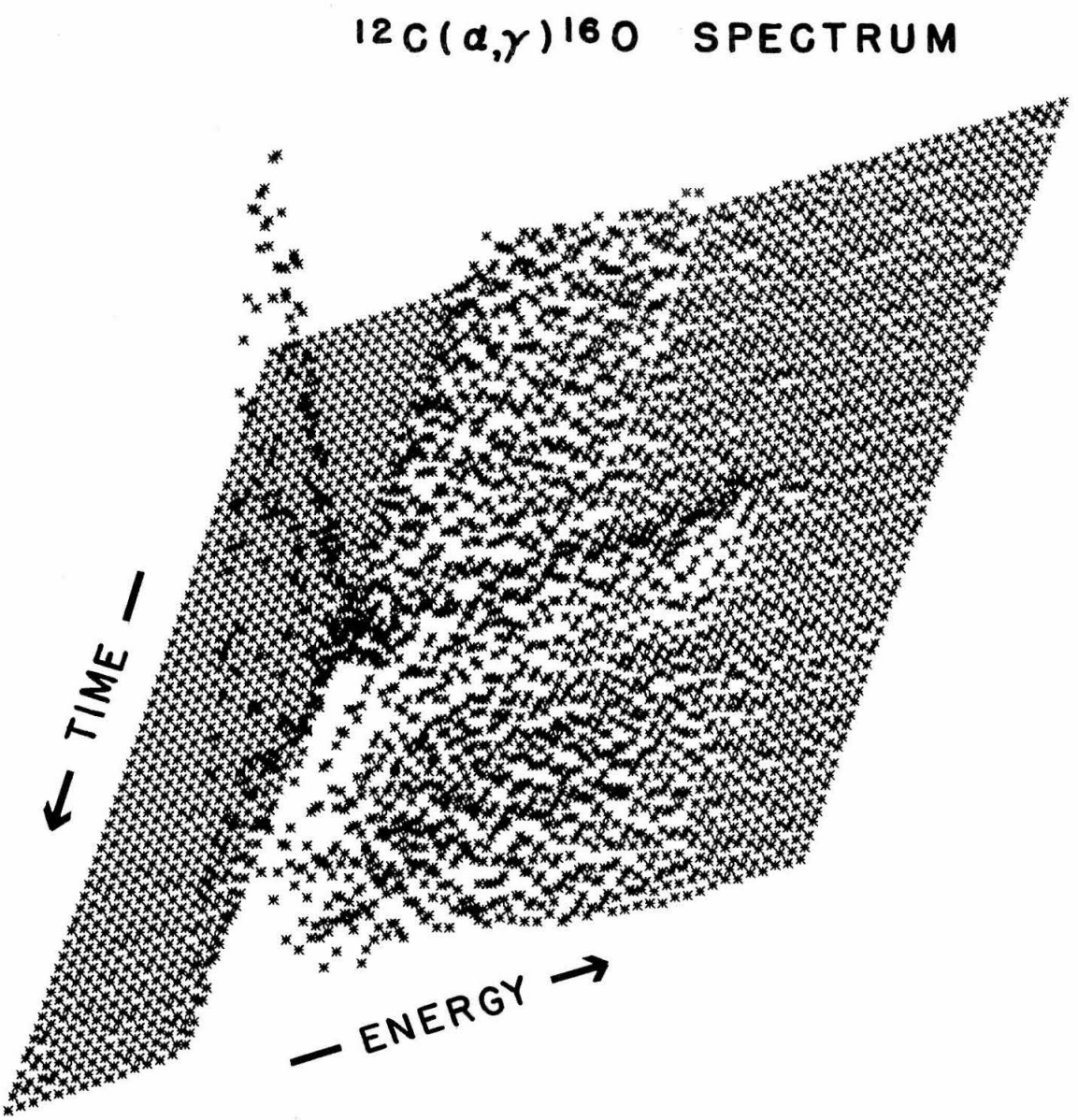

Figure 7.

Figure 8

Energy Spectra of Gamma Rays from the $^{12}C(\alpha,\gamma)^{16}O$ Reaction

These spectra are obtained from the two-dimensional spectra by summing counts over the time channels corresponding to the arrival of gamma rays from the target, and subtracting the energy spectrum of the time-independent background obtained from the same two-dimensional spectrum. Channel zero corresponds to zero gamma-ray energy; channel 64 to about 12 MeV. The c.m. alpha energies are displayed on the plots. Gamma rays of about 7 MeV are visible in the spectra measured at the higher alpha energies. For additional details see pages 34, 35 and 38.

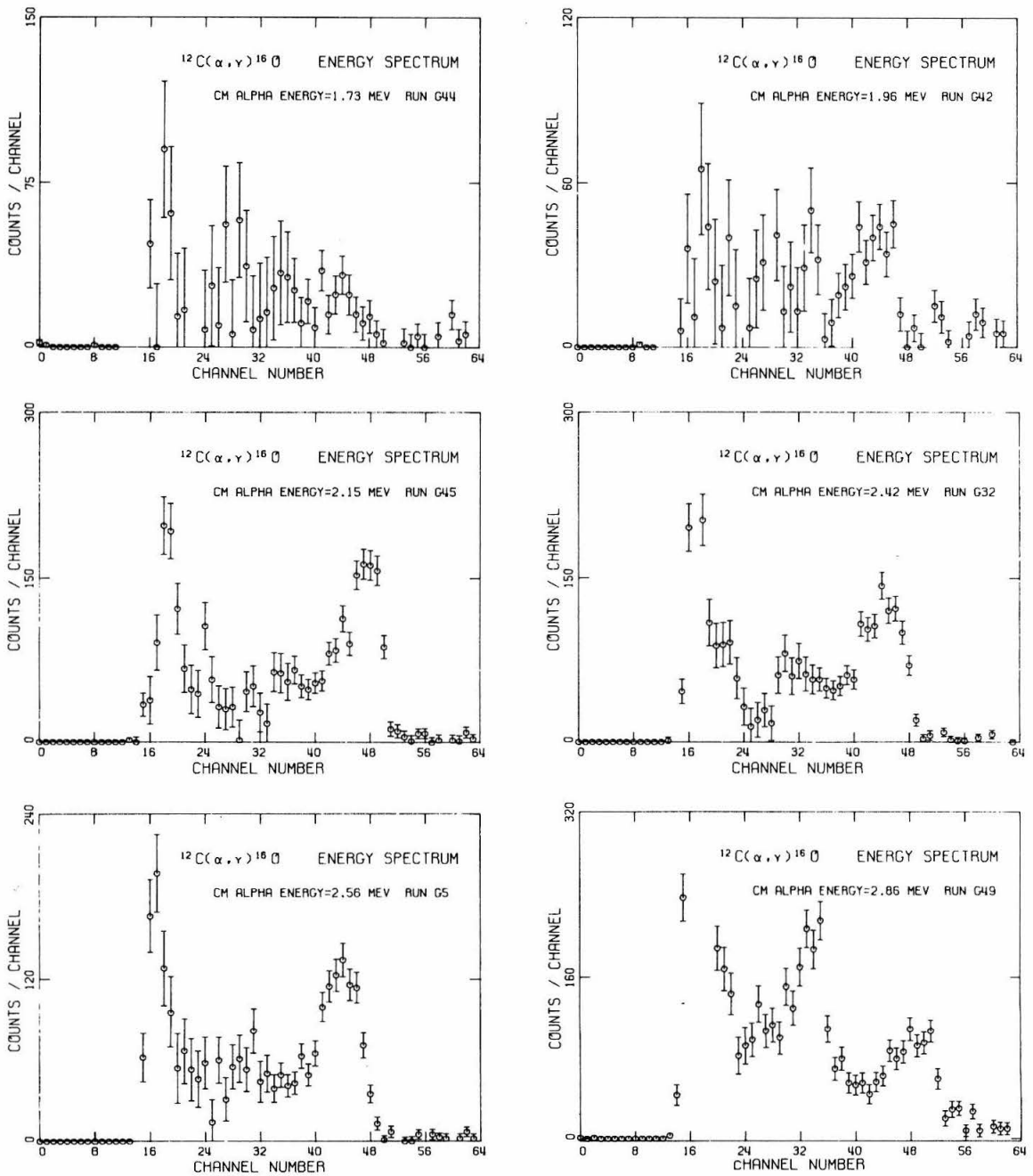
$^{12}C(\alpha,\gamma)^{16}O$ ENERGY SPECTRUM
CM ALPHA ENERGY=1.73 MEV RUN G44
CM ALPHA ENERGY=1.96 MEV RUN G42
CM ALPHA ENERGY=2.15 MEV RUN G45
CM ALPHA ENERGY=2.42 MEV RUN G32
CM ALPHA ENERGY=2.56 MEV RUN G5
CM ALPHA ENERGY=2.86 MEV RUN G49
COUNTS / CHANNEL
CHANNEL NUMBER

Figure 8.

Figure 9

Time Spectra of 9-MeV Events from the $^{12}C(\alpha,\gamma)^{16}O$ Reaction

These spectra were obtained from the two-dimensional spectra by summing counts over the energy channels corresponding to the gamma-ray energy of the ground state transition in ^{16}O (9.60 MeV at the peak of the resonance corresponding to the 9.60-MeV state in ^{16}O). The region of summation is taken from $0.8 * E_\gamma$ to $1.1 * E_\gamma$. Time increases to the left. The circles with error bars correspond to data taken with an enriched ^{12}C target; the crosses, to data taken with a natural carbon target which have been normalized to match the prompt-neutron peak and the time-independent background. Some $^{12}C(\alpha,\gamma)^{16}O$ events are present in this background. These are taken into account in the yield analysis. The narrow peak in the center of each spectrum corresponds to the gamma rays; the broad peak at the left end, to prompt neutrons from the $^{13}C(\alpha,n)^{16}O$ reaction. The difference in flight times for neutrons and gamma rays is about 3 nsec, but the peaks are separated by about 6 nsec. The reason is that most neutrons lose their energy in the NaI(Tl) crystals in a series of several collisions, so that the risetime of the pulse produced at the anode of the photomultiplier tube is greater than that of a gamma-ray pulse. The discriminator will thus be triggered at a later time. For additional details, see page 35.

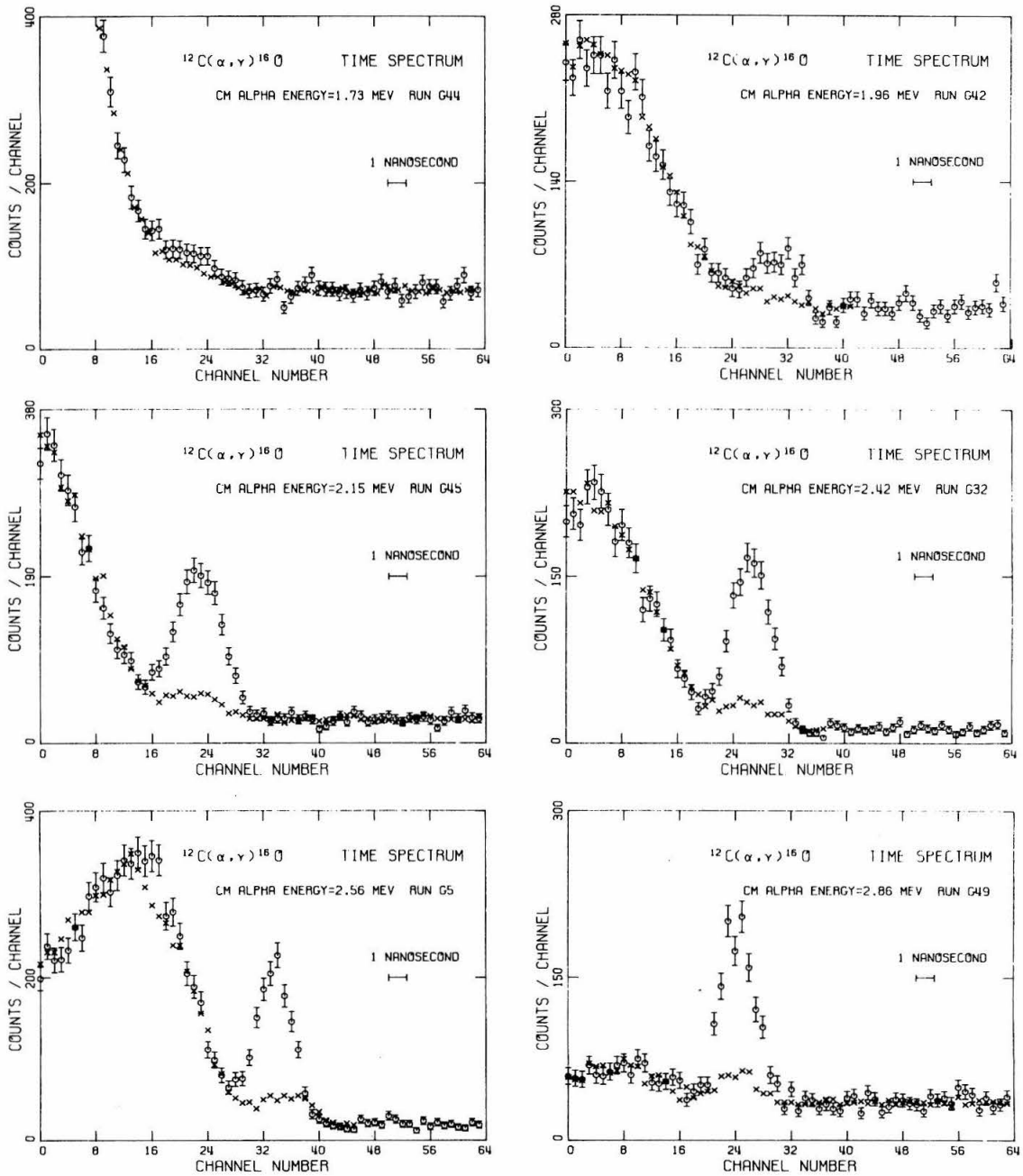
$^{12}C(\alpha,\gamma)^{16}O$ TIME SPECTRUM
CM ALPHA ENERGY=1.73 MEV RUN G44
1 NANOSECOND
COUNTS / CHANNEL
CHANNEL NUMBER
$^{12}C(\alpha,\gamma)^{16}O$ TIME SPECTRUM
CM ALPHA ENERGY=1.96 MEV RUN G42
1 NANOSECOND
COUNTS / CHANNEL
CHANNEL NUMBER
$^{12}C(\alpha,\gamma)^{16}O$ TIME SPECTRUM
CM ALPHA ENERGY=2.15 MEV RUN G45
1 NANOSECOND
COUNTS / CHANNEL
CHANNEL NUMBER
$^{12}C(\alpha,\gamma)^{16}O$ TIME SPECTRUM
CM ALPHA ENERGY=2.42 MEV RUN G32
1 NANOSECOND
COUNTS / CHANNEL
CHANNEL NUMBER
$^{12}C(\alpha,\gamma)^{16}O$ TIME SPECTRUM
CM ALPHA ENERGY=2.56 MEV RUN G5
1 NANOSECOND
COUNTS / CHANNEL
CHANNEL NUMBER
$^{12}C(\alpha,\gamma)^{16}O$ TIME SPECTRUM
CM ALPHA ENERGY=2.86 MEV RUN G49
1 NANOSECOND
COUNTS / CHANNEL
CHANNEL NUMBER

Figure 9.

Figure 10

$^{12}C(\alpha,\gamma)^{16}O$ Angular Distributions

The yields, expressed in arbitrary units, are plotted versus the angle θ, measured with respect to the direction of the incident beam of alpha particles. Angular distributions were measured for four alpha energies. The dashed curves are fits to the data obtained by assuming interference between 1^- and 2^+ contributions to the cross section, taking into account the finite size of the detectors. The solid curves indicate the angular distributions which would be measured by a point detector. For additional details see pages 44 to 47.

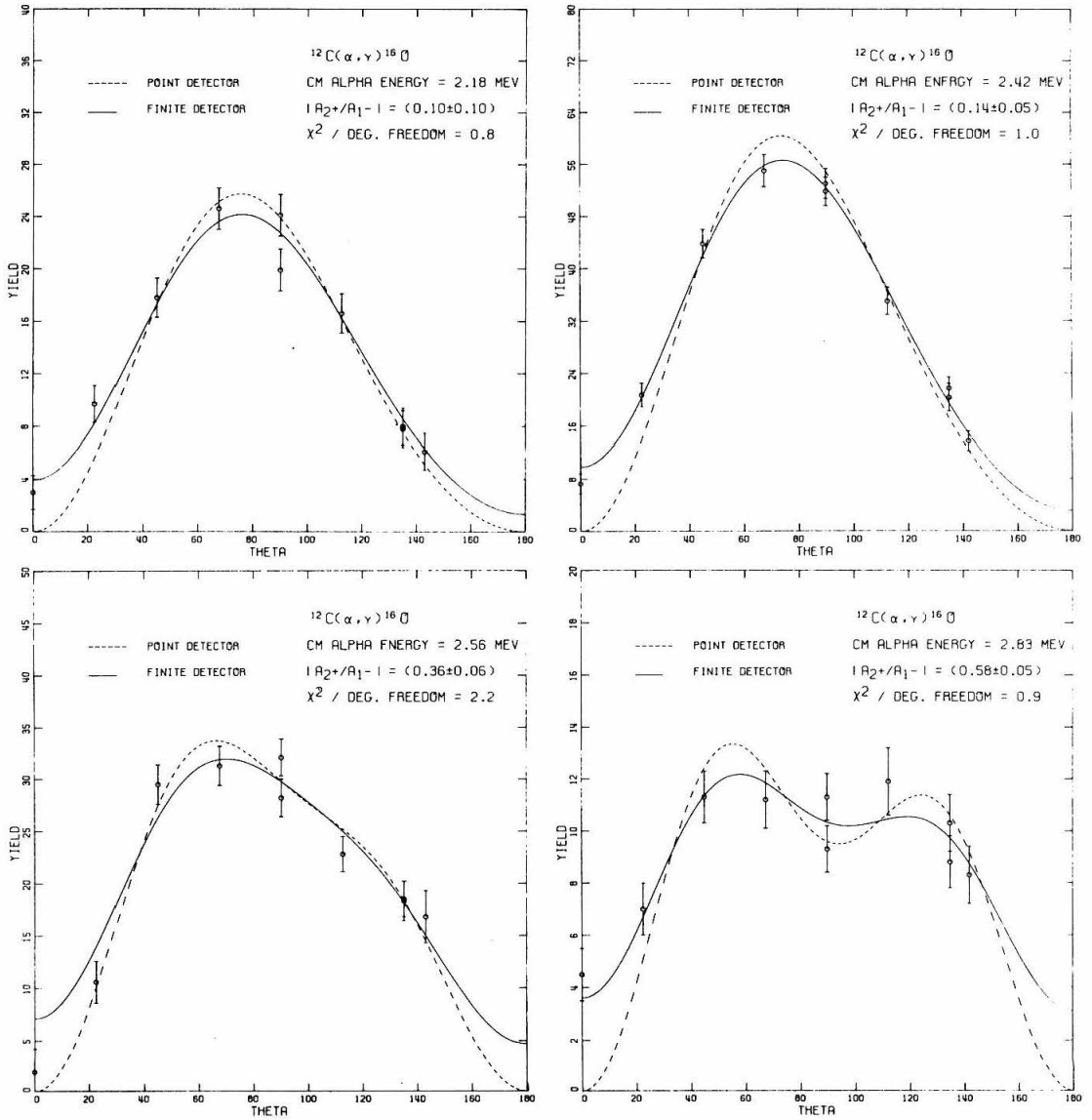
$^{12}C(\alpha,\gamma)^{16}O$
POINT DETECTOR
FINITE DETECTOR
CM ALPHA ENERGY = 2.18 MEV
$|A_2+/A_1-| = (0.10\pm0.10)$
χ^2 / DEG. FREEDOM = 0.8
CM ALPHA ENERGY = 2.42 MEV
$|A_2+/A_1-| = (0.14\pm0.05)$
χ^2 / DEG. FREEDOM = 1.0
CM ALPHA ENERGY = 2.56 MEV
$|A_2+/A_1-| = (0.36\pm0.06)$
χ^2 / DEG. FREEDOM = 2.2
CM ALPHA ENERGY = 2.83 MEV
$|A_2+/A_1-| = (0.58\pm0.05)$
χ^2 / DEG. FREEDOM = 0.9
YIELD
THETA

Figure 10.

Figure 11

Variation of $|A_{2+}|^2$ with Alpha Energy

This figure shows the results of calculations of the 2^+ direct capture cross section from the formulation of Tombrello (1961). The scale is 30% uncertain, because of the error in the quantity $\theta_\alpha^2(g.s., {}^{16}O) = 0.043 \pm 0.012$, which is determined by fitting amplitude ratios from the measured angular distributions. These values were used to extract the electric dipole contributions to the total cross sections. For additional details see pages 44 to 48.

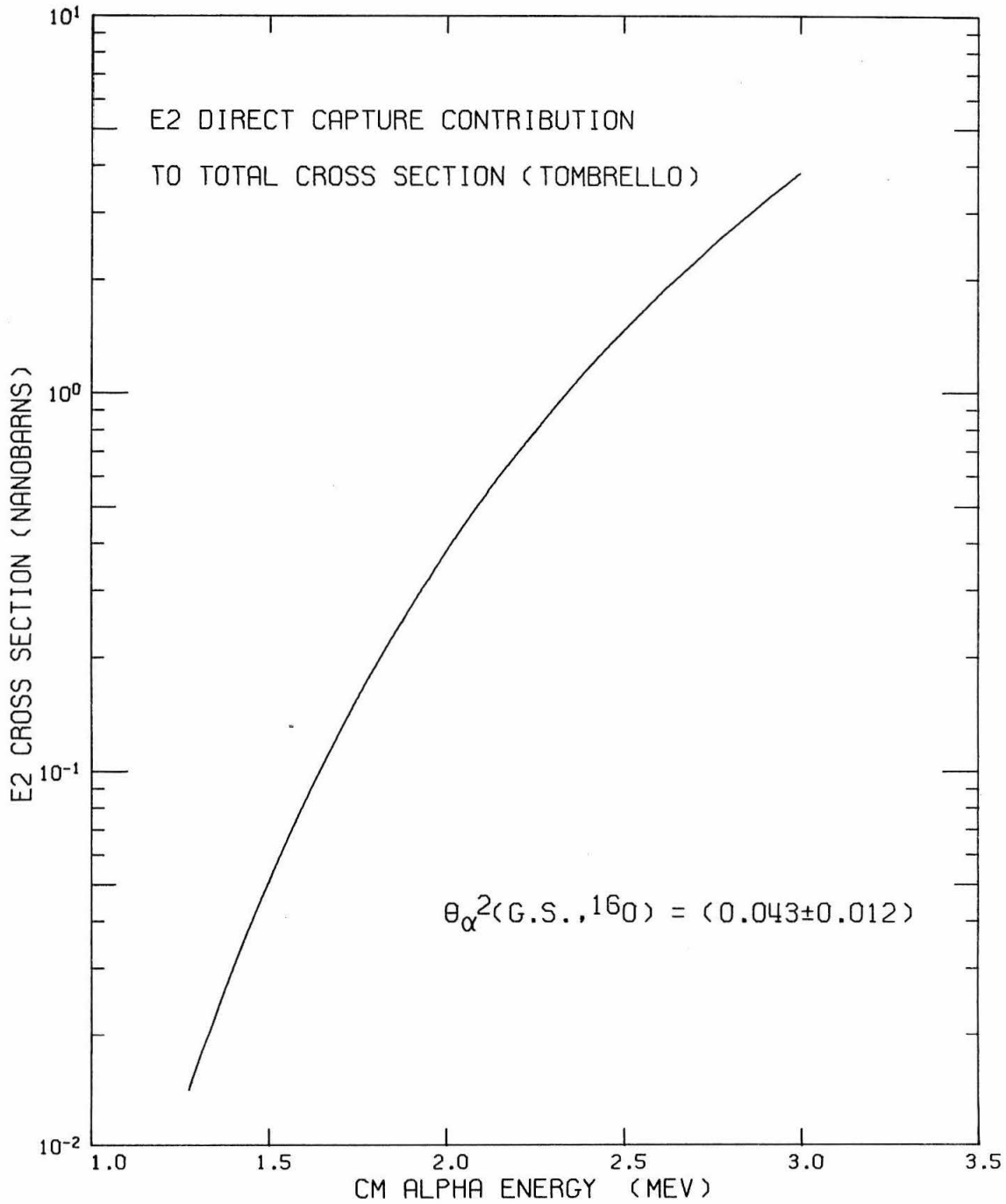
E2 DIRECT CAPTURE CONTRIBUTION
TO TOTAL CROSS SECTION (TOMBRELLO)
θ_α^2(G.S., ^{16}O) = (0.043±0.012)
E2 CROSS SECTION (NANOBARNS)
CM ALPHA ENERGY (MEV)
10^1
10^0
10^{-1}
10^{-2}
1.0
1.5
2.0
2.5
3.0
3.5

Figure 11.

Figure 12

Measured 1^- Contributions to the $^{12}C(\alpha,\gamma)^{16}O$ Total Cross Sections and 3-level R-Matrix Fits

The quantity $|A_{1-}|^2$ is plotted versus E_α(c.m.). The solid curve is the best 3-level R-matrix fit to the data (Weisser 1970). Three parameters are free to vary. The χ^2 per degree of freedom is 1.4. The dashed curve represents a fit in which Θ_α^2 is constrained to 0 and the remaining two parameters are free to vary (χ^2 per degree of freedom = 2.8); the dotted curve is also a fit with two parameters free to vary, but with Θ_α^2 constrained to 0.4 (χ^2 per degree of freedom = 1.5). For further details see pages 48 and 49.

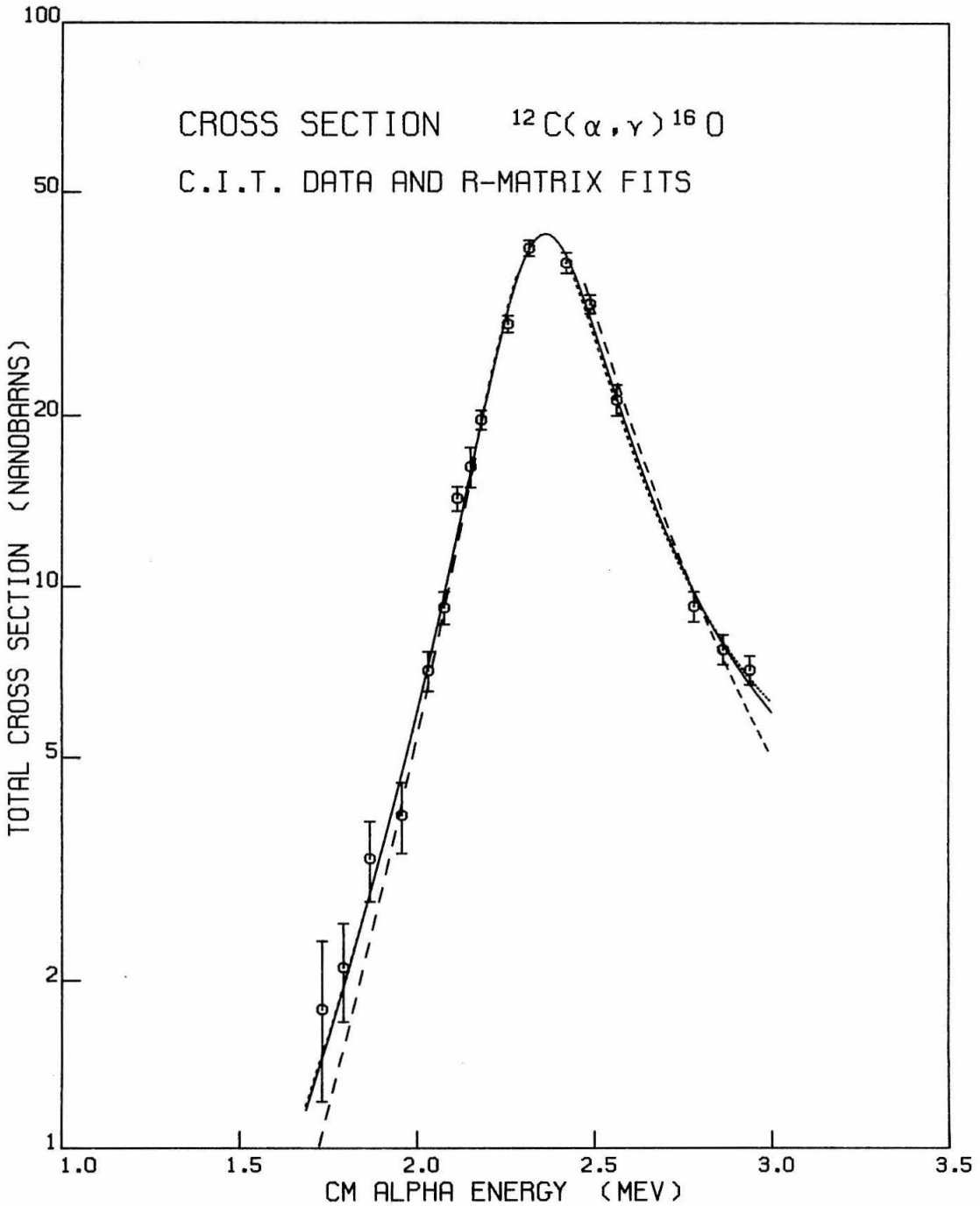
CROSS SECTION $^{12}C(\alpha,\gamma)^{16}O$
C.I.T. DATA AND R-MATRIX FITS
TOTAL CROSS SECTION (NANOBARNS)
100
50
20
10
5
2
1
1.0
1.5
2.0
2.5
3.0
3.5
CM ALPHA ENERGY (MEV)

Figure 12.

Figure 13

Variation of the Ratio $|A_{2+}|^2/|A_{1-}|^2$ with Alpha Energy

The points with error bars are values derived directly from the angular distribution measurements; the solid curve represents calculated ratios. The calculated values for $|A_{2+}|^2$ are taken from the 2^+ direct capture formulation of Tombrello (1961), using $\Theta_\alpha^2(\text{g.s.}, {}^{16}\text{O}) = 0.043 \pm 0.012$. The calculated values for $|A_{1-}|^2$ are taken from the 3-level R-matrix fit to the E1 contributions to the total cross sections (Weisser 1970). The ratio becomes very small at low alpha energies; it can be seen that the 2^+ direct capture process is not significant at astrophysically interesting energies. For additional details see pages 44 to 49, 67 and 68.

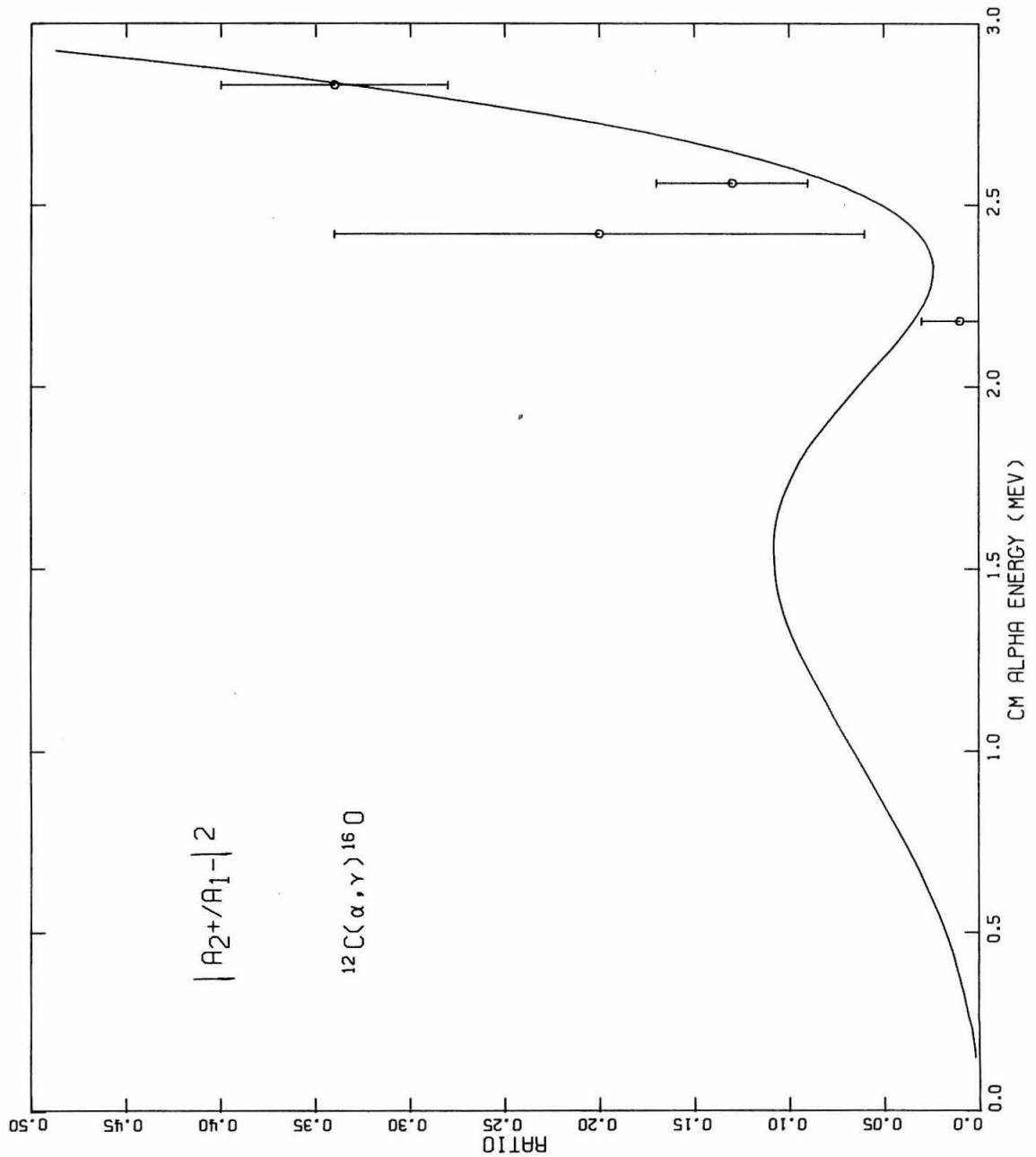
$|A_{2^+}/A_{1^-}|^2$
$^{12}C(\alpha,\gamma)^{16}O$
RATIO
0.0
0.05
0.10
0.15
0.20
0.25
0.30
0.35
0.40
0.45
0.50
0.0
0.5
1.0
1.5
2.0
2.5
3.0
CM ALPHA ENERGY (MEV)

Figure 13.

Figure 14

Measured 1^- Contributions to the $^{12}C(\alpha,\gamma)^{16}O$ S-factor and 3-Level R-Matrix Fits

The data and fits shown here are the same as those of Figure 12, but the ordinate corresponds to the S-factor rather than the cross section. ($S = \sigma E e^{2\pi\eta}$. See Appendix A.) The solid curve is the best fit; three parameters are free to vary. The other two fits are made with θ_α^2 constrained and two parameters free to vary. The dashed curve corresponds to $\theta_\alpha^2 = 0$; the dotted, to $\theta_\alpha^2 = 0.4$. It can be seen that more data at lower alpha energies is desperately needed in order to obtain a reliable extrapolation of the data to E_α(c.m.) = 300 keV. For additional details see pages 48 and 49.

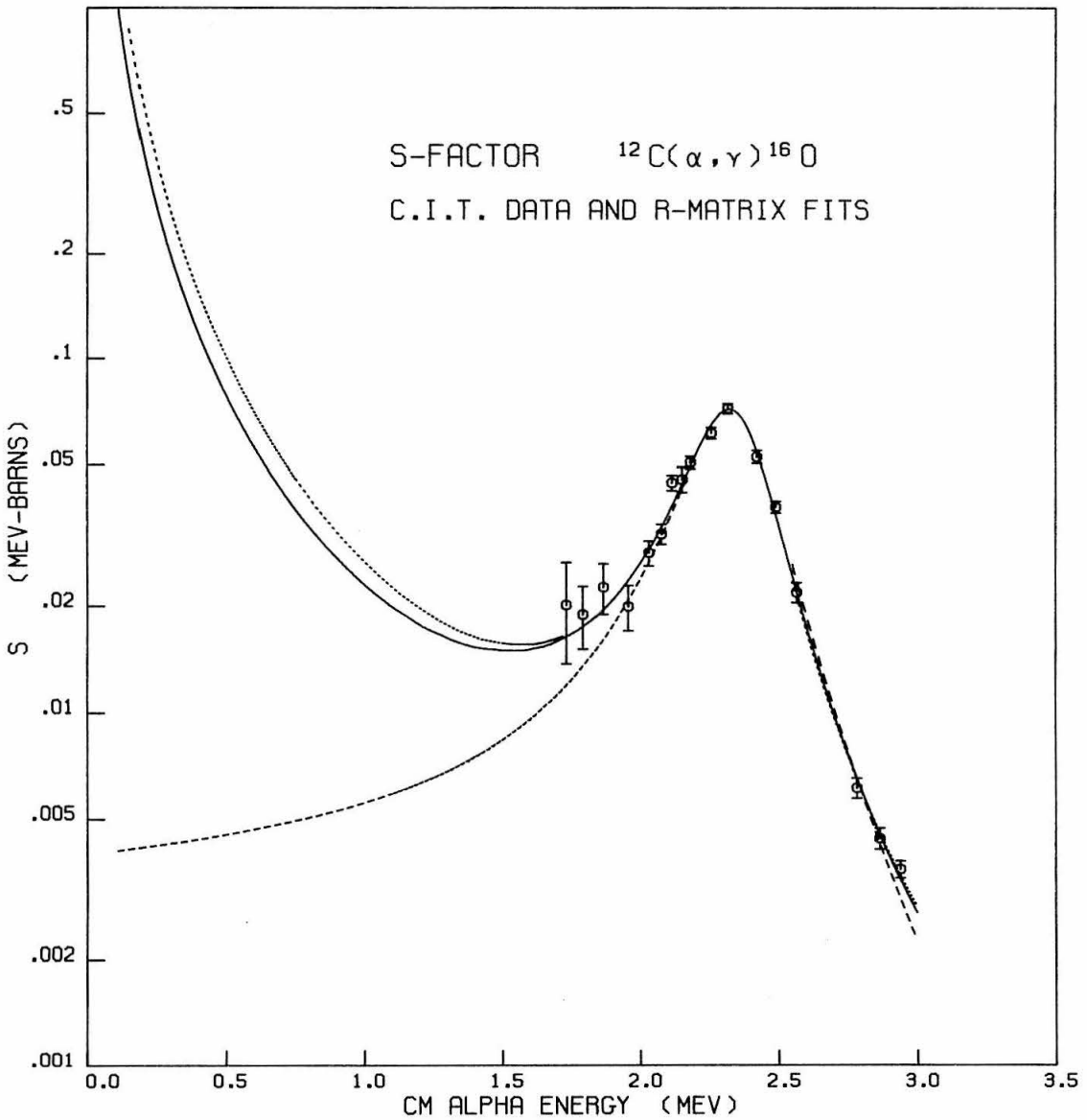
S-FACTOR $^{12}C(\alpha,\gamma)^{16}O$
C.I.T. DATA AND R-MATRIX FITS
S (MEV-BARNS)
.5
.2
.1
.05
.02
.01
.005
.002
.001
0.0
0.5
1.0
1.5
2.0
2.5
3.0
3.5
CM ALPHA ENERGY (MEV)

Figure 14.

Figure 15

Measured 1^- Contributions to the $^{12}C(\alpha,\gamma)^{16}O$ Total Cross Sections and "Hybrid" R-Matrix-Optical-Model Fits

The quantity $|A_{1^-}|^2$ is plotted versus E_α(c.m.). The solid curve is the best fit to the data (Koonin 1972). Two parameters are free to vary. The χ^2 per degree of freedom is 1.3. The dashed curve represents a fit in which the bound state at 7.12-MeV in ^{16}O is omitted (χ^2 per degree of freedom = 7). For additional details see pages 48 to 50.

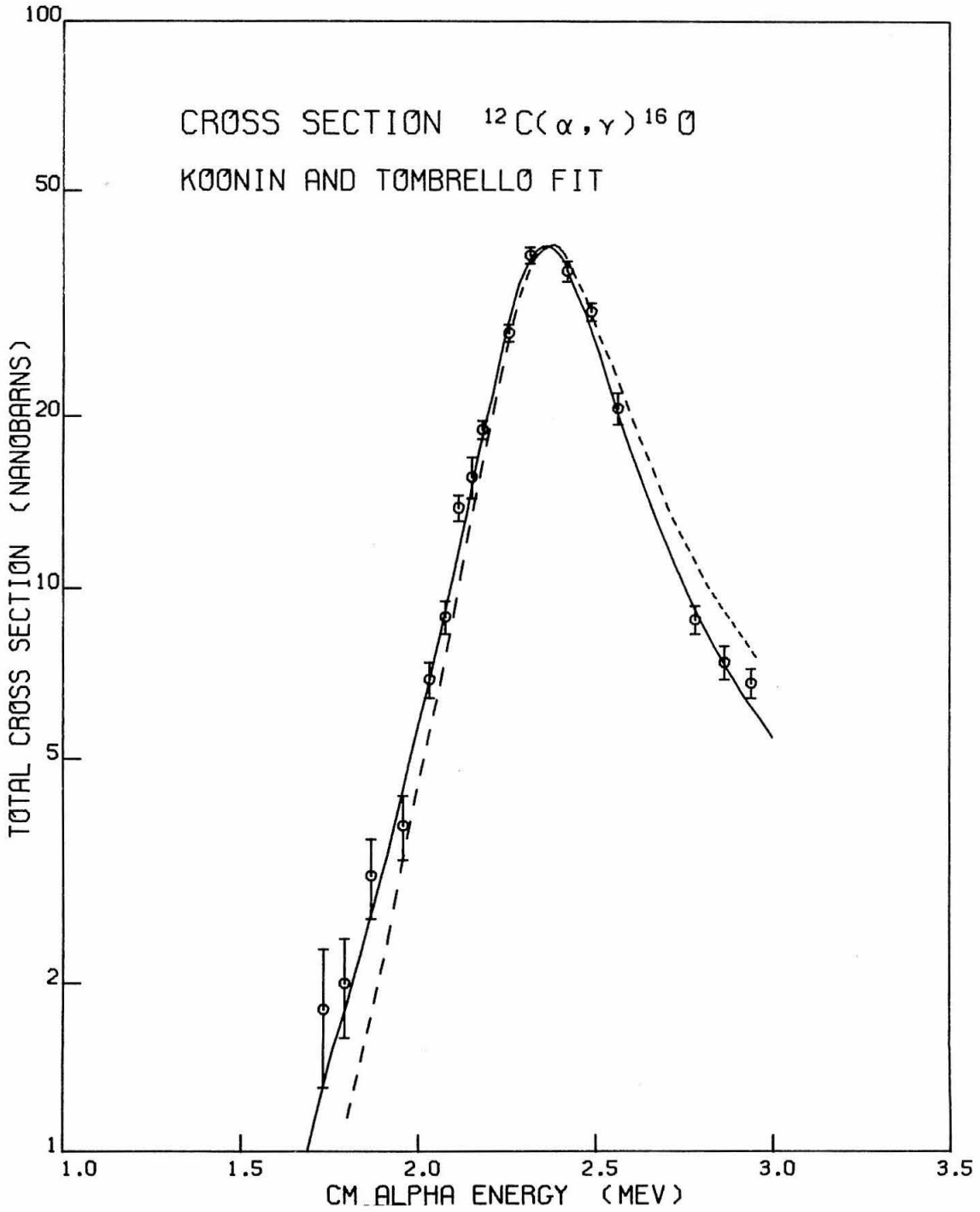
CROSS SECTION $^{12}C(\alpha,\gamma)^{16}O$
KOONIN AND TOMBRELLO FIT
TOTAL CROSS SECTION (NANOBARNS)
100
50
20
10
5
2
1
1.0
1.5
2.0
2.5
3.0
3.5
CM ALPHA ENERGY (MEV)

Figure 15.

Figure 16

Measured 1^- Contributions to the $^{12}C(\alpha,\gamma)^{16}O$ S-factor and "Hybrid" R-Matrix-Optical-Model Fit

The data and best fit shown here are the same as those of Figure 15, but the ordinate corresponds to the S-factor rather than the cross section. ($S = \sigma E e^{2\pi\eta}$. See Appendix A.) For additional details see pages 49 and 50.

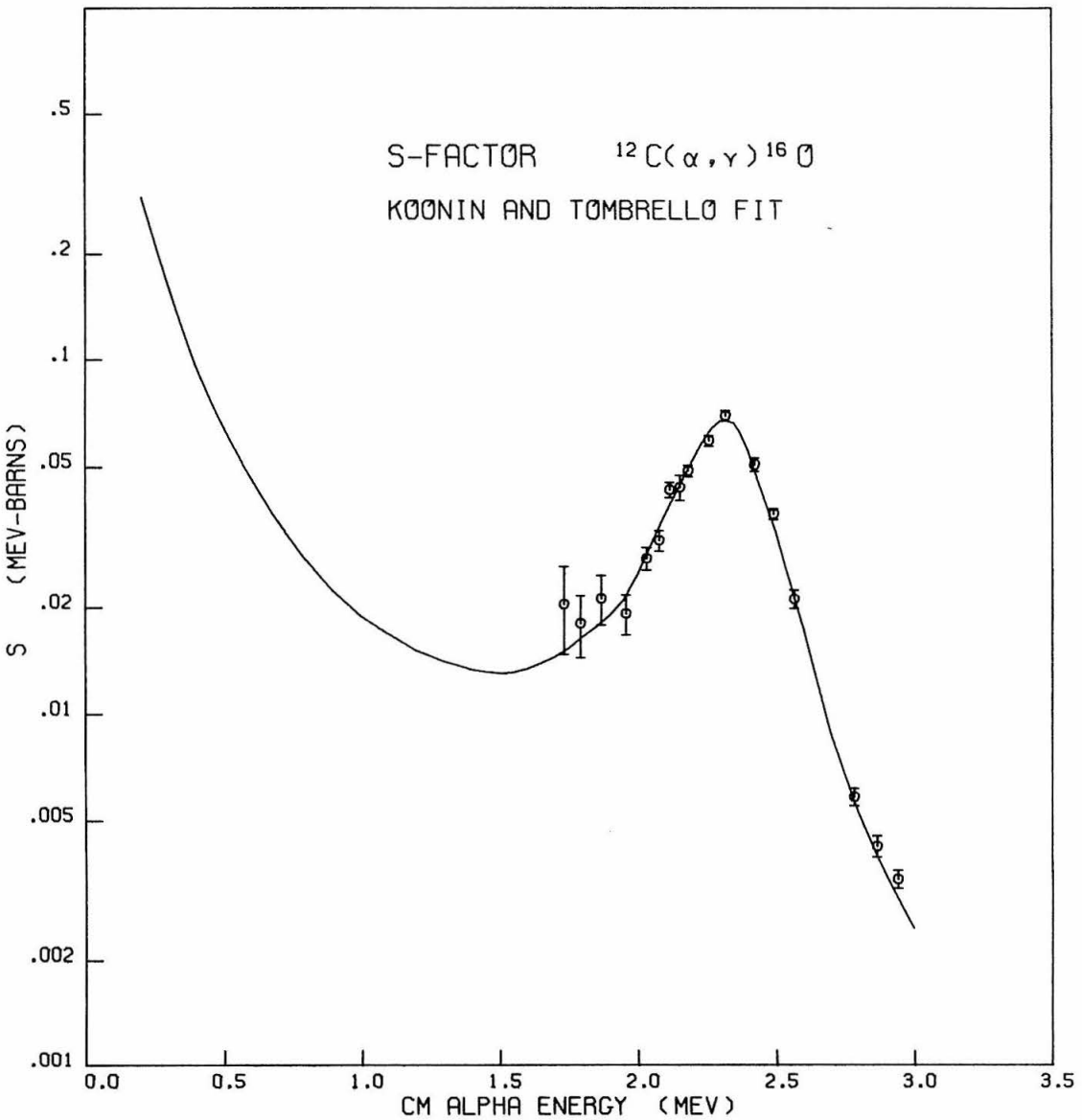
S-FACTOR $^{12}C(\alpha,\gamma)^{16}O$
KOONIN AND TOMBRELLO FIT
S (MEV-BARNS)
.5
.2
.1
.05
.02
.01
.005
.002
.001
0.0
0.5
1.0
1.5
2.0
2.5
3.0
3.5
CM ALPHA ENERGY (MEV)

Figure 16.

Figure 17

$^{12}C(\alpha,\gamma)^{16}O$ Cross Sections of Jaszczak et al. Compared with Fit to Caltech Data

The data of Jaszczak et al. (1970,1970a) is shown with the 3-level R-matrix fit to the Caltech data (1^- contributions only). The cross sections of Jaszczak et al. were obtained by assuming the transitions to be pure electric dipole. (This does not account for the discrepancy between the two sets of data.) For additional details see pages 11, 12 and 50.

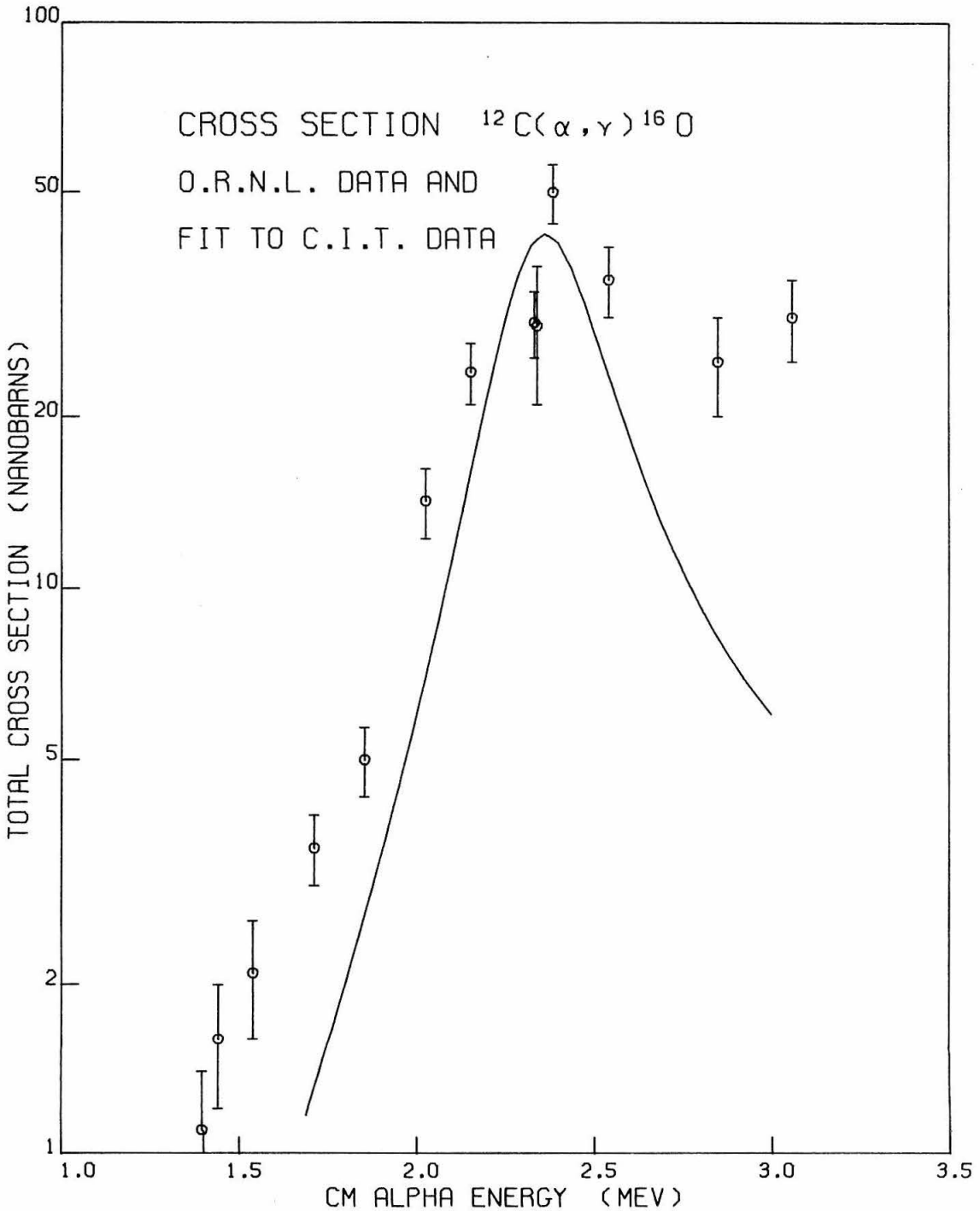
CROSS SECTION $^{12}C(\alpha,\gamma)^{16}O$
O.R.N.L. DATA AND
FIT TO C.I.T. DATA
TOTAL CROSS SECTION (NANOBARNS)
100
50
20
10
5
2
1
1.0
1.5
2.0
2.5
3.0
3.5
CM ALPHA ENERGY (MEV)

Figure 17.

Figure 18

Dependence of ^{12}C Mass Fraction on Core Mass and $\Theta^2_{\alpha,F}$

The mass fraction of ^{12}C at the end of core helium burning is plotted as a function of the mass of the helium core. The values are obtained by a combination of the calculations of Deinzer and Salpeter (1964) and Arnett (1972). The three curves represent different rates of the $^{12}C(\alpha,\gamma)^{16}O$ reaction; they are labeled by the corresponding values of $\Theta^2_{\alpha,F}$. The solid curve corresponds to the best value for $\Theta^2_{\alpha,F}$ obtained from the experimental data; the dashed curves correspond to values of $\Theta^2_{\alpha,F}$ one standard deviation above and below the best value. For additional details see pages 51 and 52.

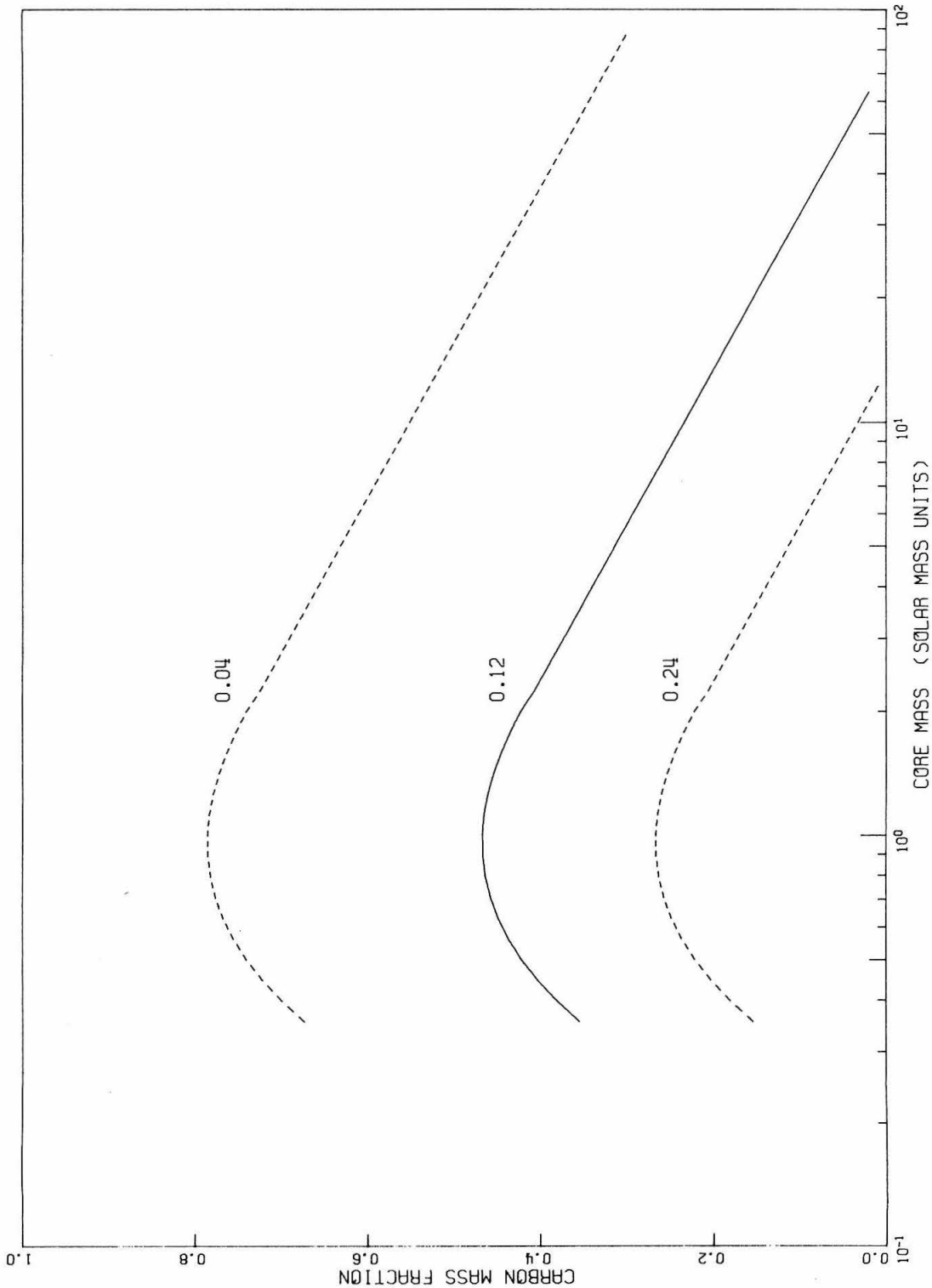
0.04
0.12
0.24
CARBON MASS FRACTION
CORE MASS (SOLAR MASS UNITS)
0.0
0.2
0.4
0.6
0.8
1.0
10^{-1}
10^{0}
10^{1}
10^{2}

Figure 18.

Figure 19

^{19}F Content of Enriched ^{12}C Targets

The yields of 6.13-MeV gamma rays from the $^{19}F(p,\alpha\gamma)^{16}O$ reaction are given for three targets: (1) a 20 $\mu g/cm^2$ CaF_2 target, (2) a 158 $\mu g/cm^2$ enriched ^{12}C target, referred to as target A in the text, and (3) a 185 $\mu g/cm^2$ enriched ^{12}C target, referred to as target B in the text. All targets were mounted on tantalum backings. Target A and other targets from the same tantalum strip were used for all of the $^{12}C(\alpha,\gamma)^{16}O$ measurements discussed in this thesis.

The width of the 872-keV resonance for the two carbon targets is due to the energy loss of the protons in the targets. The measurements for these two targets extend over the thicknesses of the targets; the yield thus represents the ^{19}F content as a function of depth in the target. It appears that in both cases there is a relatively large amount of ^{19}F near the surface of the target and near the tantalum backing, whereas there is a minimum in the content halfway through the target. For additional details see pages 75 to 78.

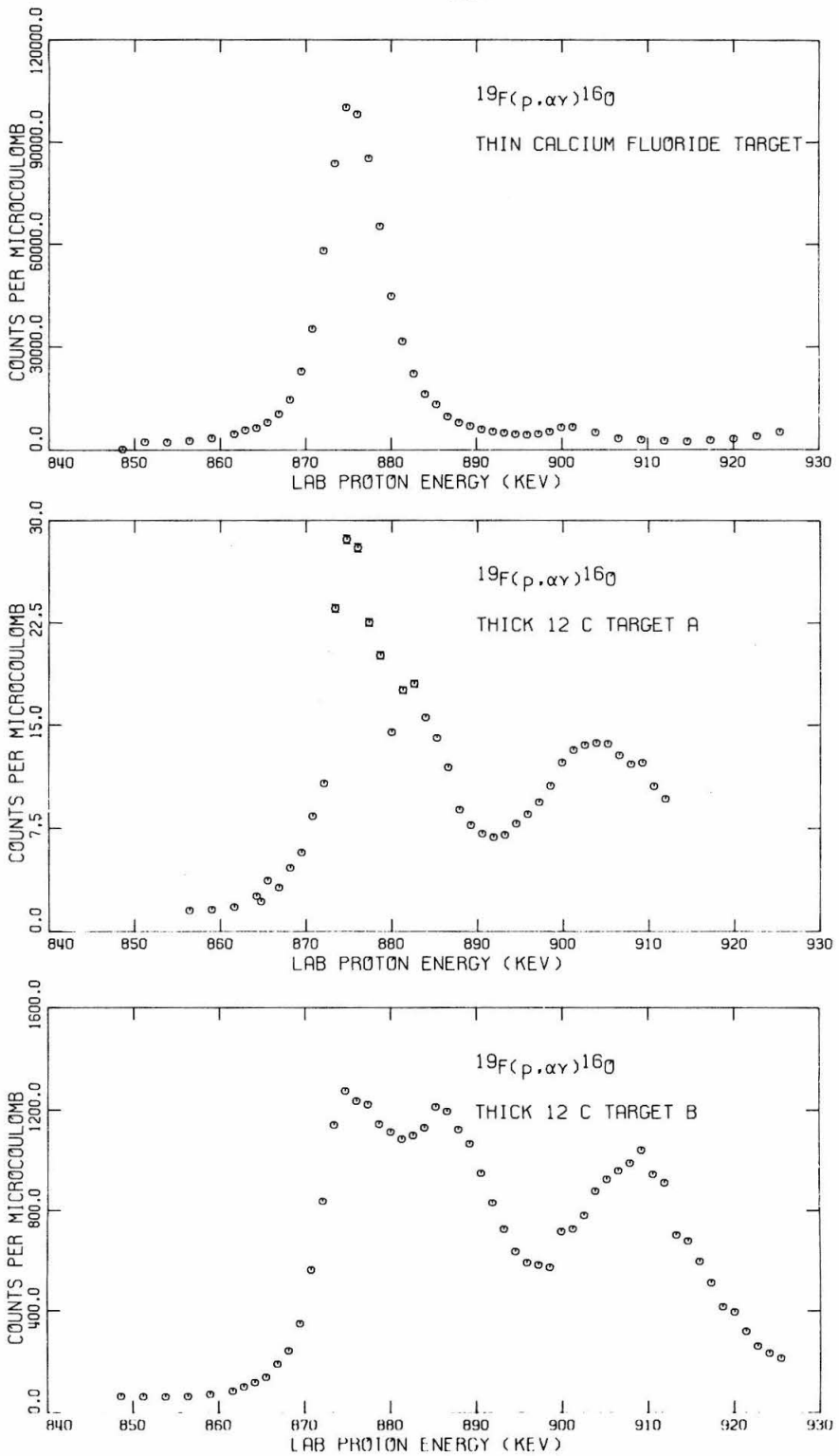
19F(p,αγ)16O
THIN CALCIUM FLUORIDE TARGET
COUNTS PER MICROCOULOMB
0.0
30000.0
60000.0
90000.0
120000.0
840
850
860
870
880
890
900
910
920
930
LAB PROTON ENERGY (KEV)
19F(p,αγ)16O
THICK 12 C TARGET A
COUNTS PER MICROCOULOMB
0.0
7.5
15.0
22.5
30.0
LAB PROTON ENERGY (KEV)
19F(p,αγ)16O
THICK 12 C TARGET B
COUNTS PER MICROCOULOMB
0.0
400.0
800.0
1200.0
1600.0
LAB PROTON ENERGY (KEV)

Figure 19.

Figure 20

The 13-MeV Gamma-Ray Yield of the $^{19}F(\alpha,\gamma)^{23}Na$ Reaction

The yield of the gamma-rays of energy corresponding to the ground-state transition in ^{23}Na is given as a function of the lab alpha energy (displayed here as the incident energy minus half the energy loss in the target). These yields were obtained with a 20 $\mu g/cm^2$ CaF_2 target, a singly-charged ^4He beam, and two 20.3-cm-diameter by 12.7-cm-long NaI(Tℓ) detectors placed 10.5 cm from the target and at angles of 90^o with respect to the incident beam. For additional details, see page 76.

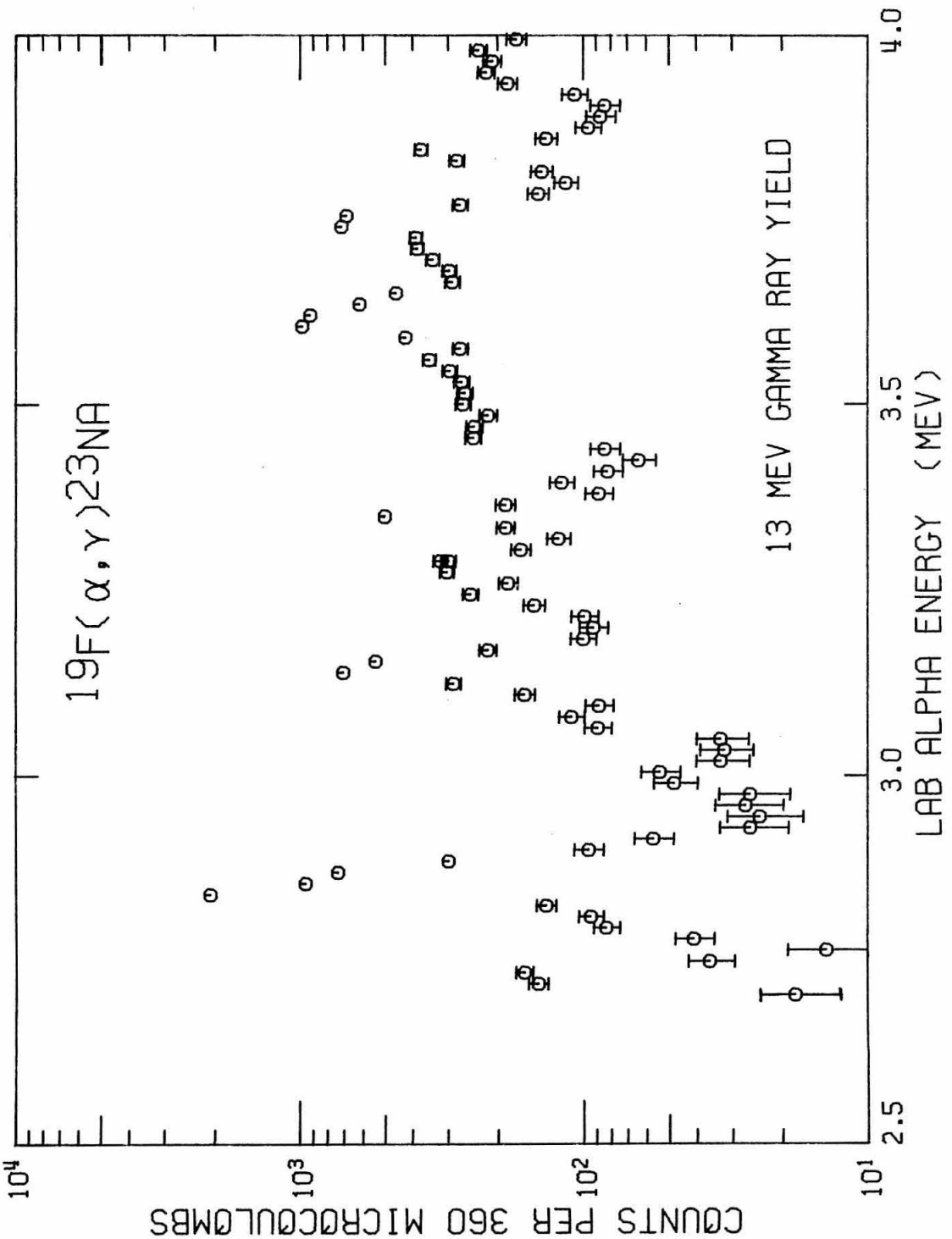
19F(α,γ)23NA
13 MEV GAMMA RAY YIELD
COUNTS PER 360 MICROCOULOMBS
LAB ALPHA ENERGY (MEV)
10^4
10^3
10^2
10^1
2.5
3.0
3.5
4.0

Figure 20.

Figure 21

The 9-MeV Gamma-Ray Yield of the $^{19}F(\alpha,\gamma)^{23}Na$ Reaction

These yields were extracted from the same spectra as those of Figure 20. In this case, the region of summation was that of gamma rays of energy corresponding to the $^{12}C(\alpha,\gamma)^{16}O$ ground-state transition for the particular lab alpha energy. These yields were used to determine the effect of the ^{19}F impurity on the $^{12}C(\alpha,\gamma)^{16}O$ yields. For additional details see pages 76 to 79.

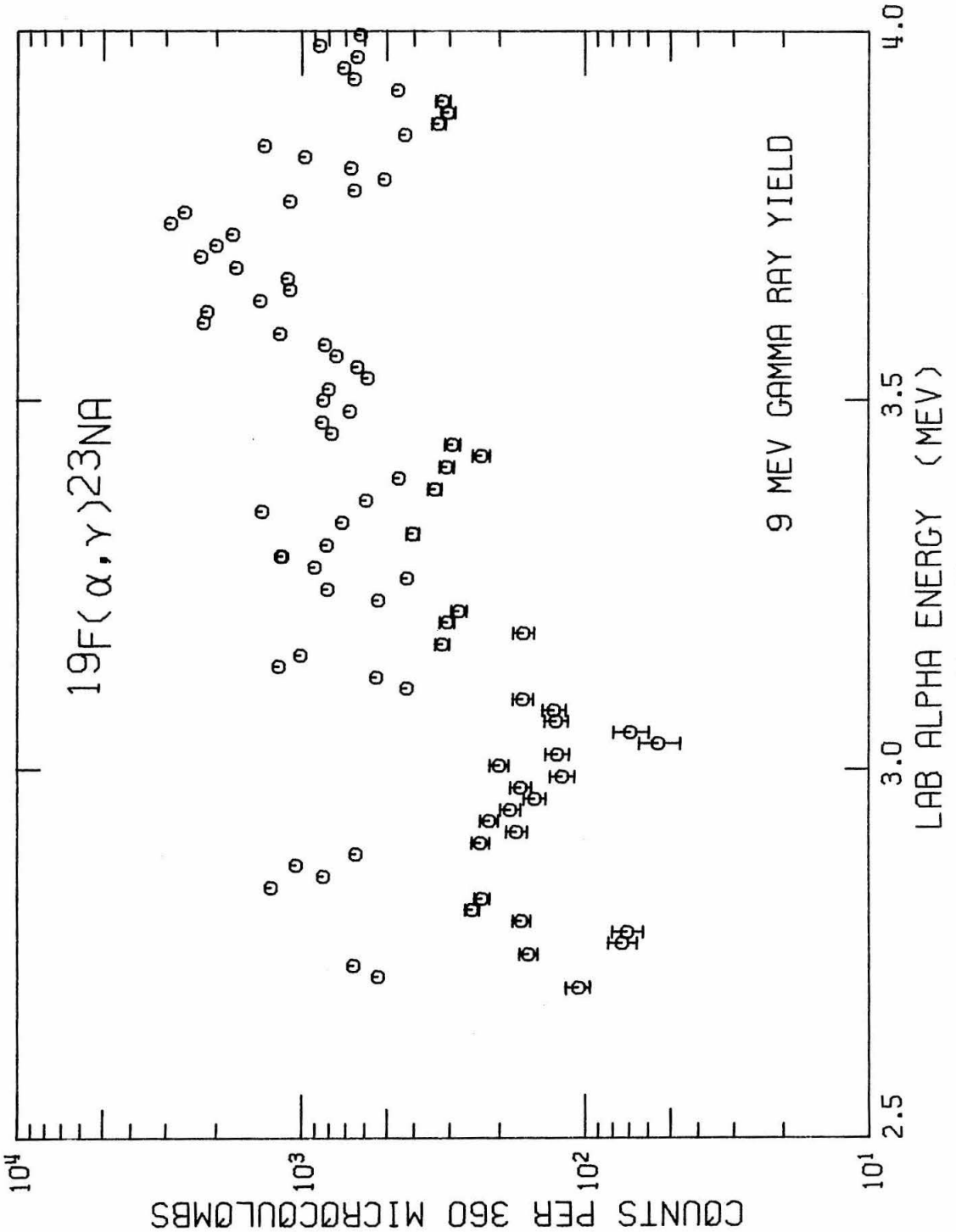
19F(α,γ)23NA
9 MEV GAMMA RAY YIELD
COUNTS PER 360 MICROCOULOMBS
LAB ALPHA ENERGY (MEV)
10^4
10^3
10^2
10^1
2.5
3.0
3.5
4.0

Figure 21.